RADIOSCIENCE LABORATORY

STANFORD ELECTRONICS LABORATORIES
DEPARTMENT OF ELECTRICAL ENGINEERING
STANFORD UNIVERSITY · STANFORD, CA 94305

SEL 79-025

COMPENDIUM OF THE ULF/ELF ELECTROMAGNETIC FIELDS GENERATED ABOVE A SEA OF FINITE DEPTH BY SUBMERGED HARMONIC DIPOLES

by
A. C. Fraser-Smith
D. M. Bubenik

Technical Report E715-1

January 1980

Sponsored by
The Office of Naval Research
through Contract No. N00014-77-C-0292
Task Area NR 089-121

UNCLASSIFIED

SECURITY CLASSIFICATION OF THIS PAGE (When Data Entered)

REPORT DOCUMENTATION PAGE		READ INSTRUCTIONS BEFORE COMPLETING FORM
1. REPORT NUMBER: Tech. Report No. E715-1	2. GOVT ACCESSION NO.	3. RECIPIENT'S CATALOG NUMBER
4. TITLE (and Subtitle): Compendium of the ULF/ELF Electromagnetic Fields Generated above a Sea of Finite Depth by Submerged Harmonic Dipoles		5. TYPE OF REPORT & PERIOD COVERED: Technical Rept. Jul [redacted] 78-30 Jun [redacted] 79
		6. PERFORMING ORG. REPORT NUMBER: SEL 79-025
7. AUTHOR(s): A. C. Fraser-Smith, D. M. Bubenik		8. CONTRACT OR GRANT NUMBER(s): N000[redacted]14-77-C-0292 (new)
9. PERFORMING ORGANIZATION NAME AND ADDRESS: Radioscience Laboratory, Stanford Electronics Laboratories, Stanford University, Stanford, California 94305		10. PROGRAM ELEMENT, PROJECT, TASK AREA & WORK UNIT NUMBERS: Task Area NR 089-121
11. CONTROLLING OFFICE NAME AND ADDRESS: Office of Naval Research, Code 465, 800 North Quincy Street, Arlington, Virginia 22217		12. REPORT DATE: Jan [redacted] 80 / 13. NO. OF PAGES: 114
14. MONITORING AGENCY NAME & ADDRESS (if diff. from Controlling Office): SU-SEL-79-025, TR-E715-1		15. SECURITY CLASS. (of this report): UNCLASSIFIED
		15a. DECLASSIFICATION/DOWNGRADING SCHEDULE

16. DISTRIBUTION STATEMENT (of this report)

Approved for public release; distribution unlimited.

17. DISTRIBUTION STATEMENT (of the abstract entered in Block 20, if different from report)

18. SUPPLEMENTARY NOTES

19. KEY WORDS (Continue on reverse side if necessary and identify by block number)

ULF/ELF Electromagnetic Fields
VMD, VED, HED, HMD
Submerged Dipoles
Undersea/Air Communication
Seafloor

20. ABSTRACT (Continue on reverse side if necessary and identify by block number)

In this report we extend earlier computations of the amplitudes of the quasi-static electromagnetic fields produced on and above the surface of a sea of finite depth by a submerged vertically directed harmonic magnetic dipole (VMD) to other dipoles. Specifically, we now present data for the fields produced by a submerged vertically directed harmonic electric dipole (VED) and by submerged horizontally directed magnetic and electric dipoles

DD FORM 1 JAN 73 1473

EDITION OF 1 NOV 65 IS OBSOLETE

UNCLASSIFIED 332400

SECURITY CLASSIFICATION OF THIS PAGE (When Data Entered)

19 KEY WORDS (Continued)

20 ABSTRACT (Continued)

(HMD and HED, respectively). The primary purpose of these computations is to determine the conditions under which an electrically conducting seafloor can produce significant changes in the fields, as compared with the fields produced on and above an infinitely deep sea, for frequencies in the ULF/ELF bands (frequencies less than 3 kHz). As in earlier work, we find that even a comparatively highly conducting seafloor (conductivity $\sigma_f \geq 0.4$ S/m) can produce substantial changes in the field amplitudes for some source-receiver configurations, and, in the case of the horizontal dipoles (as previously found for the VMD), alterations of two orders of magnitude or more can occur in the amplitudes on the sea surface for smaller values of σ_f. The VED fields are more strongly affected by a seafloor, and some field quantities can be changed by over four orders of magnitude for $\sigma_f \leq 0.04$ S/m. Reviewing the dipole field data as a whole, it appears that the vertical electric component produced by the HED in the plane of the dipole ($\phi = 0°$) should be the most useful for undersea-to-air communication at large distances. This component is comparatively large, varies at large distances as the inverse square of the distance, and tends to be enhanced by the presence of a seafloor. Finally, despite many differences in the fields and in the seafloor effects, we find that our previously derived criteria for estimating when a seafloor effect is likely to occur for a VMD source are valid for all dipole sources. Thus, the largest seafloor induced changes occur when the dipole is within 1 seawater skin depth (δ) of the seafloor, and there is essentially no seafloor effect when the dipoles are more than 3δ above the floor.

SEL 79-025

COMPENDIUM OF THE ULF/ELF ELECTROMAGNETIC FIELDS GENERATED ABOVE A SEA OF FINITE DEPTH BY SUBMERGED HARMONIC DIPOLES

by

A. C. Fraser-Smith

D. M. Bubenik*

Technical Report E715-1

January 1980

Sponsored by

The Office of Naval Research

through

Contract No. N00014-77-C-0292

*Present address: Electromagnetic Sciences Laboratory, SRI International, Menlo Park, California 94025.

ACKNOWLEDGEMENTS

We wish to thank Oswald G. Villard, Jr., for many stimulating discussions and encouragement during the course of this work. We would also like to thank Sidney G. Reid, Jr., and R. Gracen Joiner of the Office of Naval Research for helpful discussions and for making the work possible. The invaluable assistance provided by Paula Renfro in the preparation of the report is gratefully acknowledged.

A preliminary presentation of some of the material in this report was made at the Workshop on Ocean Floor Electromagnetics held at the Naval Postgraduate School, Monterey, California, August 20-22, 1979.

Support for the work was provided by the Office of Naval Research through Contract No. N00014-77-C-0292.

ABSTRACT

In this report we extend earlier computations of the amplitudes of the quasi-static electromagnetic fields produced on and above the surface of a sea of finite depth by a submerged vertically directed harmonic magnetic dipole (VMD) to other dipoles. Specifically, we now present data for the fields produced by a submerged vertically directed harmonic electric dipole (VED) and by submerged horizontally directed mangetic and electric dipoles (HMD and HED, respectively). The primary purpose of these computations is to determine the conditions under which an electrically conducting seafloor can produce significant changes in the fields, as compared with the fields produced on and above an infinitely deep sea, for frequencies in the ULF/ELF bands (frequencies less than 3 kHz). As in our earlier work, we find that even a comparatively highly conducting seafloor (conductivity $\sigma_f \sim 0.4$ S/m) can produce substantial changes in the field amplitudes for some source-receiver configurations, and, in the case of the horizontal dipoles (as previously found for the VMD), alterations of two orders of magnitude or more can occur in the amplitudes on the sea surface for smaller values of σ_f. The VED fields are more strongly affected by a seafloor, and some field quantities can be changed by over four orders of magnitude for $\sigma_f \leq 0.04$ S/m. Reviewing the dipole field data as a whole, it appears that the vertical electric component produced by the HED in the plane of the dipole ($\phi = 0°$) should be the most useful for undersea-to-air communication at large distances. This component is comparatively large, varies at large distances as the inverse square of the distance, and tends to be enhanced by the presence of a seafloor. Finally, despite many differences in the fields and in the seafloor effects, we find that our previously derived criteria for estimating when a seafloor effect is likely to occur for a VMD source are valid for all dipole sources. Thus, the largest seafloor induced changes occur when the dipole is within 1 seawater skin depth (δ) of the seafloor, and there is essentially no seafloor effect when the dipoles are more than 3δ above the floor.

TABLE OF CONTENTS

Note: In this report we use the abbreviation ULF (ultra-low-frequencies) for frequencies less than 5 Hz. Pc 1 geomagnetic pulsations are observed in the upper part of this frequency range (0.2 to 5 Hz). ELF (extremely-low-frequencies) is used to designate frequencies in the range 5 Hz to 3 kHz, and VLF (very-low-frequencies) is used for frequencies in the range 3 to 30 kHz.

I. INTRODUCTION

In a recent paper [Fraser-Smith and Bubenik, 1979] we described the ULF/ELF electromagnetic fields generated on and above the surface of a sea of finite depth by a submerged vertically directed harmonic magnetic dipole (VMD). By comparing the field amplitudes produced in the presence of a seafloor with those produced when no seafloor was present (i.e., for an infinitely deep sea), we showed that a seafloor could produce substantial changes in the fields for certain source-receiver configurations. Further, our computations showed that these changes did not require a seafloor with an exceptionally low electrical conductivity: changes of up to an order of magnitude occurred in some field amplitudes when a seafloor was introduced with a conductivity (σ_f) only one tenth of the conductivity of seawater (σ_s; where σ_s = 4 Siemen/m). In addition to drawing attention to the existence of these potentially large seafloor effects, the primary purpose of our paper was to present quantitative data on the changes produced by a seafloor and to introduce criteria for estimating when seafloor effects were most likely to occur. Summarizing these criteria, we found that the seafloor effects were most marked in seas that were electrically shallow, i.e., for seas that were less than a few seawater skin depths (δ) deep. More quantitatively, we found that the largest changes in the fields were produced when the VMD was within 1δ of the seafloor, and there was essentially no seafloor effect when the VMD was more than 3δ above the floor.

Another purpose of the paper was to point out that seafloor effects would probably be important, or at least significant, at most sea locations if measurements were made at frequencies in the ULF range (frequencies less than 5 Hz). This conclusion follows from the criteria described above and from consideration of representative seawater skin depths (Table 1). In particular, because the skin depth at 0.01 Hz is nearly 2.5 km, a seafloor as deep as 7 km can produce perceptible changes in the electromagnetic fields produced on and above the surface by a submerged VMD operating at 0.01 Hz (or at lower frequencies). Since only very little of the world's seafloor area is located at depths

Table 1. Representative Skin Depths
(for σ_s = 4.0 S/m)

Frequency (Hz)	Skin depth (m)	Frequency (Hz)	Skin depth (m)
100	25.2	1	251.6
80	28.1	0.8	281.3
60	32.5	0.6	324.9
40	39.8	0.4	397.9
20	56.3	0.2	562.7
10	79.6	0.1	795.8
8	89.0	0.08	889.7
6	102.7	0.06	1027.3
4	125.8	0.04	1258.2
2	177.9	0.02	1779.4
1	251.6	0.01	2516.5

greater than 7 km, and then only in narrow trenches, the seas everywhere can be considered to be electrically shallow for electromagnetic signals with frequencies less than 0.01 Hz.

The results we have just described could have application in geophysical prospecting or in the detection of wrecks on the seafloor, as noted by Fraser-Smith and Bubenik [1979]. Another possible geophysical application is in the derivation of effective seafloor electrical conductivities: a calibrated dipole source could be submerged at a known depth and its electromagnetic field measured on or above the surface; comparison of the measured fields with the theoretically computed values would give the effective seafloor conductivity. (Other electromagnetic methods for obtaining seafloor conductivities have been suggested by Brock-Nannestad, 1965; Bannister, 1968; and Coggon and Morrison, 1970.) Specific Navy applications include submarine detection and undersea-to-air communication. Because of these many possible applications, we have now extended the work of Fraser-Smith and Bubenik [1979] on the VMD to the remaining three major dipole categories: the horizontal magnetic dipole (HMD) and vertical and horizontal electric dipoles (VED and HED, respectively). To insure the general application of the new data, we have computed the amplitudes of all the relevant electric and magnetic field components for each dipole. Also, in the case of the horizontal dipoles (where the fields have an azimuthal variation), our field computations cover the two principal azimuthal angles $\phi = 0°$ and $\phi = 90°$. The primary purpose of this report is to present these new field data.

As in our earlier work, we have used a parametric approach by measuring all distances in units of the seawater skin depth δ, where

$$\delta = (2/\omega\mu_0\sigma_s)^{1/2} , \qquad (1)$$

and $\omega = 2\pi f$, where f is the frequency, and μ_0 is the permeability of free space ($4\pi \times 10^{-7}$ H/m). The seafloor conductivities are normalized to the conductivity of seawater. It is not difficult to convert the parametric field data into the actual electric and magnetic field amplitudes. To assist in this conversion, and in the interpretation

of the data, representative skin depths for seawater (we assume σ_s = 4.0 Siemen/m, where the unit Siemen/m is identical to the older mho/m unit of conductivity) are listed in Table 1.

We assume that both the sea and the seafloor are nonmagnetic, i.e., that their permeabilities are the same as the permeability of free space. It seems clear that the ULF/ELF electromagnetic fields of submerged harmonic dipoles are influenced predominantly in practice by the electrical conductivities of the sea and seafloor, as described in this report, and that the effects of a magnetic seafloor can generally be neglected. However, studies of the electromagnetic properties of the seafloor at ULF/ELF frequencies are in their infancy, and there may be special circumstances in the future where a knowledge of the effects produced by a weakly magnetic (or even strongly magnetic) seafloor would be of interest. Our field data provide no information about these effects, but the field equations presented in the following section can be simply modified to include permeabilities differing from μ_0. (The equation for Z_n is changed to $Z_n = i\omega\mu_n/\gamma_n$, and the μ_0 in the equations for the HED and HMD becomes the permeability of the layer containing the dipole sources, in accordance with our notation convention.)

The data in this report, when taken together with our previous data for the VMD, provide moderately complete information about the ULF/ELF electromagnetic fields produced on and above a sea of finite depth by submerged harmonic magnetic and electric dipoles.

II. METHOD OF CALCULATION

Figure 1 shows the geometry used in the field calculations. The harmonic dipoles of moment m (magnetic dipole) or p (electric dipole) and angular frequency ω are located at the point (−d,0,0) in a cylindrical coordinate system (r,ϕ,z). The sea surface is the plane $z = 0$, and the seafloor is the plane $z = -D$. The region $z > 0$ is free space, while the region $z < -D$ is a homogeneous conducting half-space corresponding to the seafloor. Using the notation of Fraser-Smith and Bubenik [1979], the air, water, and floor regions have been labeled +1, 0, and −1, respectively, and the surface and floor boundaries are correspondingly denoted +1 and −1.

In Figure 1 the HMD source is directed along the x axis. We will use this particular geometry for both the HMD and for the HED. Our approach in this respect differs from that of Kraichman [1976], who oriented his HED along the x-direction and his HMD along the y-direction.

The expressions for the electromagnetic field components produced by the VED, HED, and HMD at a point P (r,ϕ,z) in the space above the sea have been derived using a method adapted from Morrison et al. [1969], and Kong [1975]. The same method was used in our earlier work to obtain the expressions for the VMD field components. The field expressions for the three dipole types are:

Vertical Electric Dipole

$$E_r = \frac{p}{2\pi\sigma_0} \int_0^\infty F_{2M} \lambda^2 \, d\lambda \, , \tag{2}$$

$$E_z = \frac{p}{2\pi\sigma_0} \int_0^\infty F_{1M} \lambda^2 \, d\lambda \, , \tag{3}$$

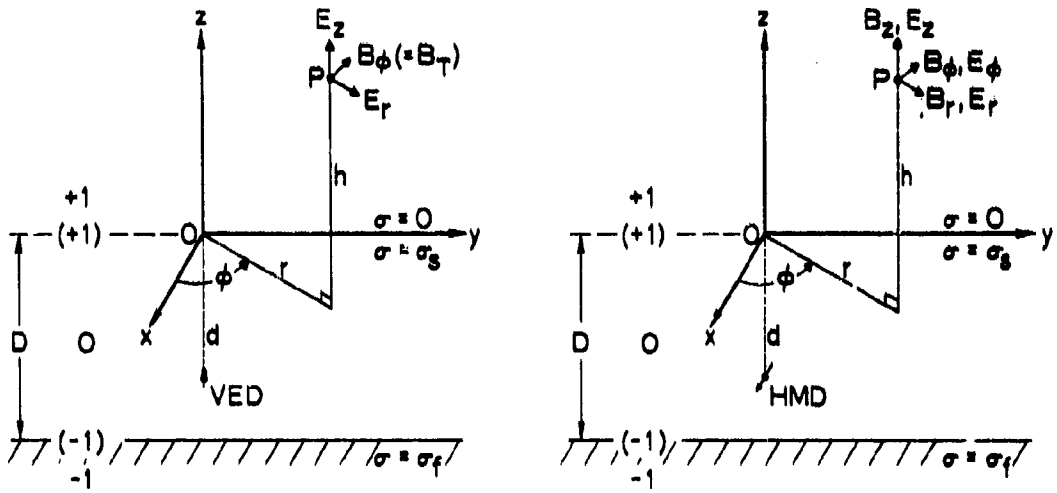

Figure 1. The geometry employed in computing the electromagnetic field components E_r, E_z, and B_ϕ (VED source; left) or B_r, B_z, B_ϕ and E_r, E_z, E_ϕ (HMD source; right) produced at P on and above the surface of a sea of finite depth D by dipole sources located at a depth d ($d \leq D$) below the surface.

$$B_\phi = \frac{i\omega\mu_0\varepsilon_1 p}{2\pi\sigma_0} \int_0^\infty F_{2M}\lambda \, d\lambda \, . \tag{4}$$

Horizontal Electric Dipole

$$E_r = -\frac{p \cos\phi}{2\pi\sigma_0} \left\{ \int_0^\infty \gamma_0 F_{3M}\lambda \, d\lambda - \frac{1}{r} \int_0^\infty [\gamma_0 F_{4M} + (\lambda - \gamma_0) F_{2E}] \, d\lambda \right\} , \tag{5}$$

$$E_\phi = \frac{p \sin\phi}{2\pi\sigma_0} \left\{ \int_0^\infty (\gamma_0 - \lambda) F_{1E}\lambda \, d\lambda + \frac{1}{r} \int_0^\infty [\gamma_0 F_{4M} + (\lambda - \gamma_0) F_{2E}] \, d\lambda \right\} , \tag{6}$$

$$E_z = \frac{p \cos\phi}{2\pi\sigma_0} \int_0^\infty \gamma_0 F_{4M}\lambda \, d\lambda \, , \tag{7}$$

$$B_r = -\frac{\mu_0 p \sin\phi}{2\pi} \left(\int_0^\infty \frac{1}{\gamma_0 + \lambda} F_{1E}\lambda^2 \, d\lambda - \frac{1}{r} \int_0^\infty \frac{1}{\gamma_0 + \lambda} F_{2E}\lambda \, d\lambda \right) , \tag{8}$$

$$B_\phi = -\frac{\mu_0 p \cos\phi}{2\pi} \left(\frac{1}{r} \int_0^\infty \frac{1}{\gamma_0 + \lambda} F_{2E}\lambda \, d\lambda \right) , \tag{9}$$

$$B_z = \frac{\mu_0 p \sin\phi}{2\pi} \int_0^\infty \frac{1}{\gamma_0 + \lambda} F_{2E}\lambda^2 \, d\lambda \, , \tag{10}$$

Horizontal Magnetic Dipole

$$E_r = \frac{i\omega\mu_0 m \sin\phi}{2\pi}\left[\int_0^\infty F_{1M}\lambda\, d\lambda - \frac{1}{r}\int_0^\infty\left(F_{2M} - \frac{\gamma_0}{\gamma_0+\lambda}F_{4E}\right)d\lambda\right], \tag{11}$$

$$E_\phi = \frac{i\omega\mu_0 m \cos\phi}{2\pi}\left[\int_0^\infty \frac{\gamma_0}{\gamma_0+\lambda}F_{3E}\lambda\, d\lambda + \frac{1}{r}\int_0^\infty\left(F_{2M} - \frac{\gamma_0}{\gamma_0+\lambda}F_{4E}\right)d\lambda\right], \tag{12}$$

$$E_z = -\frac{i\omega\mu_0 m \sin\phi}{2\pi}\int_0^\infty F_{2M}\lambda\, d\lambda, \tag{13}$$

$$B_r = -\frac{\mu_0 m \cos\phi}{2\pi}\left(\int_0^\infty \frac{\gamma_0}{\gamma_0+\lambda}F_{3E}\lambda^2\, d\lambda - \frac{1}{r}\int_0^\infty \frac{\gamma_0}{\gamma_0+\lambda}F_{4E}\lambda\, d\lambda\right), \tag{14}$$

$$B_\phi = \frac{\mu_0 m \sin\phi}{2\pi}\left(\frac{1}{r}\int_0^\infty \frac{\gamma_0}{\gamma_0+\lambda}F_{4E}\lambda\, d\lambda\right), \tag{15}$$

$$B_z = \frac{\mu_0 m \cos\phi}{2\pi}\int_0^\infty \frac{\gamma_0}{\gamma_0+\lambda}F_{4E}\lambda^2\, d\lambda, \tag{16}$$

where

$$F_{1M} = F_{TM}^{(a)} e^{-(\gamma_0 d+\lambda h)} J_0(\lambda r),$$

$$F_{2M} = F_{TM}^{(a)} e^{-(\gamma_0 d+\lambda h)} J_1(\lambda r),$$

$$F_{3M} = F_{TM}^{(b)} e^{-(\gamma_0 d+\lambda h)} J_0(\lambda r),$$

$$F_{4M} = F_{TM}^{(b)} e^{-(\gamma_0 d + \lambda h)} J_1(\lambda r) ,$$

$$F_{1E} = F_{TE}^{(a)} e^{-(\gamma_0 d + \lambda h)} J_0(\lambda r) ,$$

$$F_{2E} = F_{TE}^{(a)} e^{-(\gamma_0 d + \lambda h)} J_1(\lambda r) ,$$

$$F_{3E} = F_{TE}^{(b)} e^{-(\gamma_0 d + \lambda h)} J_0(\lambda r) ,$$

$$F_{4E} = F_{TE}^{(b)} e^{-(\gamma_0 d + \lambda h)} J_1(\lambda r) ,$$

and where

$$F_{TM}^{(a)} = (1 + \rho_{-1TM})/(1 - \rho_{-1TM}\rho_{1TM}) ,$$

$$F_{TM}^{(b)} = (1 - \rho_{-1TM})/(1 - \rho_{-1TM}\rho_{1TM}) ,$$

$$\rho_{1TM} = [(Y_1 - Y_0)/(Y_1 + Y_0)] \, e^{-2\gamma_0 d} ,$$

$$\rho_{-1TM} = [(Y_{-1} - Y_0)/(Y_{-1} + Y_0)] \, e^{+2\gamma_0 (d-D)} ,$$

$$F_{TE}^{(a)} = (1 + \rho_{-1TE})/(1 - \rho_{-1TE}\rho_{1TE}) ,$$

$$F_{TE}^{(b)} = (1 - \rho_{-1TE})/(1 - \rho_{-1TE}\rho_{1TE}) ,$$

$$\rho_{1TE} = [(Z_1 - Z_0)/(Z_1 + Z_0)] \, e^{-2\gamma_0 d} ,$$

$$\rho_{-1TE} = [(Z_{-1} - Z_0)/(Z_{-1} + Z_0)] \, e^{+2\gamma_0 (d-D)} ,$$

$$Y_n = (\sigma_n + i\omega\varepsilon_n)/\gamma_n ,$$

$$Z_n = i\omega\mu_0/\gamma_n ,$$

$$\gamma_n^2 = \lambda^2 + k_n^2 ,$$

$$k_n^2 = \omega^2 \mu_n \varepsilon_n - i\omega\mu_n\sigma_n \ ,$$

ε_n, σ_n = permittivity and electrical conductivity in region n, and

$$\mu_0 = 4\pi \times 10^{-7} \text{ H/m} \ .$$

Note that the expression for ρ_{-1TE} differs from the one given by Bubenik and Fraser-Smith [1978] and by Fraser-Smith and Bubenik [1979]. The correct form of this expression is the one given here; this correct form was also used in our earlier computations, but it was reported incorrectly owing to a copy error.

The equations listed above are valid at all frequencies. In our computations, however, we use the quasi-static approximation [e.g., Kraichman, 1976], which is equivalent to neglecting most displacement current terms. Thus, with the exception of the $i\omega\mu_0\varepsilon_1$ factor multiplying the expression for the magnetic field component B_ϕ produced by the VED, we set $\varepsilon_1 = \varepsilon_0 = \varepsilon_{-1} = 0$. This is a commonly used approximation, and it is applicable when the source-receiver distance is much smaller than a free space wavelength. Use of this approximation clearly implies a restriction on the frequency range over which our computations are valid. It was partly for this reason that we restricted the frequency range of applicability of the data derived in our earlier work either to frequencies between 0.1 and 100 Hz [Fraser-Smith and Bubenik, 1976] or to frequencies less than about 300 Hz [Bubenik and Fraser-Smith, 1978; Fraser-Smith and Bubenik, 1979]. More important, the restrictions were prompted by the fact that the specified frequency ranges were likely to be the most useful in practice for undersea-to-air and undersea-to-undersea communication and for undersea detection. However, because of their possible use at frequencies above 300 Hz, we now point out that the data in this report and in the Bubenik and Fraser-Smith [1978] and Fraser-Smith and Bubenik [1979] articles are valid throughout the ELF and VLF ranges, i.e., they are valid up to frequencies as high as 30 kHz.

The actual validity of the parametric data depends specifically on the applicability of the quasi-static approximation at the largest

source-receiver distances. In this report, and in the last two articles cited, the largest source-receiver distance is only a little greater than 100 seawater skin depths (specifically, the greatest source-receiver distance occurs when d = 3δ, h = 10δ, and r = 100δ, and the distance is 100.84δ). Assuming that "much smaller" than a free space wavelength means less than one tenth of a wavelength, the data in Table 2 show that in our case the quasi-static approximation begins to lose validity at frequencies above about 30 kHz.

As in our earlier work we evaluated the full field expressions numerically, using the techniques described by Bubenik [1977]. We set $\sigma_1 = 0$, and both the magnetic dipole moment m and the electric dipole moment p are set equal to unity (m = 1 Am^2, and p = 1 Am). For dipoles of arbitrary moment the field values given in the figures should be multiplied by the moment to obtain the corresponding field magnitudes. We use the milligamma as our unit for the magnetic field (1 mγ = 1 picotesla), and the electric field data are presented in units of microvolts/meter.

Table 2. Comparison of the free space wavelength (λ_1) with one hundred times the seawater skin depth (100δ) for various frequencies in the range 0.1-30 kHz. Seawater is assumed to have a conductivity of 4.0 S/m.

Frequency (kHz)	100δ (km)	λ_1 (km)	$\lambda_1/100\delta$
0.1	2.52	3000	1190
0.3	1.45	1000	690
1	0.80	300	375
3	0.46	100	217
10	0.25	30	120
30	0.15	10	67

III. RESULTS

Our results consist of amplitude data for the radial and vertical components E_r and E_z, the total electric field E_{TOTAL}, and the total magnetic field B_{TOTAL} (which also represents the azimuthal magnetic field component B_ϕ) produced by the VED. We also present data for the three electric field components (E_r, E_ϕ, E_z), three magnetic field components (B_r, B_ϕ, B_z), total magnetic field B_{TOTAL}, and total electric field E_{TOTAL} produced by the submerged HED and HMD at the two principal azimuthal angles $\phi = 0°$ and 90°. Because of the sin ϕ and cos ϕ terms appearing in the equations for the field components produced by the two horizontal dipoles (Equations 5-16), only one of the horizontal electric components (E_r and E_ϕ) and one of the horizontal magnetic components (B_r and B_ϕ) are produced by each of the dipoles when $\phi = 0°$ or 90°. The vertical fields vanish at one or the other of these angles. The notation we use for these nonzero components is $E_{HORIZONTAL}$ and $B_{HORIZONTAL}$. Whether these components are radial or azimuthal can be determined quickly by noting the azimuthal angle and by referring to Equations 5-16. Alternatively, the form of the horizontal components can be determined by reference to the following list of nonzero magnetic and electric field quantities produced by each dipole type.

VMD: B_r, B_z, E_ϕ; B_{TOTAL}, $E_{TOTAL} = E_\phi$.

VED: B_ϕ, E_r, E_z; $B_{TOTAL} = B_\phi$, E_{TOTAL}.

HED, $\phi = 0°$: B_ϕ, E_r, E_z; $B_{TOTAL} = B_\phi$, E_{TOTAL}, $E_{HORIZONTAL} = E_r$.

HED, $\phi = 90°$: B_r, B_z, E_ϕ; B_{TOTAL}, $B_{HORIZONTAL} = B_r$, $E_{TOTAL} = E_\phi$.

HMD, $\phi = 0°$: B_r, B_z, E_ϕ; B_{TOTAL}, $B_{HORIZONTAL} = B_r$, $E_{TOTAL} = E_\phi$.

HMD, $\phi = 90°$: B_ϕ, E_r, E_z; $B_{TOTAL} = B_\phi$, $E_{HORIZONTAL} = E_r$, E_{TOTAL}.

Note that for each dipole category there are only three basic magnetic and electric field components.

The presentation of the new field data is very similar to the one used for the results of our VMD computations [Fraser-Smith and Bubenik, 1979]. First, we present a series of curves that give the actual fields produced by a particular unit moment dipole when submerged in a sea of infinite depth. Next, we present additional curves that give the ratios of the fields produced by the dipole in a sea of finite depth D to the fields produced under otherwise identical conditions by the dipole submerged in the sea of infinite depth. These latter curves show clearly any seafloor effect that is present, since the absence of a seafloor effect is indicated by a ratio of 1.0. The curves for the infinitely deep sea are presented for three receiver heights (h/δ = 0, 1, and 10) and for four dipole depths (d/δ = 0.1, 0.3, 1.0, and 3.0). These data are then supplemented by the seafloor effect curves, which are drawn for four sea depths (D/δ = 0.1, 0.3, 1.0, and 3.0). Finally, to illustrate the effect of a change in the seafloor electrical conductivity, we consider two seafloor conductivities $\sigma_s = 0.1\ \sigma_f$ and $0.01\ \sigma_f$, where we write $\sigma_0 = \sigma_s$ (for seawater electrical conductivity), and $\sigma_{-1} = \sigma_f$ (for seafloor electrical conductivity). The subscript has been dropped from σ_s when this conductivity appears in the ordinate labels.

The field data are presented in the following figures.

VED: Figures 2-15.

HED, $\phi = 0°$: Figures 16-29.

HED, $\phi = 90°$: Figures 30-43.

HMD, $\phi = 0°$: Figures 44-57.

HMD, $\phi = 90°$: Figures 58-71.

The same basic arrangement of figures is used for each dipole category.

IV. DISCUSSION

At horizontal distances greater than 10δ the curves for the fields produced by the dipoles in an infinitely deep sea begin to decrease linearly (see Figures 2, 3 [VED]; 16, 17 [HED, $\phi = 0°$]; 30, 31 [HED, $\phi = 90°$]; 44, 45 [HMD, $\phi = 0°$]; 58, 59 [HMD, $\phi = 90°$]). Because of our use of logarithmic scales, the linear decline implies a power law decrease of the fields with distance. Further, because the slopes of the linear portions of the curves are not all the same, our data indicate that the dipole fields for $r > 10\delta$ decrease with distance as r^{-n}, where the power n depends both on the dipole type and on the electric or magnetic field component under consideration. Since distance is an important factor in any communication or detection application of these data, we will examine the range of values assumed by n.

As previously described by Fraser-Smith and Bubenik [1979], the total magnetic and electric fields for the VMD had $n = 4$, and the two magnetic field components B_r and B_z for this dipole had $n = 4$ and 5, respectively. These values of n, together with the values of n derived from our new data, are listed in Table 3. It can be seen than n ranges from 5, implying a very rapid decline of the field quantity with distance, down to 2, implying a comparatively slow variation of the field quantity with distance. These powers of n are all consistent with the distance variations in the approximate expressions for the fields tabulated by Kraichman [1976] for large source-receiver distances.

Examining the field quantities with $n = 2$ in greater detail, we observe that they are B_ϕ (or, equivalently, B_{TOTAL}) for the VED; E_z (or, equivalently, E_{TOTAL}) for the HED, $\phi = 0°$; and E_z (or, equivalently, E_{TOTAL}) for the HMD, $\phi = 90°$. Although these three components would appear to have equivalent potential for long distance communication, we can dismiss the B_ϕ component because, as is clearly shown by the data in Figure 2, its amplitude is always very small. To illustrate, assuming $r/\delta = 100$, $h = 0$, and $d = 0.1$, we have $B_\phi \times \delta^4\sigma_s^2 = 0.255 \times 10^{-3}$ mγ $\times$ m^{2}S^2, or $B_\phi = 3.98 \times 10^{-15}$ mγ at 1 Hz, for a unit moment

Table 3. Values of the power n occurring in the long distance variation r^{-n} observed in the fields produced by each dipole. An asterisk indicates that no field component is produced.

	VMD	VED	HED, $\phi = 0°$	HED, $\phi = 90°$	HMD, $\phi = 0°$	HMD, $\phi = 90°$
B_{TOTAL}	4	2	3	3	3	3
E_{TOTAL}	4	3	2	3	3	2
B_r	4	*	*	3	3	*
B_ϕ	*	2	3	*	*	3
B_z	5	*	*	4	4	*
E_r	*	4	3	*	*	3
E_ϕ	4	*	*	3	3	*
E_z	*	3	2	*	*	2

VED. Under the same conditions, a unit moment HED ($\phi = 0°$) would give $B_\phi \times \delta^2 = 0.128$ m$\gamma \times m^2$, or $B_\phi = 2.0 \times 10^{-6}$ mγ (Figure 16). These results apply to an infinitely deep sea; in a sea of finite depth the B_ϕ amplitudes for the VED are reduced even further, as shown by the data in even-numbered Figures 4,...14. (The B_ϕ amplitudes for the HED, $\phi = 0°$, are mostly increased by the presence of a seafloor.)

Comparing the E_z components produced by the HED, $\phi = 0°$, and the HMD, $\phi = 90°$, for an infinitely deep sea and for the configuration $r = 100\delta$, $d = 0.1\delta$, and $h = 0$, we find (a) for the HED, $\phi = 0°$, $E_z \times \delta^3\sigma = 0.204 \times 10^2$ μV/m $\times m^2$S, or $E_z = 3.20 \times 10^{-7}$ μV/m at 1 Hz (Figure 17), and (b) for the HMD, $\phi = 90°$, $E_z \times \delta^4\sigma = 0.288 \times 10^2$ μV/m $\times m^3$S, or $E_z = 1.80 \times 10^{-9}$ μV/m at 1 Hz (Figure 59). This comparison is made for unit moment dipoles, of course. Without consideration of the possibility that there may be practical reasons for preferring an HMD source to an HED, it appears from this comparison that using the vertical electric field produced by an HED source in the $\phi = 0°$ plane would be preferable for long distance communication to reception of the vertical electric field produced in the $\phi = 90°$ plane by an HMD. In a sea of finite depth, our data show that the seafloor effects for E_z are predominantly positive (i.e., enhancements occur) for the HED ($\phi = 0°$), whereas the effects are predominantly negative for the HMD ($\phi = 90°$); these results therefore lend additional support to the above conclusion.

As we saw in the case of the B_ϕ component produced by the VED, it is possible to have an r^{-2} distance variation in a component, but still not to have sufficiently large amplitudes for measurements of the component to be useful in comparison to measurements of some other dipole component with a more rapid decline of amplitude with distance. Comparing the amplitudes of the E_z component produced at large distances by the HED, $\phi = 0°$, with the amplitudes of all the other electric field components considered in this work, we find that under the same conditions in an infinitely deep sea the HED, $\phi = 0°$, component is larger in all cases. With the possible exception of the electric field components produced by the VED in a sea of finite depth, which will shortly be discussed, it appears unlikely that seafloor effects can produce

significant changes in this situation. We conclude, therefore, that the E_z field produced by an HED ($\phi = 0°$) source is likely to be the most attractive electric field component for possible long distance undersea-to-air communication or for undersea detection.

Because of the great difference between magnetic field and electric field sensors, a comparison similar to those above of the possible advantages or disadvantages of magnetic field measurements versus electric field measurements is beyond the scope of this work.

Finally, we wish to point out the large seafloor effects that occur for the E_r component and, to a lesser extent, for the E_z component produced by the VED. Under certain conditions, the E_r component can be increased by nearly six orders of magnitude (Figure 7; note the expanded ordinate scale in this figure and in Figure 5). None of the other electric or magnetic field components considered in this work are affected similarly; at most, enhancements or reductions of the field amplitudes by up to two orders of magnitude are observed. The E_z component is mostly reduced at short distances ($r/\delta < 1$) and is largely unaffected at large distances ($r/\delta > 10$), whereas the E_r component tends also to be reduced at short distances before being enhanced at large distances. The total electric field, reflecting this behavior as well as the differences in amplitudes of the two field components (Figure 3), is somewhat more stable than its components, but also exhibits a moderately large seafloor effect.

Although it may not immediately appear to be true in the case of the VED, all the criteria developed in our VMD study [Fraser-Smith and Bubenik, 1979] for estimating when seafloor effects are most likely to occur are valid for all the other dipole categories. Thus, for each of the VMD, VED, HED, and HMD sources, we have the following criteria: (1) the seafloor effects are most marked in seas that are electrically shallow, (2) the largest changes in the fields occur when the dipole is located within one seawater skin depth (δ) of the seafloor, and (3) there is essentially no seafloor effect when the dipole is located more than 3δ above the floor. The seafloor effects for the VED differ from the effects for the other dipoles only in their scale, not in the

applicability of our criteria (1)-(3). In particular, criterion (2) appears to be most important for the VED, with the largest seafloor effects occurring when the dipole is located on the floor.

V. REFERENCES

Bannister, P. R., "Determination of the electrical conductivity of the sea bed in shallow waters," Geophysics, 33, 995-1003, 1968.

Brock-Nannestad, L., "Determination of the electric conductivity of the seabed in shallow waters with varying conductivity profile," Electron. Letters, 1, 274-276, 1965.

Bubenik, D. M., "A practical method for the numerical evaluation of Sommerfeld integrals," IEEE Trans. Ant. Prop., AP-25, 904-906, 1977.

Bubenik, D. M., and A. C. Fraser-Smith, "ULF/ELF electromagnetic fields generated in a sea of finite depth by a submerged vertically-directed harmonic magnetic dipole," Radio Sci., 13, 1011-1020, 1978.

Coggon, J. H., and H. F. Morrison, "Electromagnetic investigation of the sea floor," Geophysics, 35, 476-489, 1970.

Fraser-Smith, A. C., and D. M. Bubenik, "ULF/ELF magnetic fields generated at the sea surface by submerged magnetic dipoles," Radio Sci., 11, 901-913, 1976.

Fraser-Smith, A. C., and D. M. Bubenik, "ULF/ELF electromagnetic fields generated above a sea of finite depth by a submerged vertically-directed harmonic magnetic dipole," Radio Sci., 14, 59-74, 1979.

Kong, J. A., Theory of Electromagnetic Waves, 339 pp., Wiley-Interscience, New York, 1975.

Kraichman, M. B., Handbook of Electromagnetic Propagation in Conducting Media, Second Printing, U.S. Government Printing Office, Washington, D.C., 1976.

Morrison, H. F., F. J. Phillips, and D. P. O'Brien, "Quantitative interpretation of transient electromagnetic fields over a layered half space," Geophys. Prosp., 17, 82-101, 1969.

Figures for the

VERTICAL ELECTRIC DIPOLE

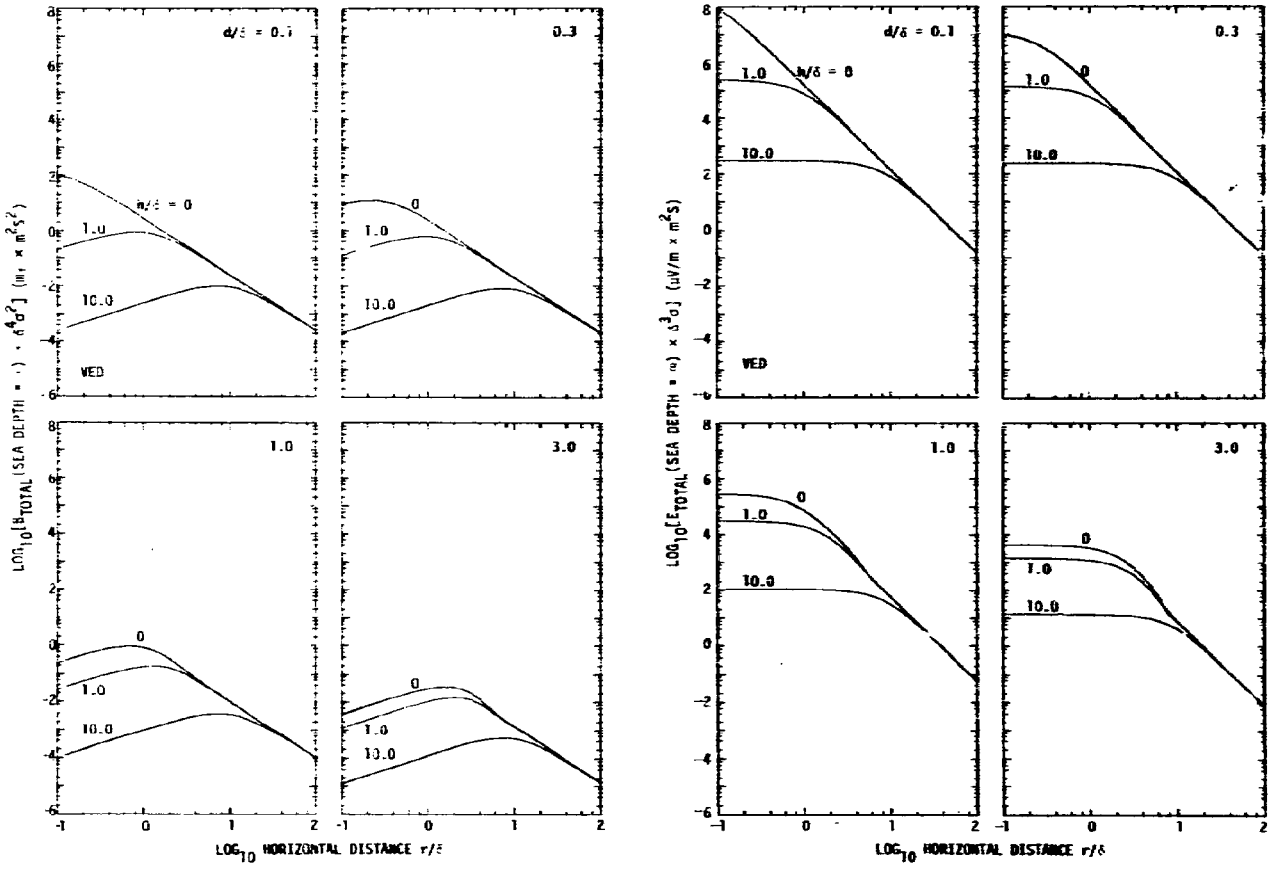

Figure 2. Variation with horizontal distance of the amplitudes of the total magnetic (B_{TOTAL}) and electric (E_{TOTAL}) fields produced on and above the surface of an infinitely deep sea by a submerged vertically directed harmonic electric dipole (VED).

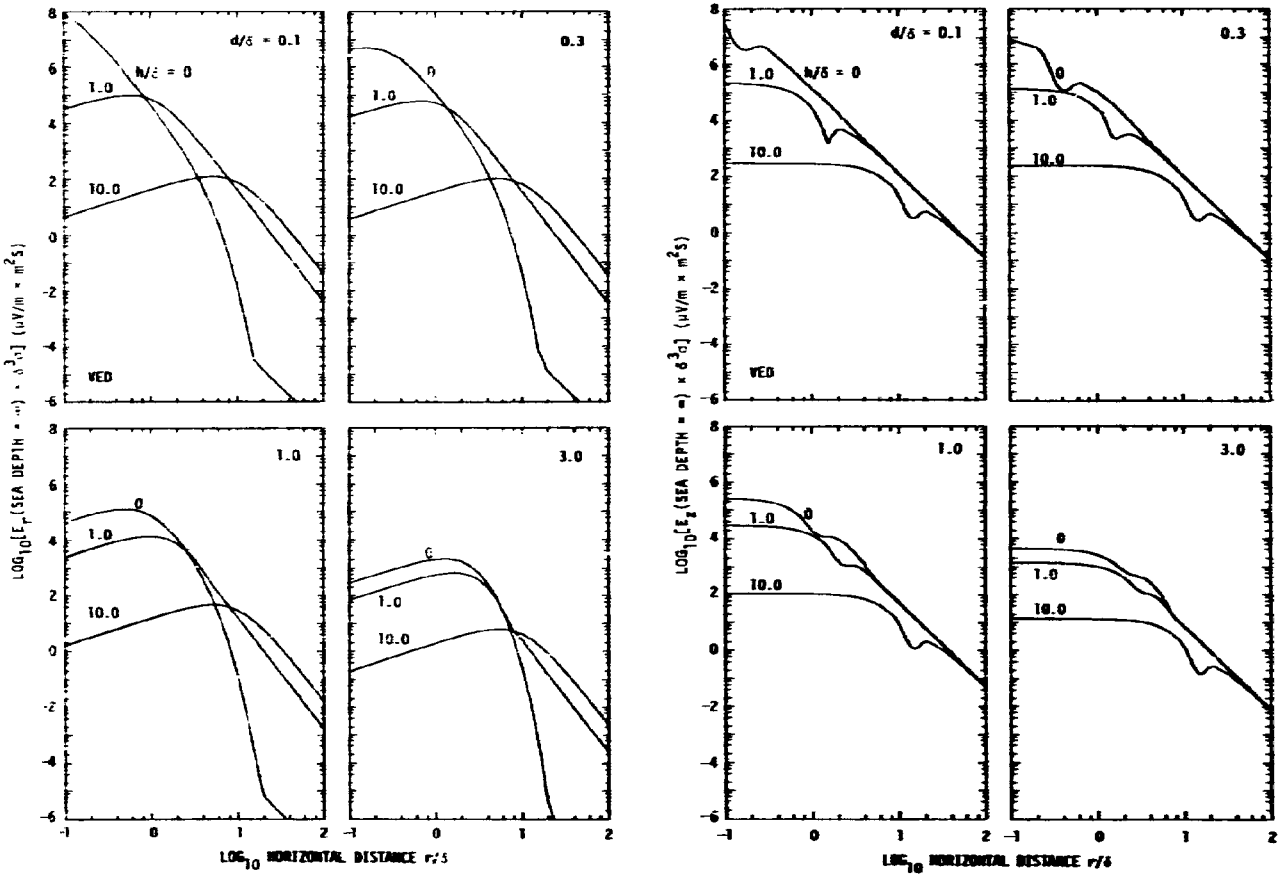

Figure 3. Variation with horizontal distance of the amplitudes of the two electric field components E_r and E_z produced on and above the surface of an infinitely deep sea by a submerged vertically directed harmonic electric dipole (VED).

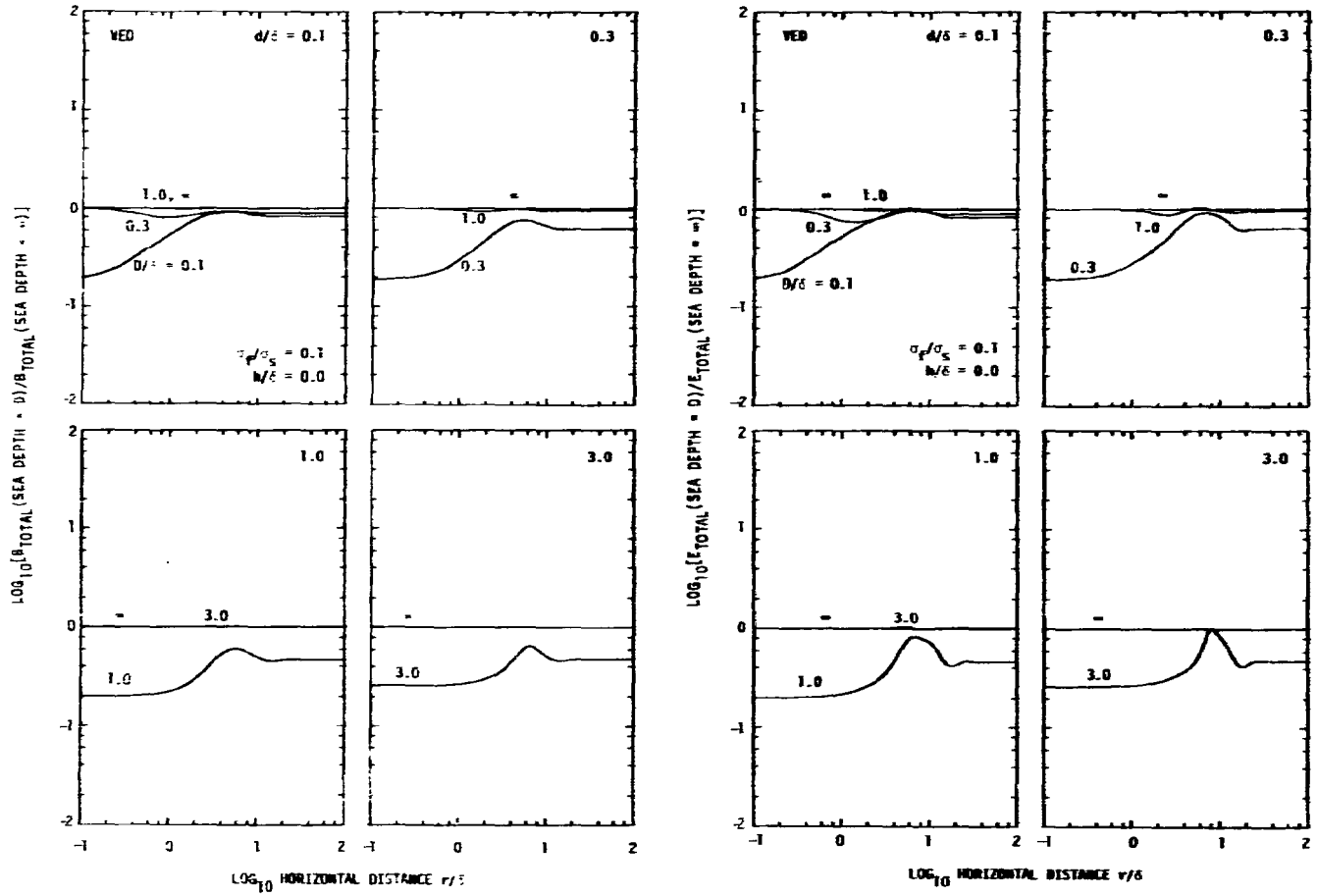

Figure 4. Curves illustrating the changes produced in the surface magnetic and electric field data presented in Figure 2 when an electrically conducting sea floor (conductivity $\sigma_f = 0.1\ \sigma_s$, depth D) is introduced.

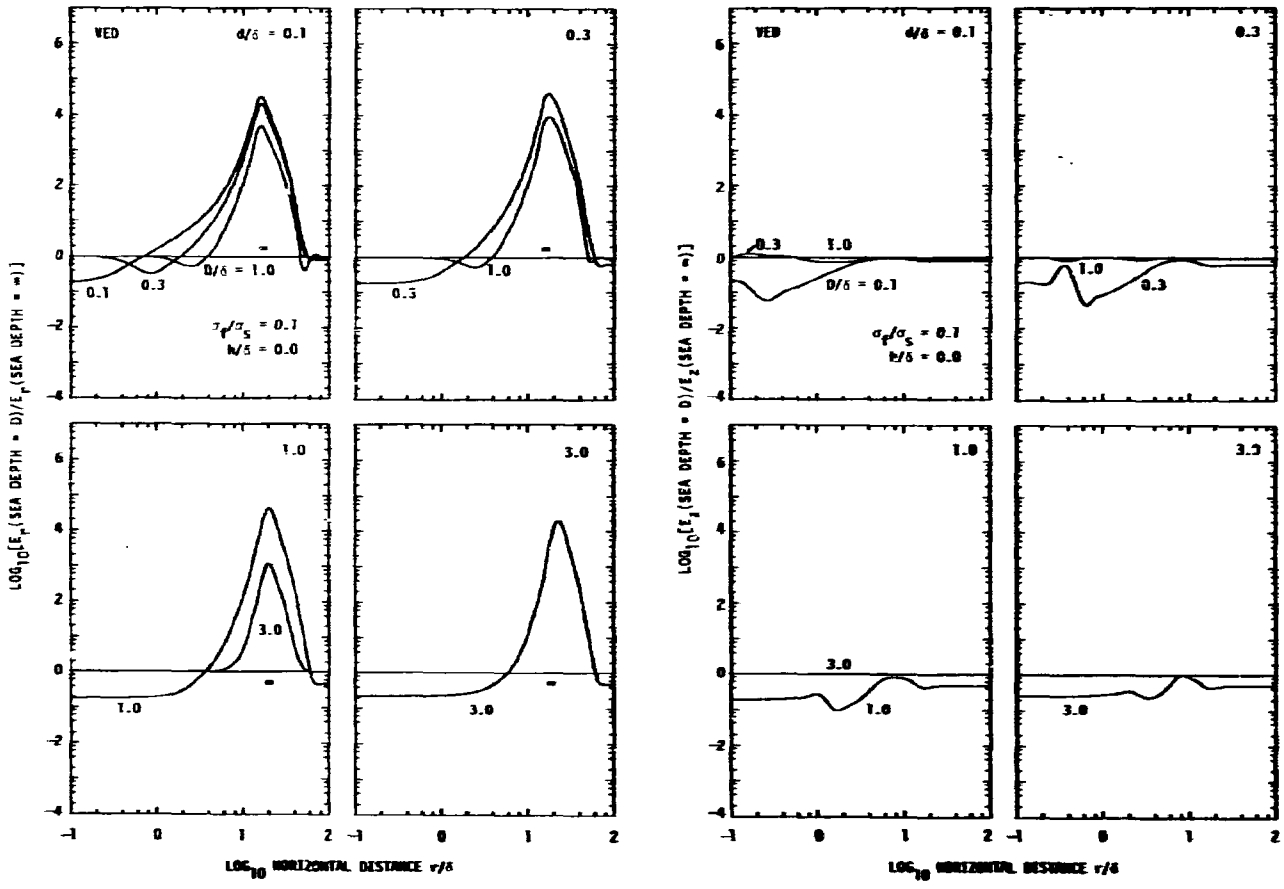

Figure 5. Curves illustrating the changes produced in the surface electric field component data presented in Figure 3 when an electrically conducting sea floor (conductivity $\sigma_f = 0.1\ \sigma_s$, depth D) is introduced.

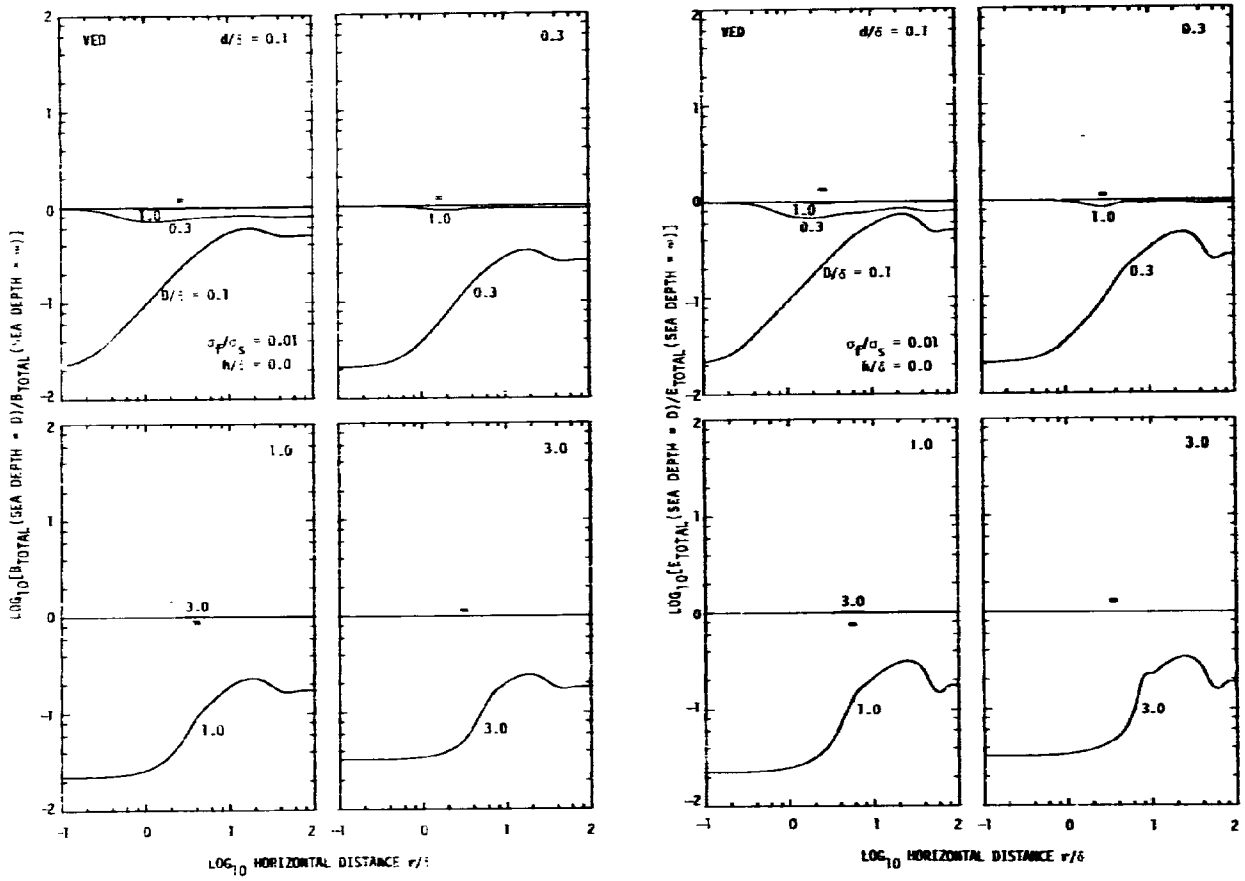

Figure 6. Curves illustrating the changes produced in the surface magnetic and electric field data presented in Figure 2 when an electrically conducting sea floor (conductivity σ_f = 0.01 σ_s, depth D) is introduced. The conductivity of this sea floor is one tenth the conductivity of the sea floor used in Figure 4.

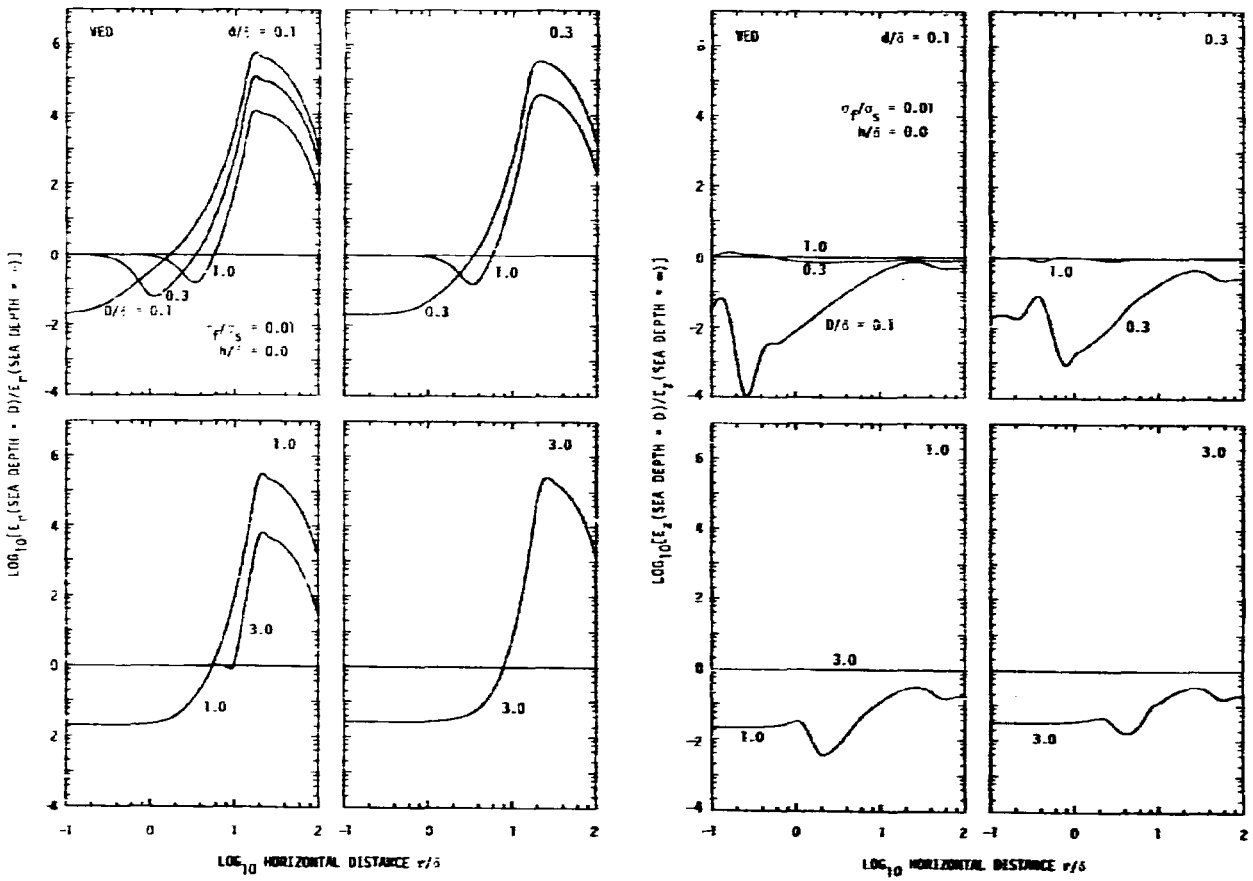

Figure 7. Curves illustrating the changes produced in the surface electric field component data presented in Figure 3 when an electrically conducting sea floor (conductivity $\sigma_f = 0.01\ \sigma_S$, depth D) is introduced. The conductivity of this sea floor is one tenth the conductivity of the sea floor used in Figure 5.

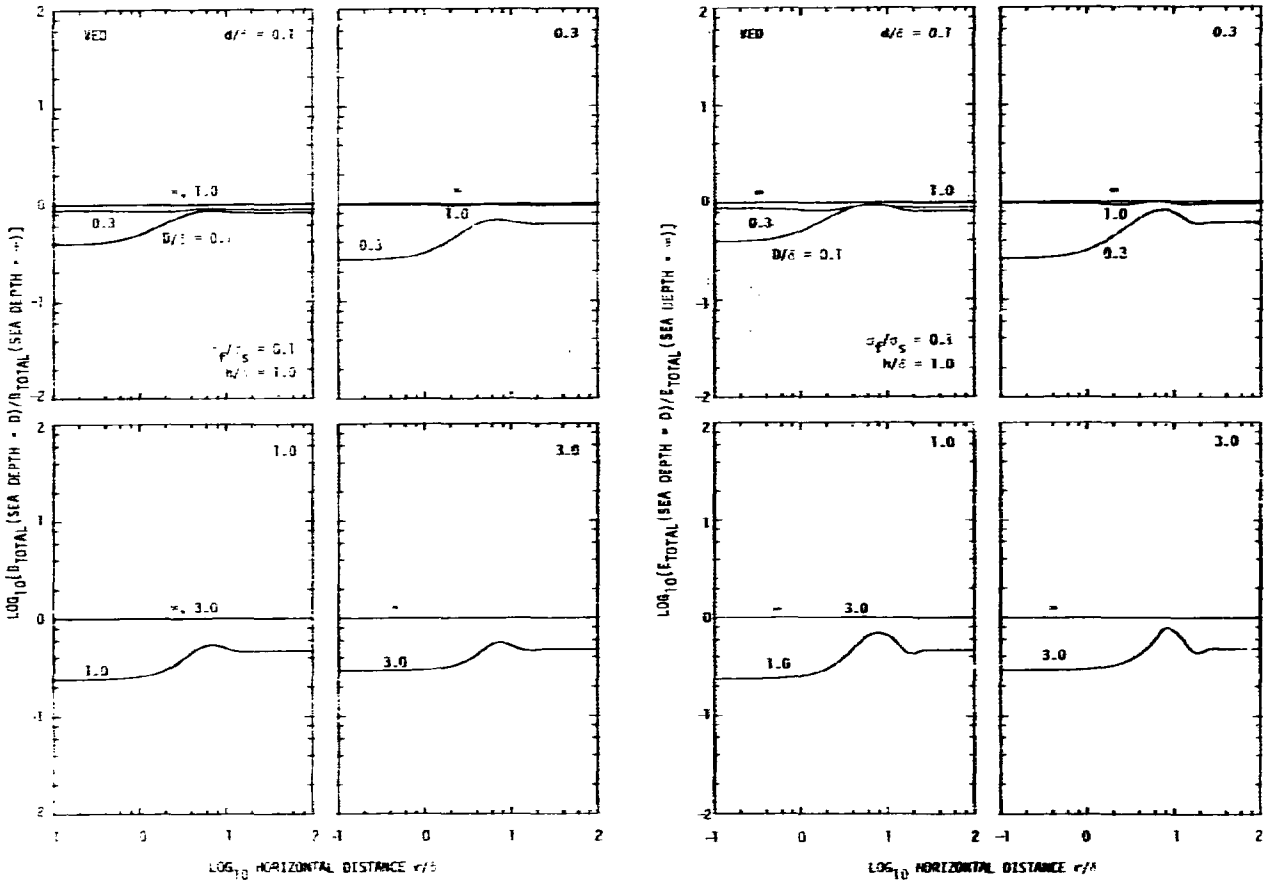

Figure 8. Curves illustrating the changes produced in the magnetic and electric field data presented in Figure 2 for a receiver altitude of one sea water skin depth ($h/\delta = 1.0$) when an electrically conducting sea floor (conductivity $\sigma_f = 0.1\ \sigma_s$, depth D) is introduced.

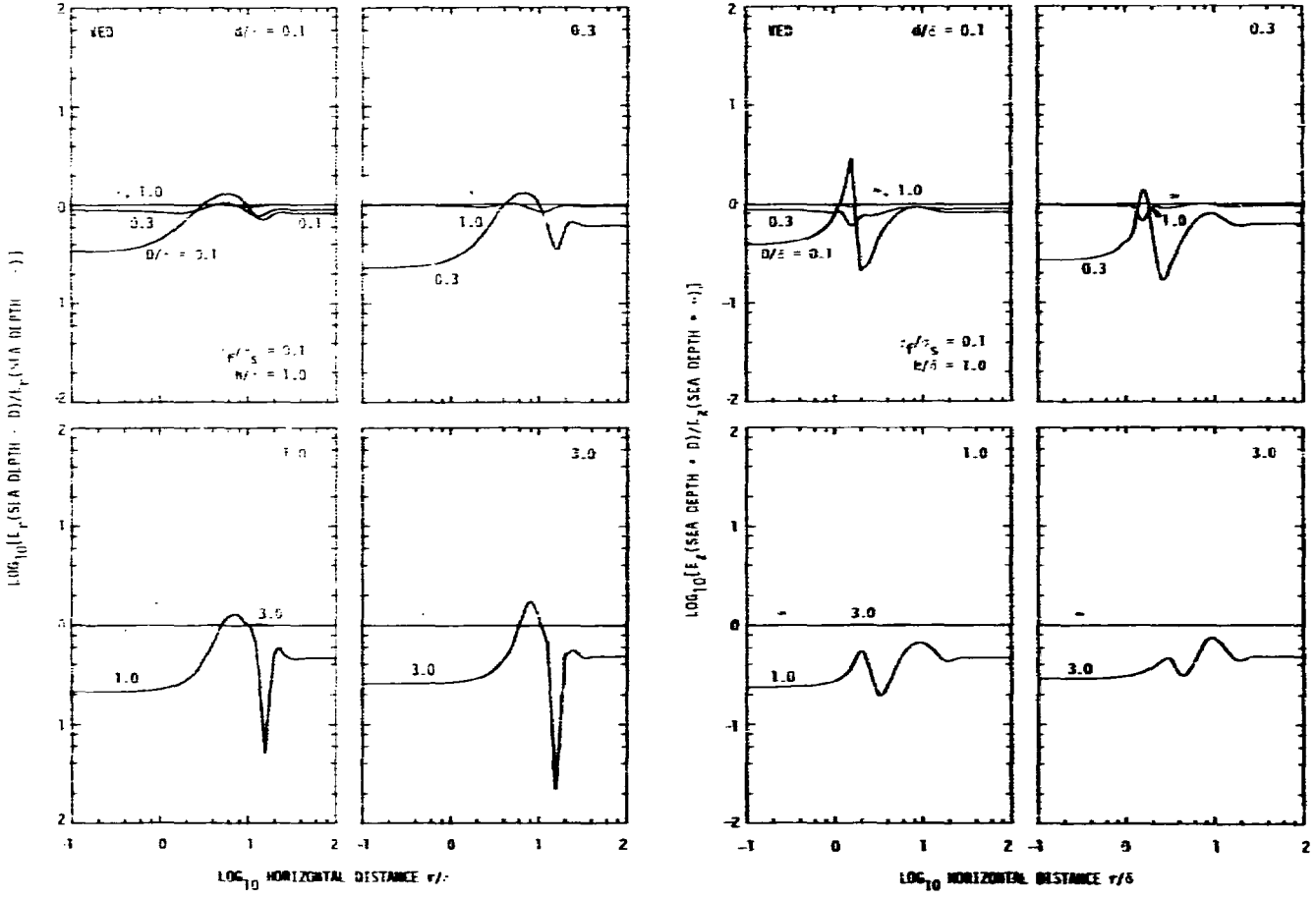

Figure 9. Curves illustrating the changes produced in the electric field component data presented in Figure 3 for a receiver altitude of one sea water skin depth ($h/\delta = 1.0$) when an electrically conducting sea floor (conductivity $\sigma_f = 0.1\ \sigma_s$, depth D) is introduced.

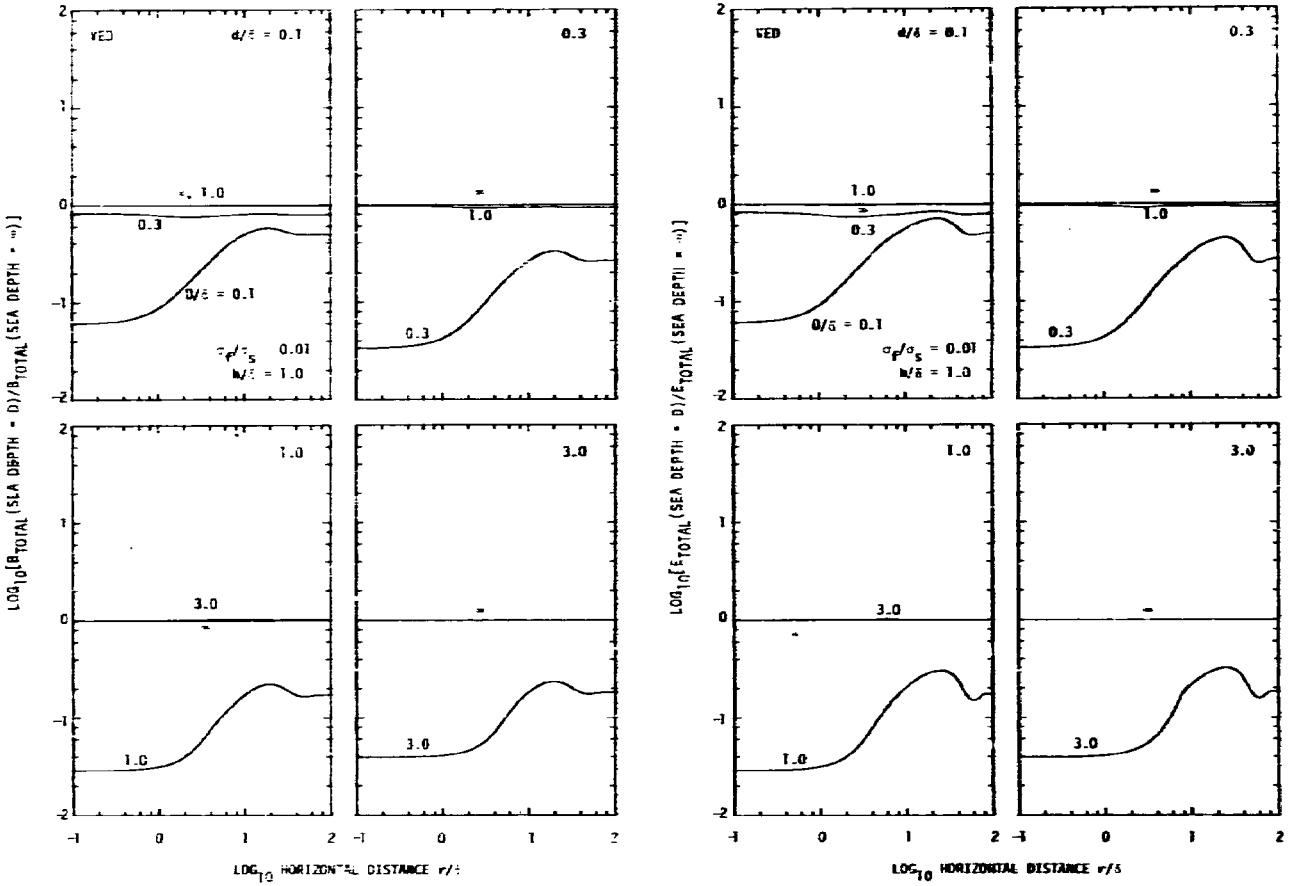

Figure 10. Curves illustrating the changes produced in the magnetic and electric field data presented in Figure 2 for a receiver altitude of one sea water skin depth ($h/\delta = 1.0$) when an electrically conducting sea floor (conductivity $\sigma_f = 0.01\ \sigma_s$, depth D) is introduced. The conductivity of this sea floor is one tenth the conductivity of the sea floor used in Figure 8.

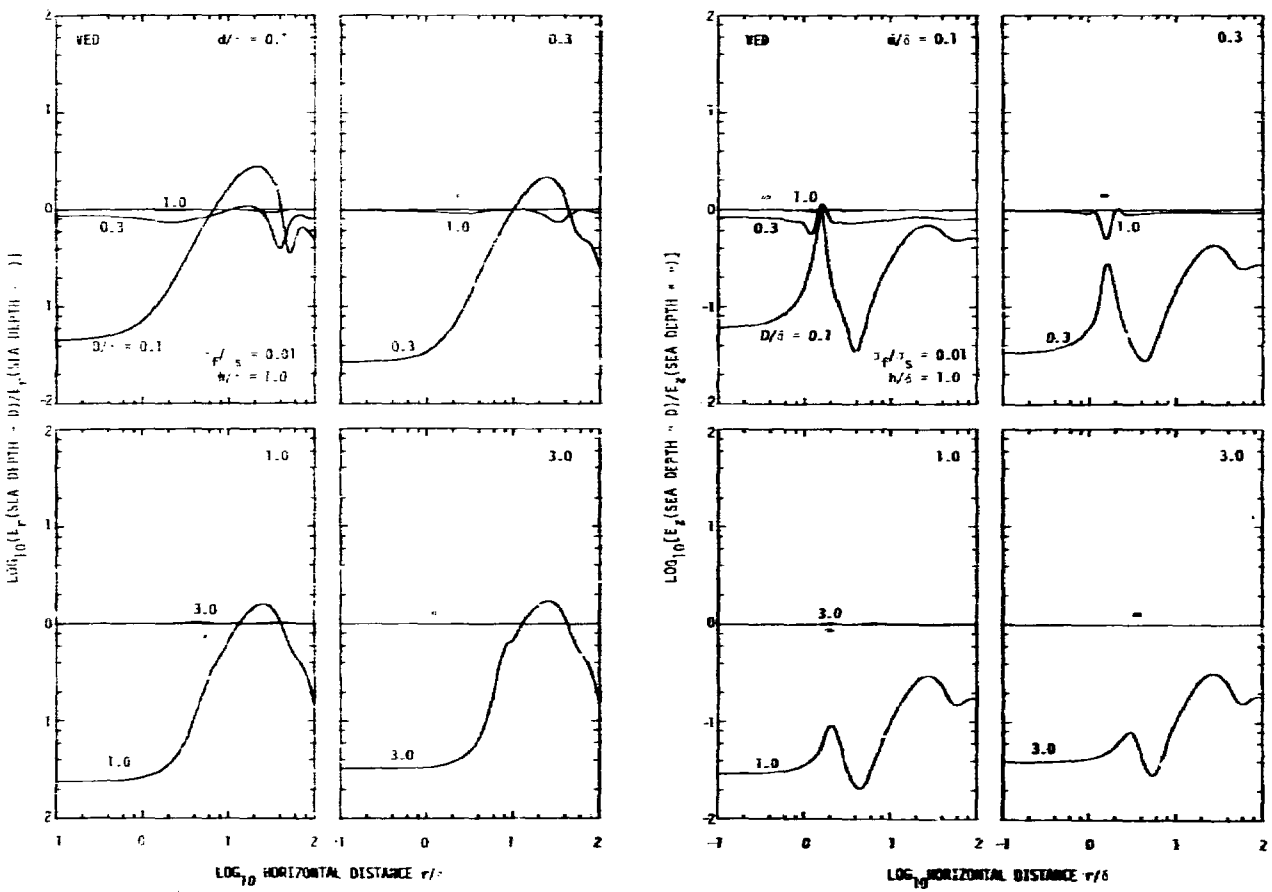

Figure 11. Curves illustrating the changes produced in the electric field component data presented in Figure 3 for a receiver altitude of one sea water skin depth ($h/\delta = 1.0$) when an electrically conducting sea floor (conductivity $\sigma_f = 0.01\ \sigma_S$, depth D) is introduced. The conductivity of this sea floor is one tenth the conductivity of the sea floor used in Figure 9.

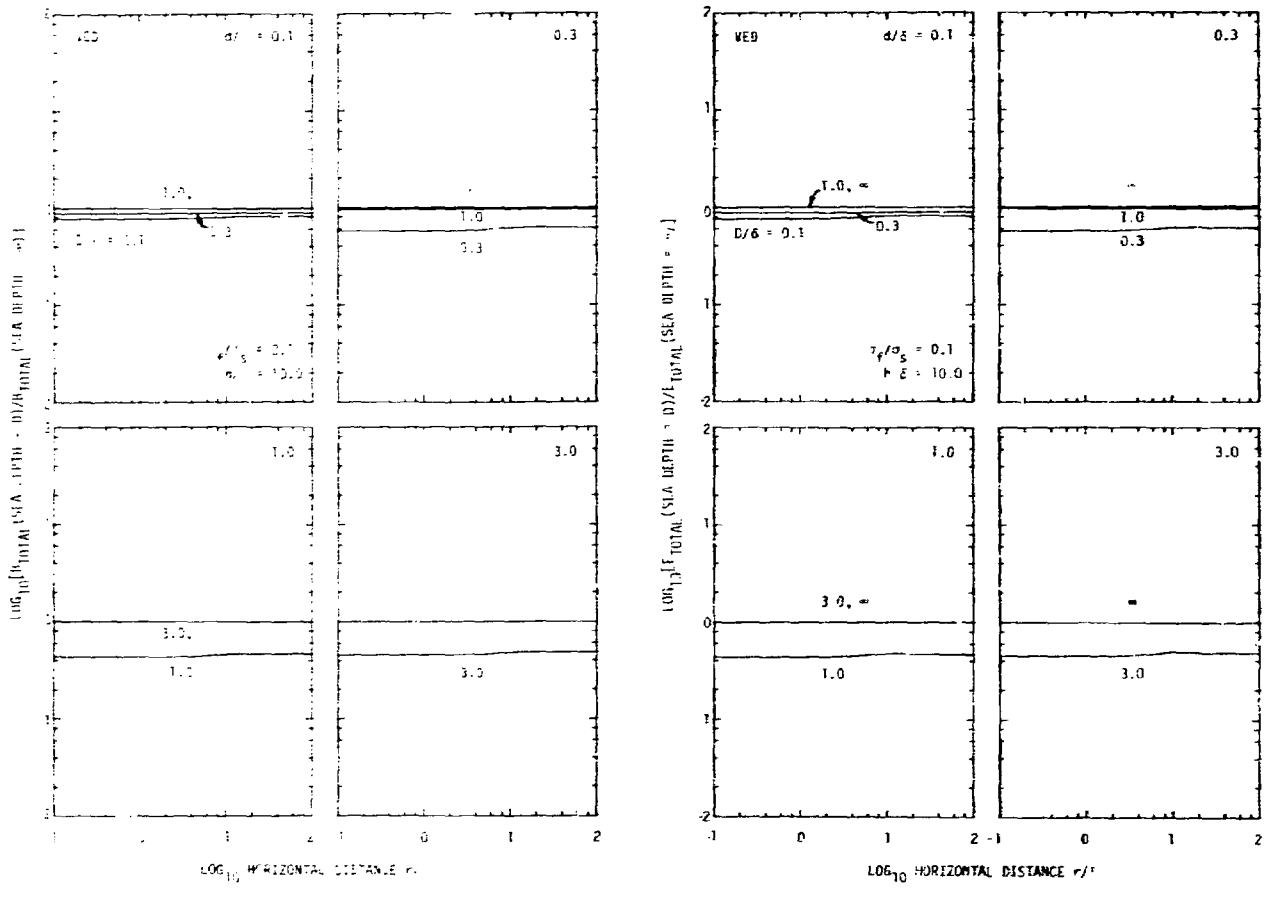

Figure 12. Curves illustrating the changes produced in the magnetic and electric field data presented in Figure 2 for a receiver altitude of ten sea water skin depths ($h/\delta = 10.0$) when an electrically conducting sea floor (conductivity $\sigma_f = 0.1\ \sigma_s$, depth D) is introduced.

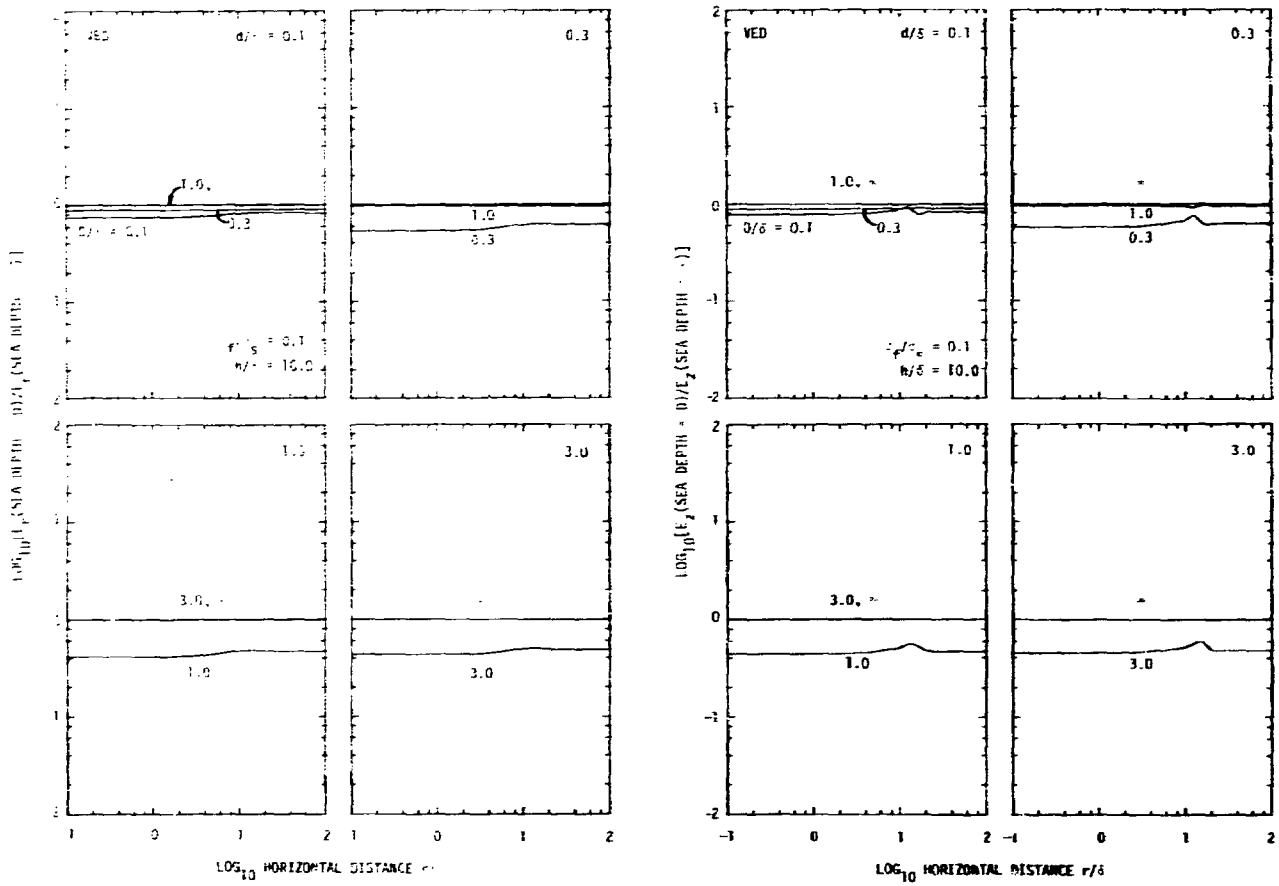

Figure 13. Curves illustrating the changes produced in the electric field component data presented in Figure 3 for a receiver altitude of ten sea water skin depths ($h/\delta = 10.0$) when an electrically conducting sea floor (conductivity $\sigma_f = 0.1\ \sigma_s$, depth D) is introduced.

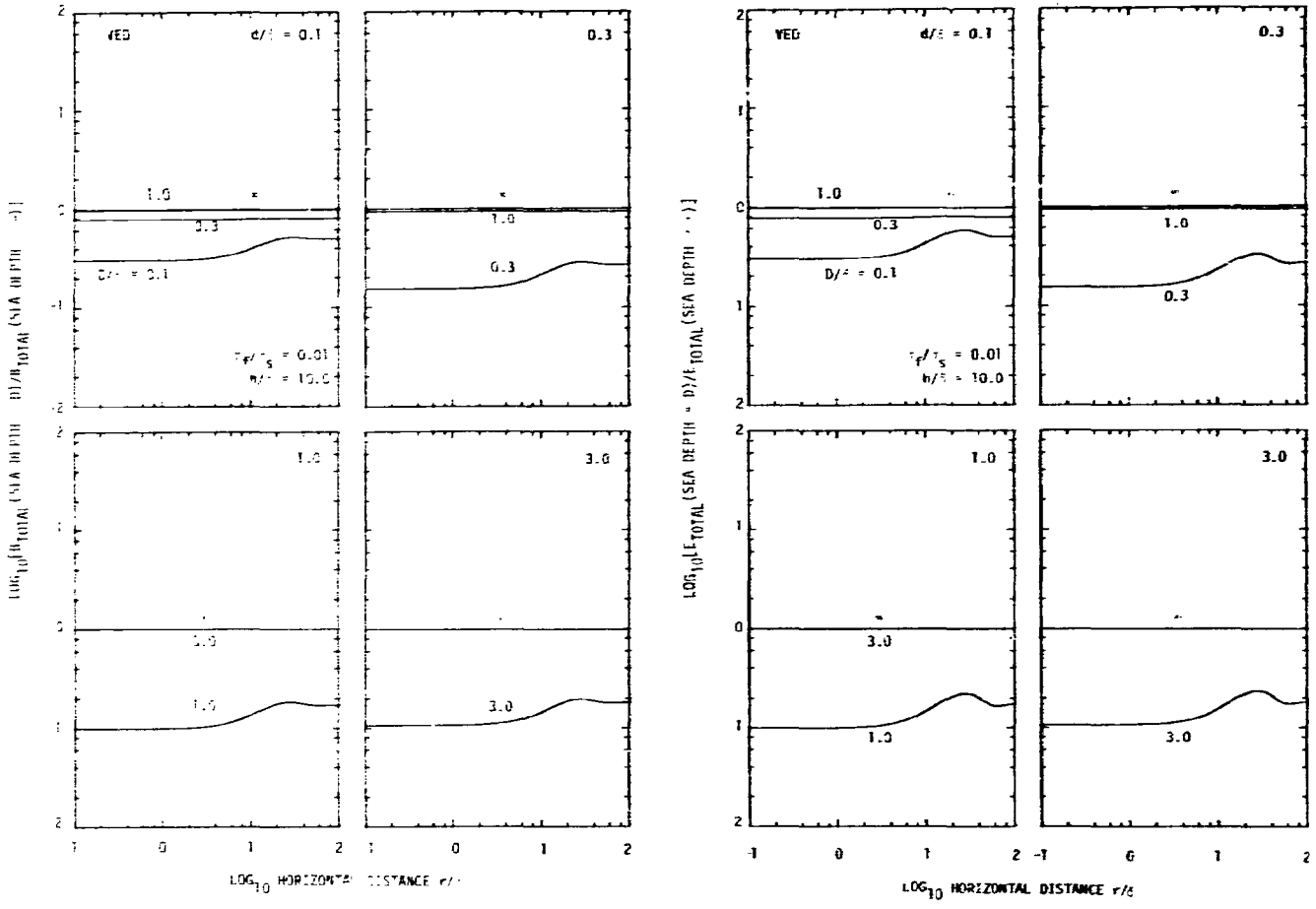

Figure 14. Curves illustrating the changes produced in the magnetic and electric field data presented in Figure 2 for a receiver altitude of ten sea water skin depths (h/δ = 10.0) when an electrically conducting sea floor (conductivity $\sigma_f = 0.01\ \sigma_s$, depth D) is introduced. The conductivity of this sea floor is one tenth the conductivity of the sea floor used in Figure 12.

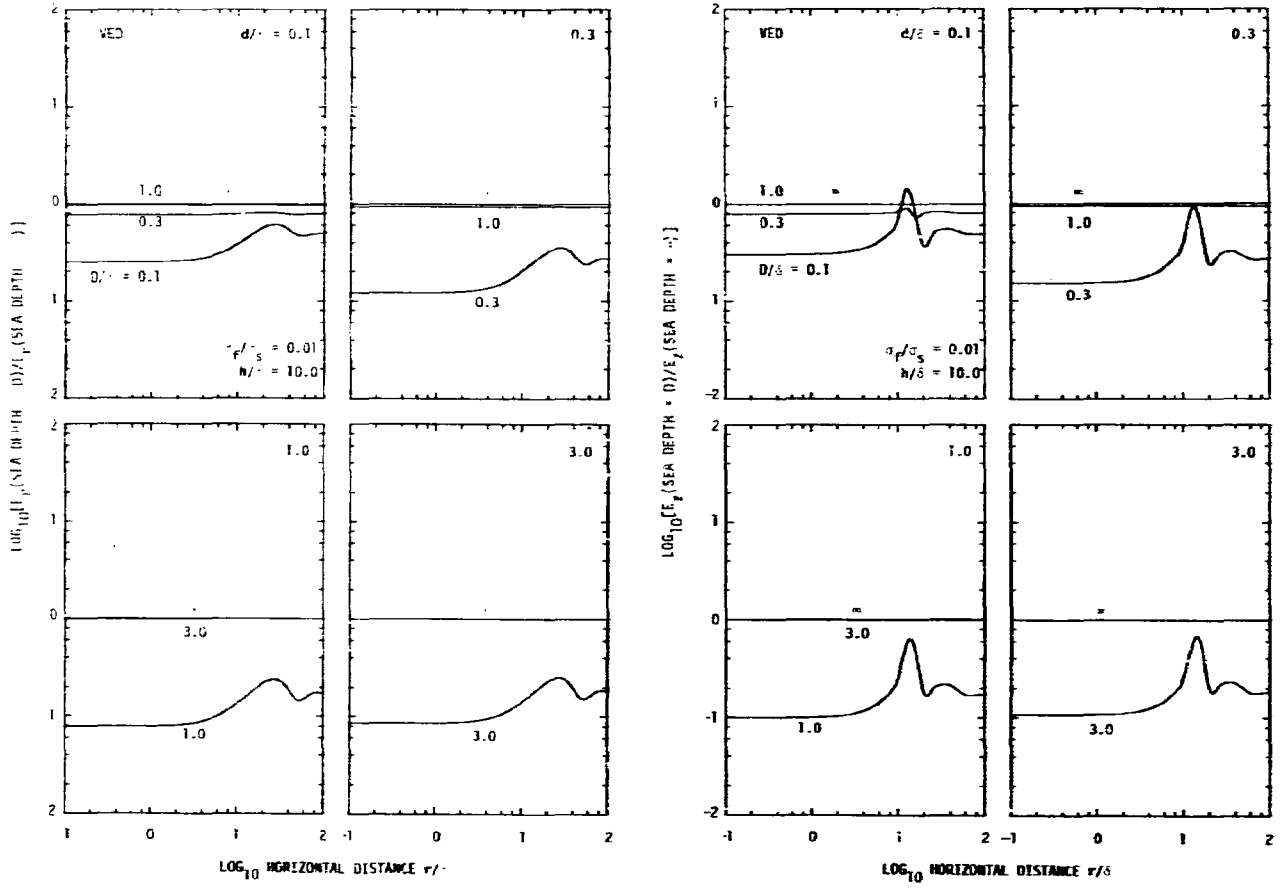

Figure 15. Curves illustrating the changes produced in the electric field component data presented in Figure 3 for a receiver altitude of ten sea water skin depths ($h/\delta = 10.0$) when an electrically conducting sea floor (conductivity $\sigma_f = 0.01\ \sigma_s$, depth D) is introduced. The conductivity of this sea floor is one tenth the conductivity of the sea floor used in Figure 13.

Figures for the

HORIZONTAL ELECTRIC DIPOLE, $\phi = 0°$

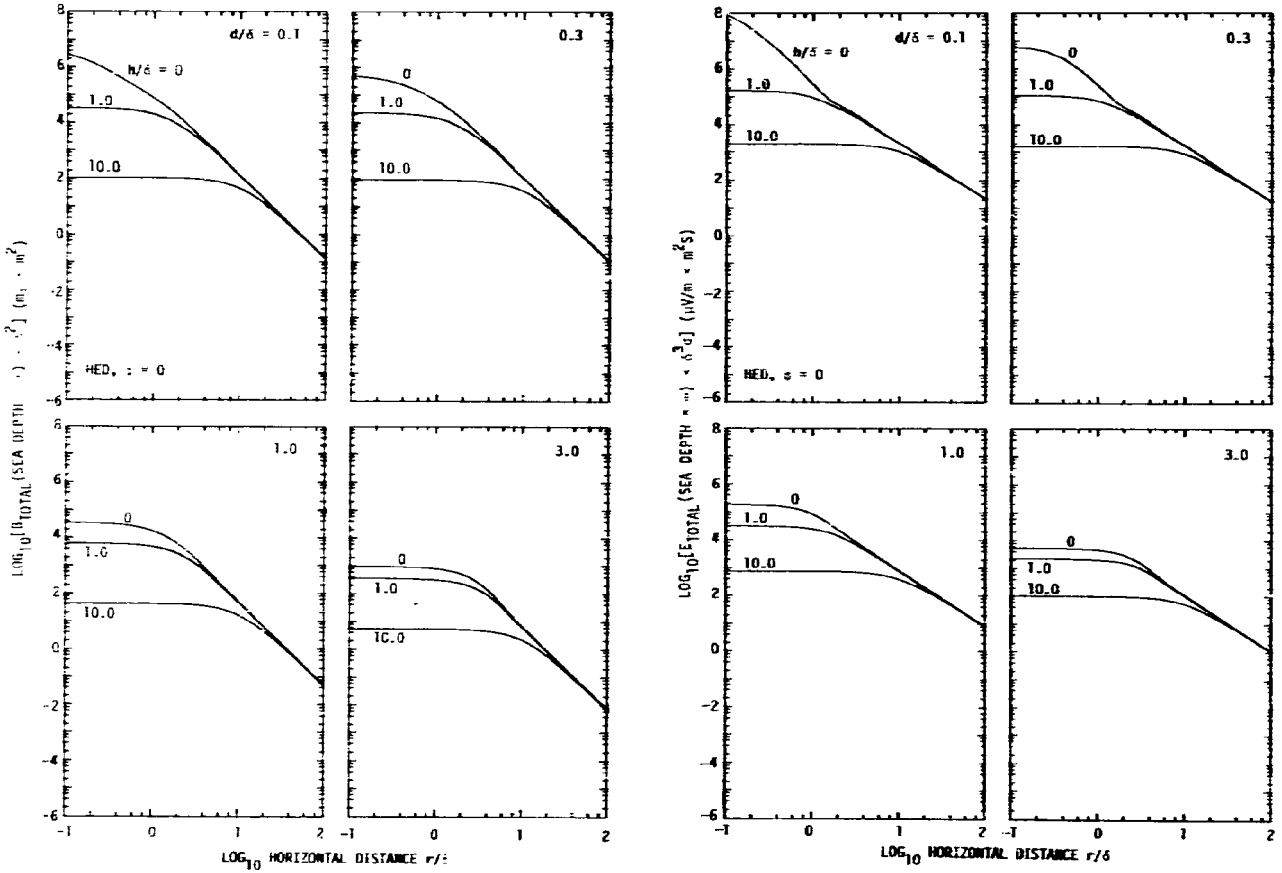

Figure 16. Variation with horizontal distance of the amplitudes of the total magnetic (B_{TOTAL}) and electric (E_{TOTAL}) fields produced on and above the surface of an infinitely deep sea by a submerged horizontally directed electric dipole (HED). The fields are given for an azimuthal angle (ϕ) of 0°.

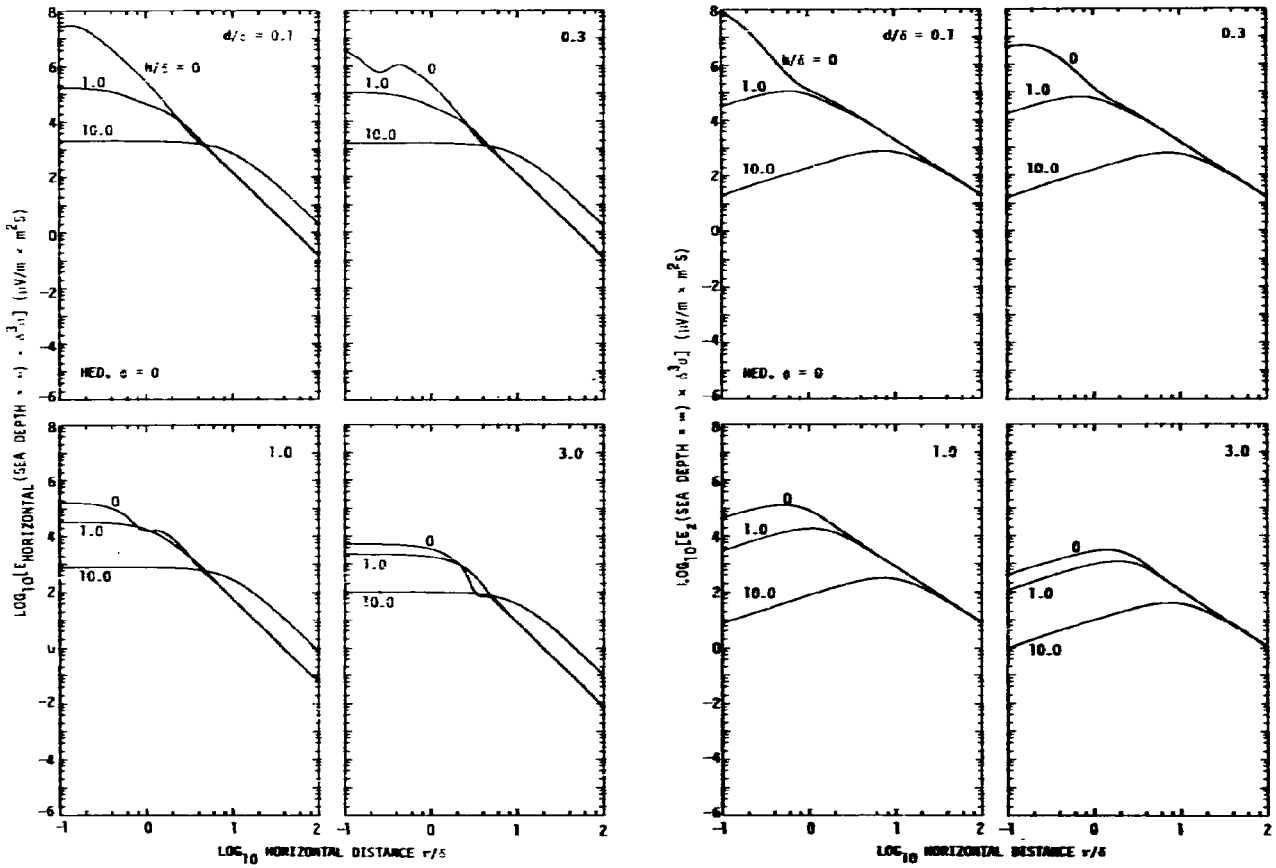

Figure 17. Variation with horizontal distance of the amplitudes of the two electric field components $E_{HORIZONTAL}$ and E_z produced on and above the surface of an infinitely deep sea by a submerged horizontally directed harmonic electric dipole (HED). The fields are given for an azimuthal angle (ϕ) of 0°.

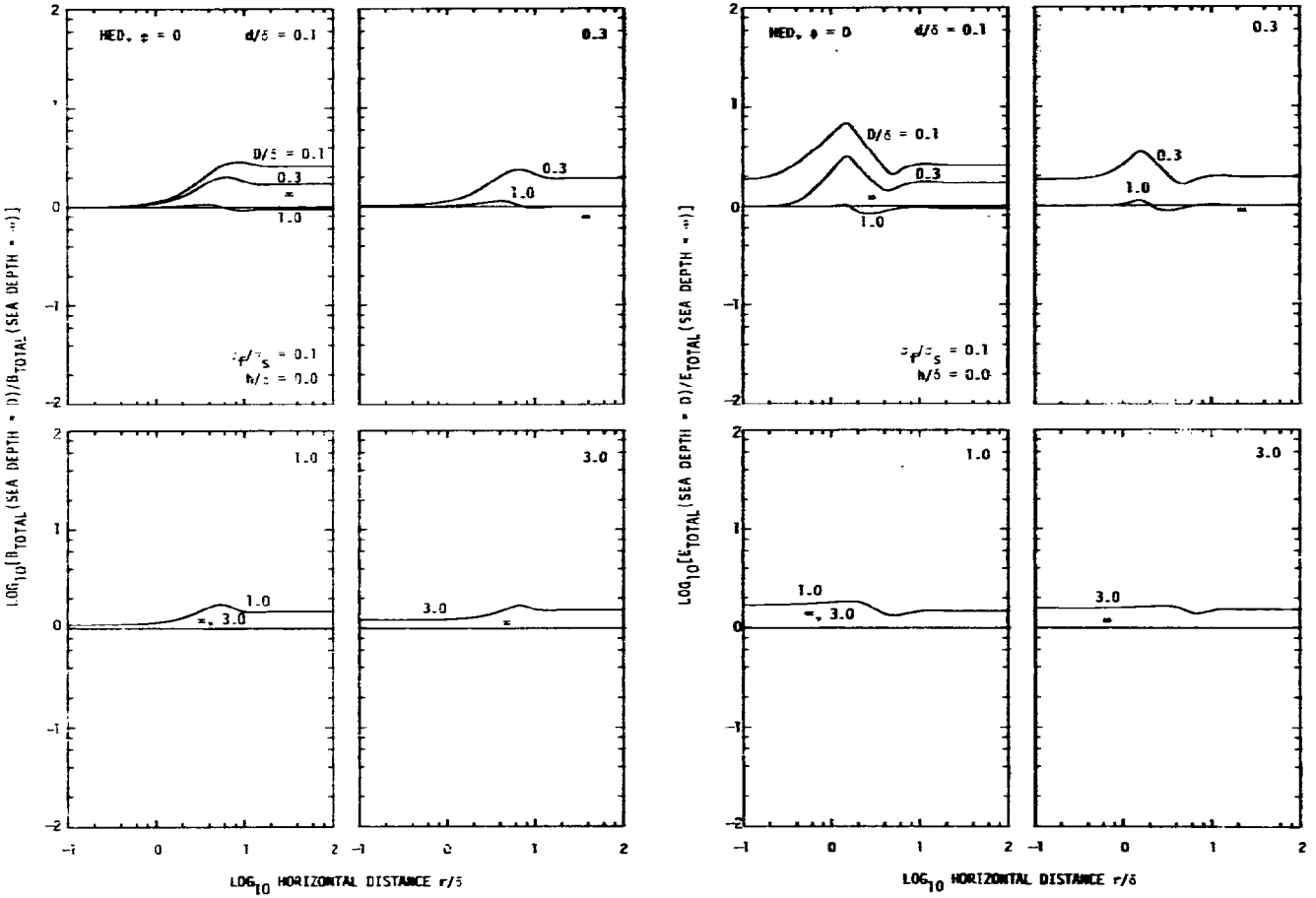

Figure 18. Curves illustrating the changes produced in the surface magnetic and electric field data presented in Figure 16 when an electrically conducting sea floor (conductivity $\sigma_f = 0.1\ \sigma_s$, depth D) is introduced.

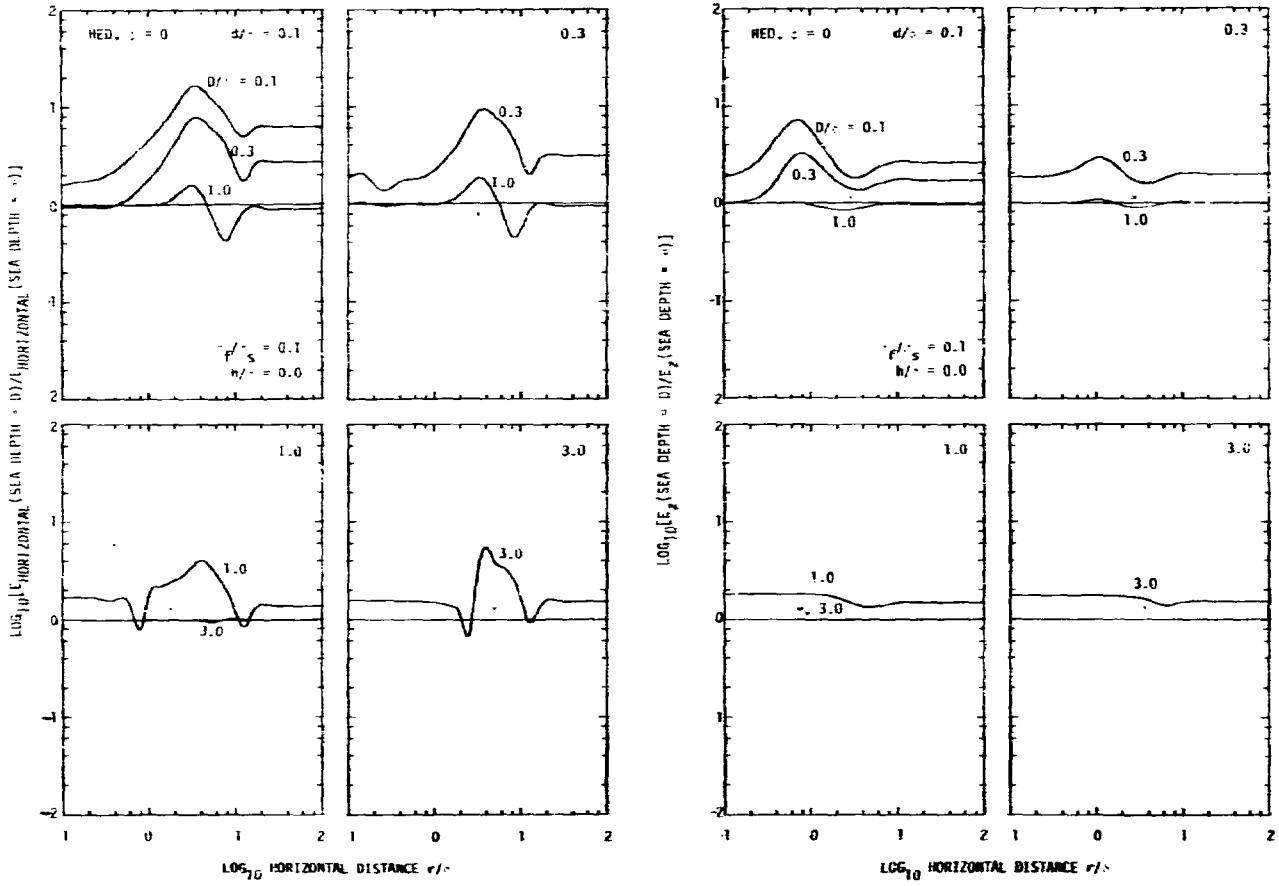

Figure 19. Curves illustrating the changes produced in the surface electric field component data plotted in Figure 17 when an electrically conducting sea floor (conductivity σ_f = 0.1 σ_s, depth D) is introduced.

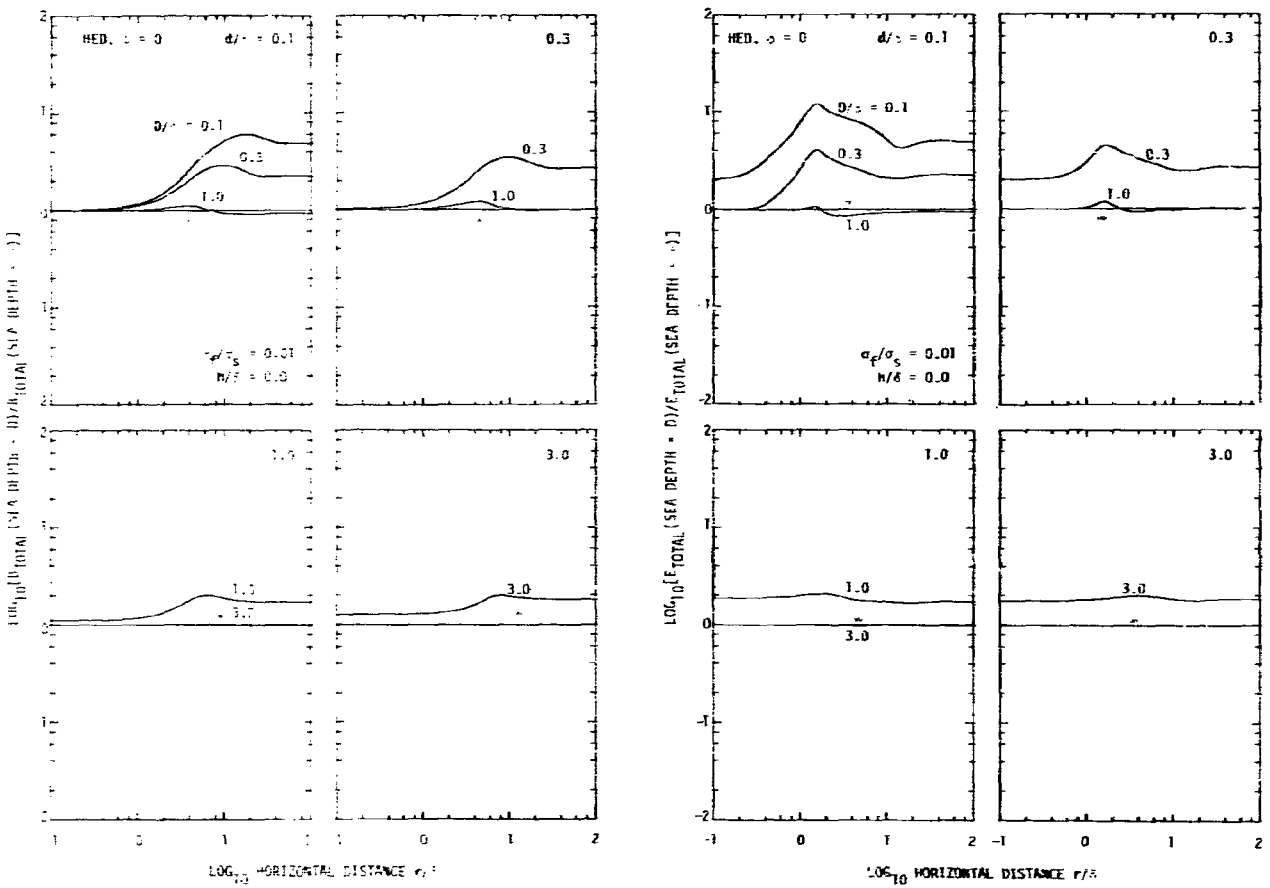

Figure 20. Curves illustrating the changes produced in the surface magnetic and electric field data presented in Figure 16 when an electrically conducting sea floor (conductivity σ_f = 0.01 σ_s, depth D) is introduced. The conductivity of this sea floor is one tenth the conductivity of the sea floor used in Figure 18.

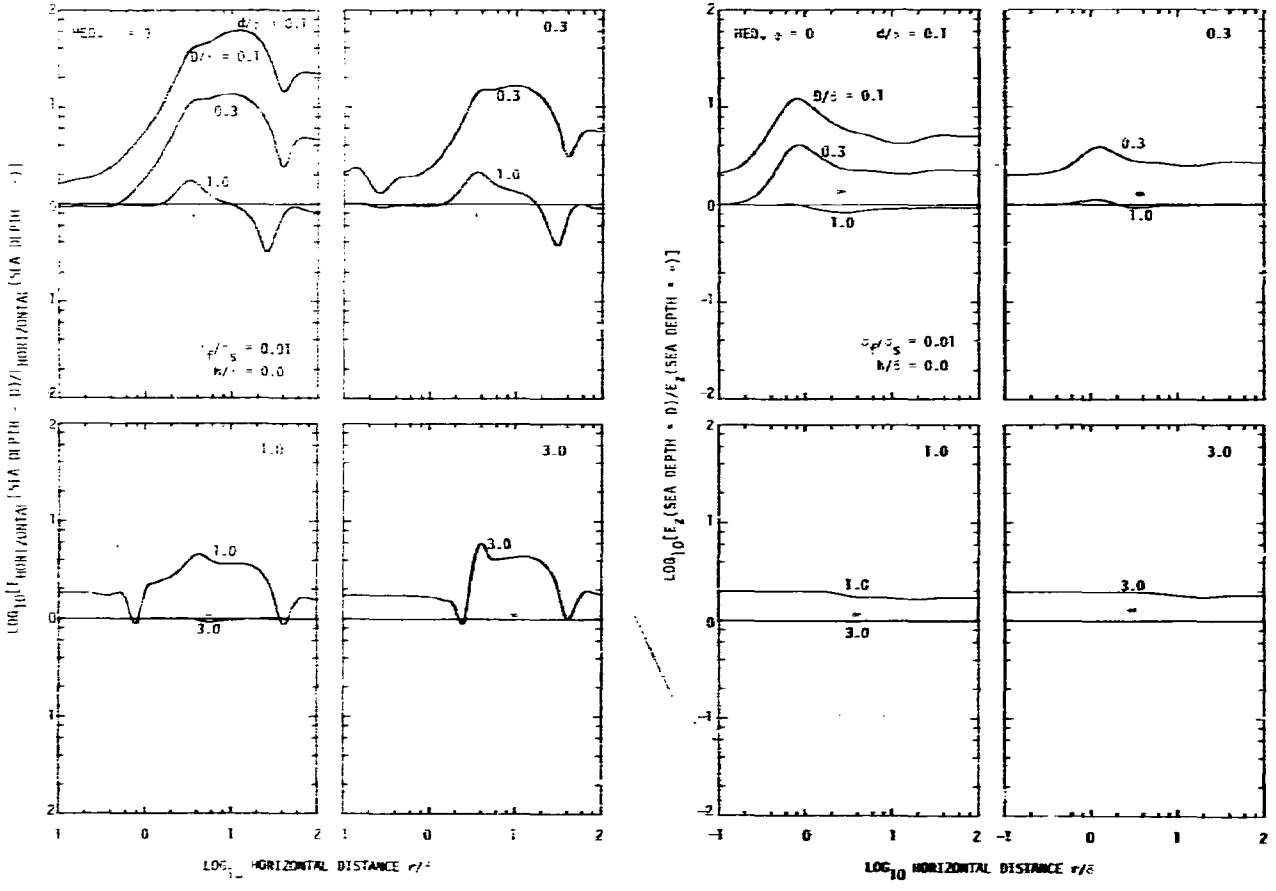

Figure 21. Curves illustrating the changes produced in the surface electric field component data presented in Figure 17 when an electrically conducting sea floor (conductivity $\sigma_f = 0.01\ \sigma_s$, depth D) is introduced. The conductivity of this sea floor is one tenth the conductivity of the sea floor used in Figure 19.

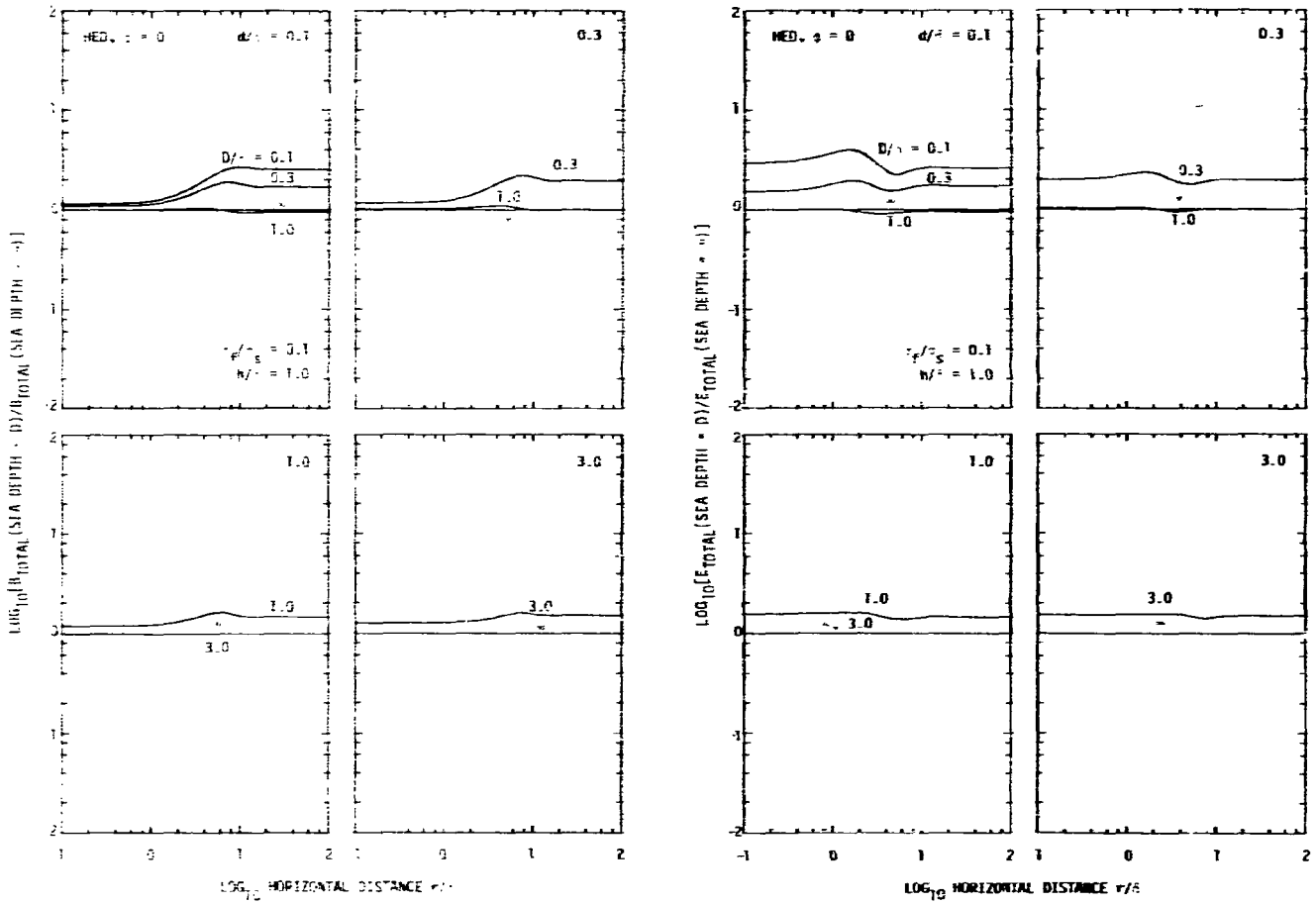

Figure 22. Curves illustrating the changes produced in the magnetic and electric field data presented in Figure 16 for a receiver altitude of one sea water skin depth ($h/\delta = 1.0$) when an electrically conducting sea floor (conductivity $\sigma_f = 0.1\ \sigma_s$, depth D) is introduced.

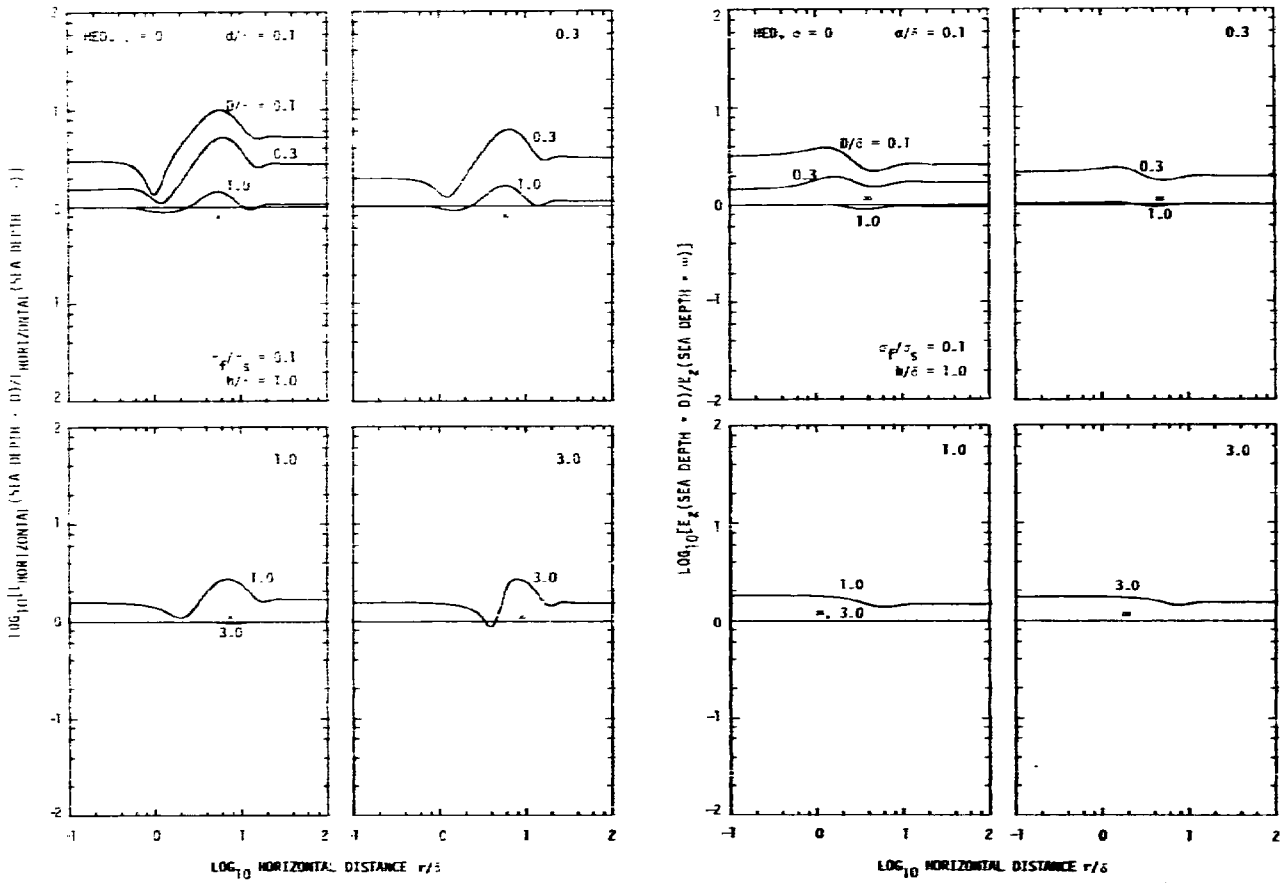

Figure 23. Curves illustrating the changes produced in the electric field component data presented in Figure 17 for a receiver altitude of one sea water skin depth ($h/\delta = 1.0$) when an electrically conducting sea floor (conductivity $\sigma_f = 0.1\ \sigma_s$, depth D) is introduced.

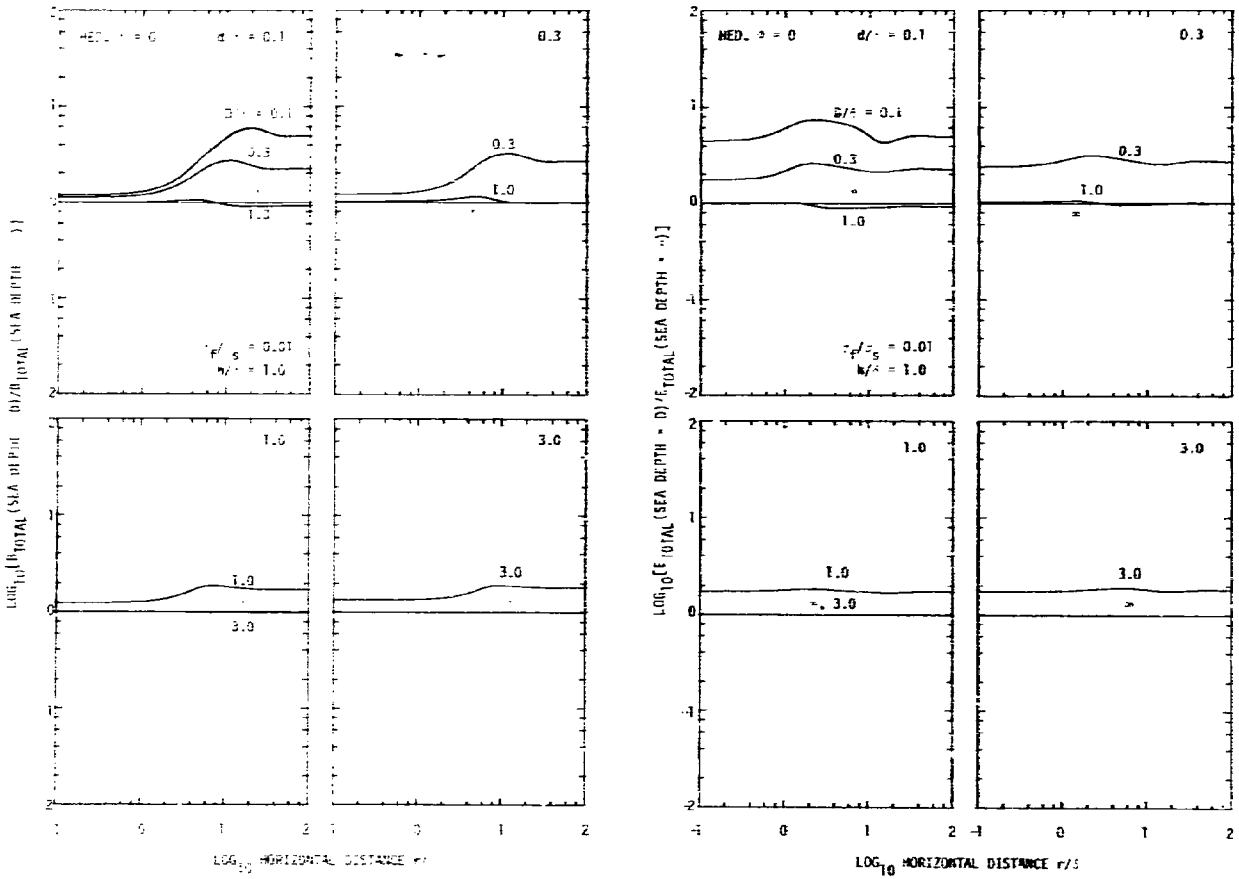

Figure 24. Curves illustrating the changes produced in the magnetic and electric field data presented in Figure 16 for a receiver altitude of one sea water skin depth (h/δ = 1.0) when an electrically conducting sea floor (conductivity $\sigma_f = 0.01\ \sigma_s$, depth D) is introduced. The conductivity of this sea floor is on tenth the conductivity of the sea flcor used in Figure 22.

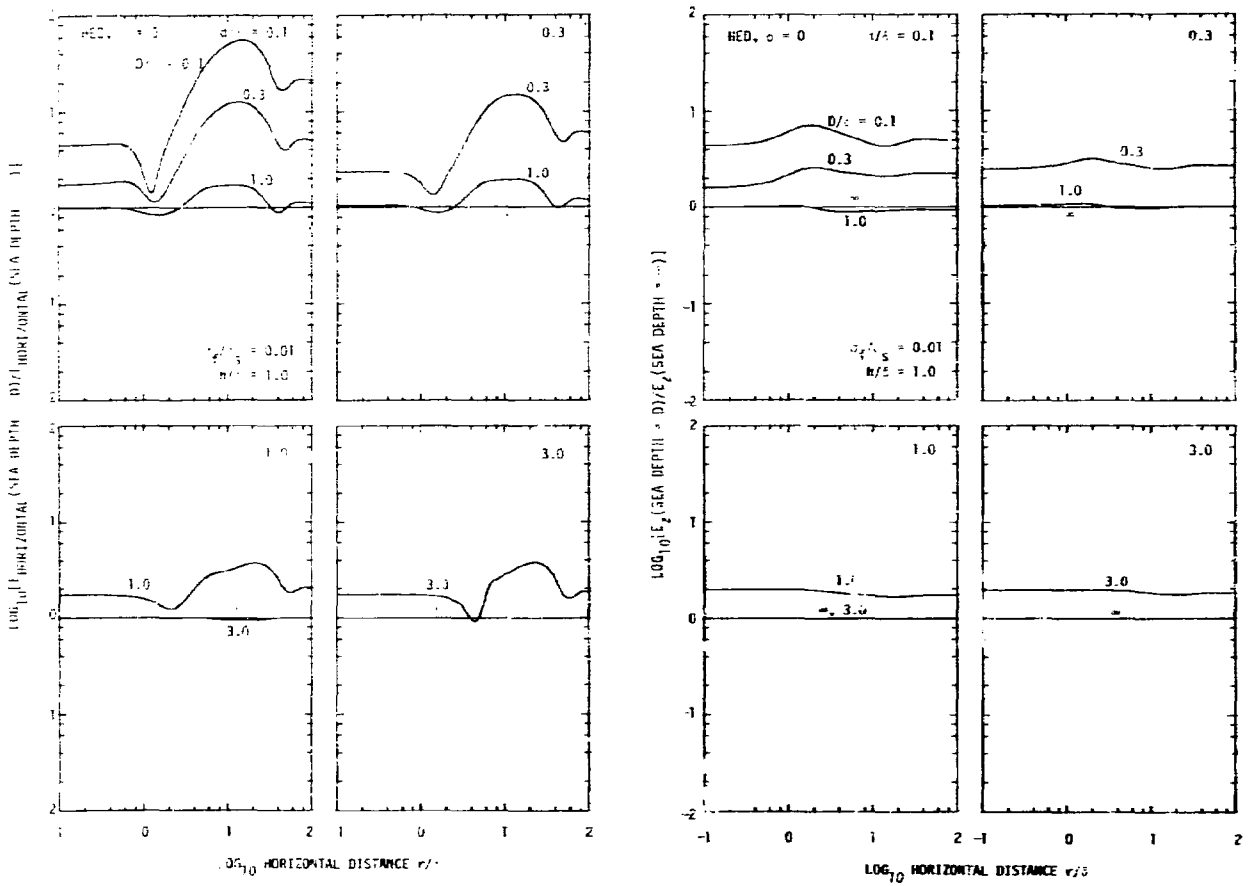

Figure 25. Curves illustrating the changes produced in the electric field component data presented in Figure 17 for a receiver altitude of one sea water skin depth ($h/\delta = 1.0$) when an electrically conducting sea floor (conductivity $\sigma_f = 0.01\ \sigma_s$, depth D) is introduced. The conductivity of this sea floor is one tenth the conductivity of the sea floor used in Figure 23.

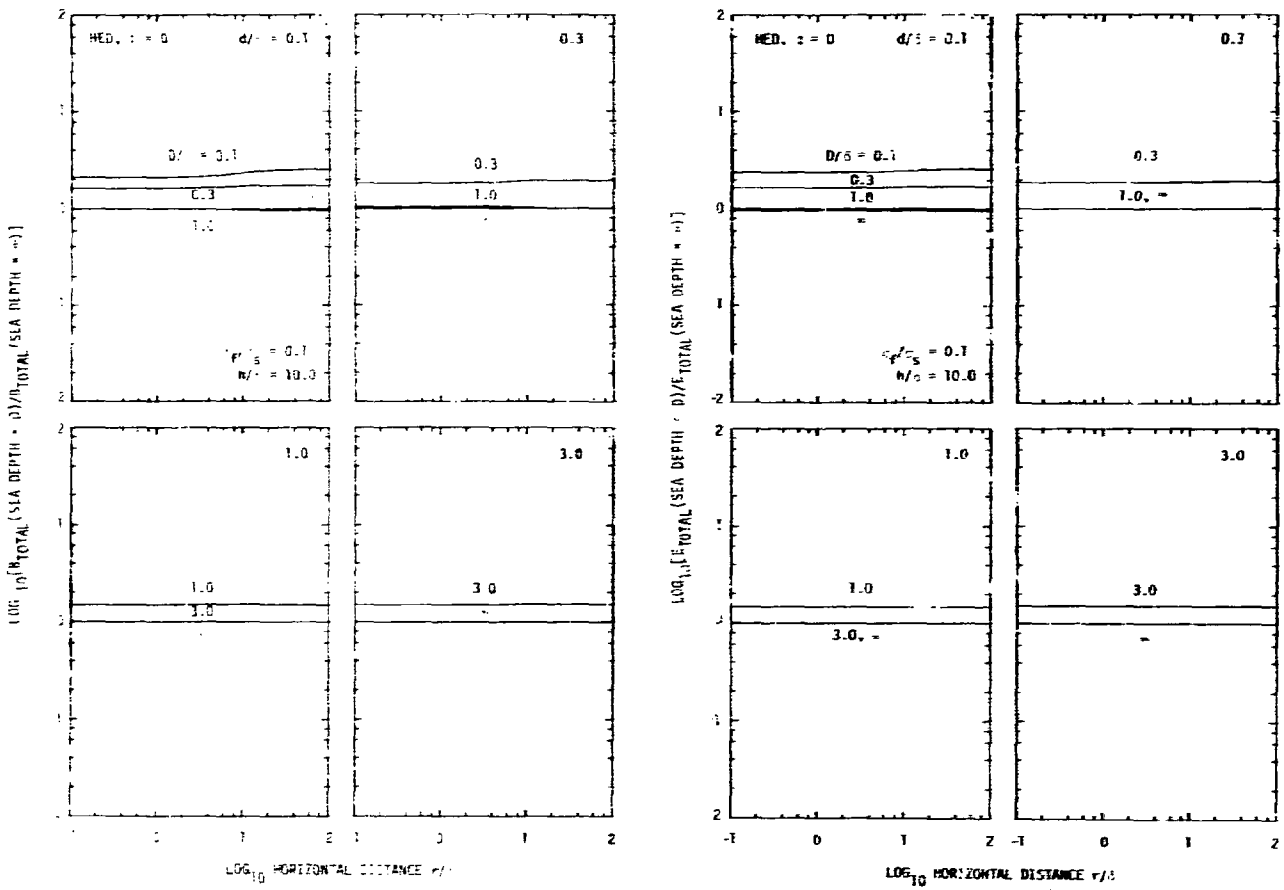

Figure 26. Curves illustrating the changes produced in the magnetic and electric field data presented in Figure 16 for a receiver altitude of ten sea water skin depths (h/δ = 10.0) when an electrically conducting sea floor (conductivity $\sigma_f = 0.1\ \sigma_s$, depth D) is introduced.

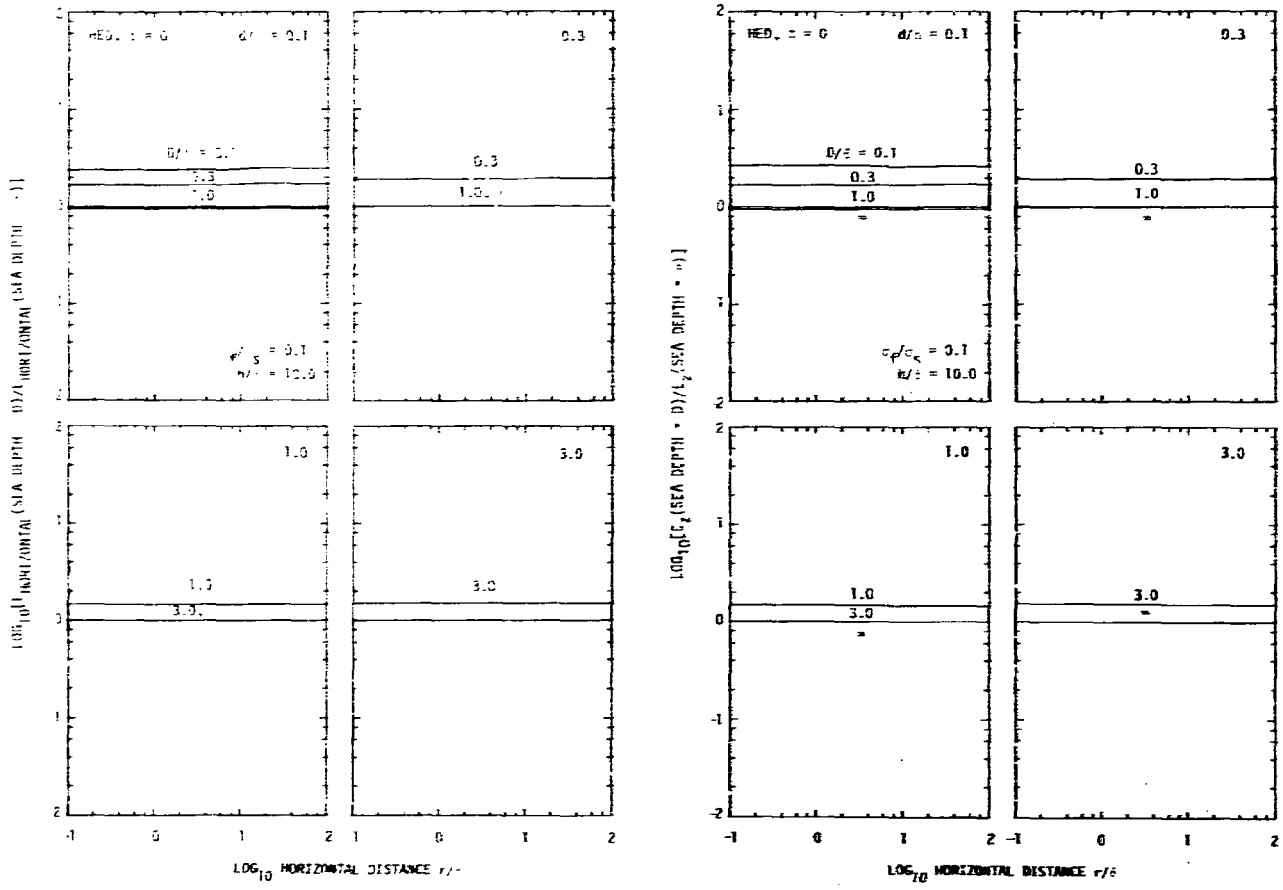

Figure 27. Curves illustrating the changes produced in the electric field component data presented in Figure 17 for a receiver altitude of ten sea water skin depths (h/δ = 10.0) when an electrically conducting sea floor (conductivity $\sigma_f = 0.1\ \sigma_s$, depth D) is introduced.

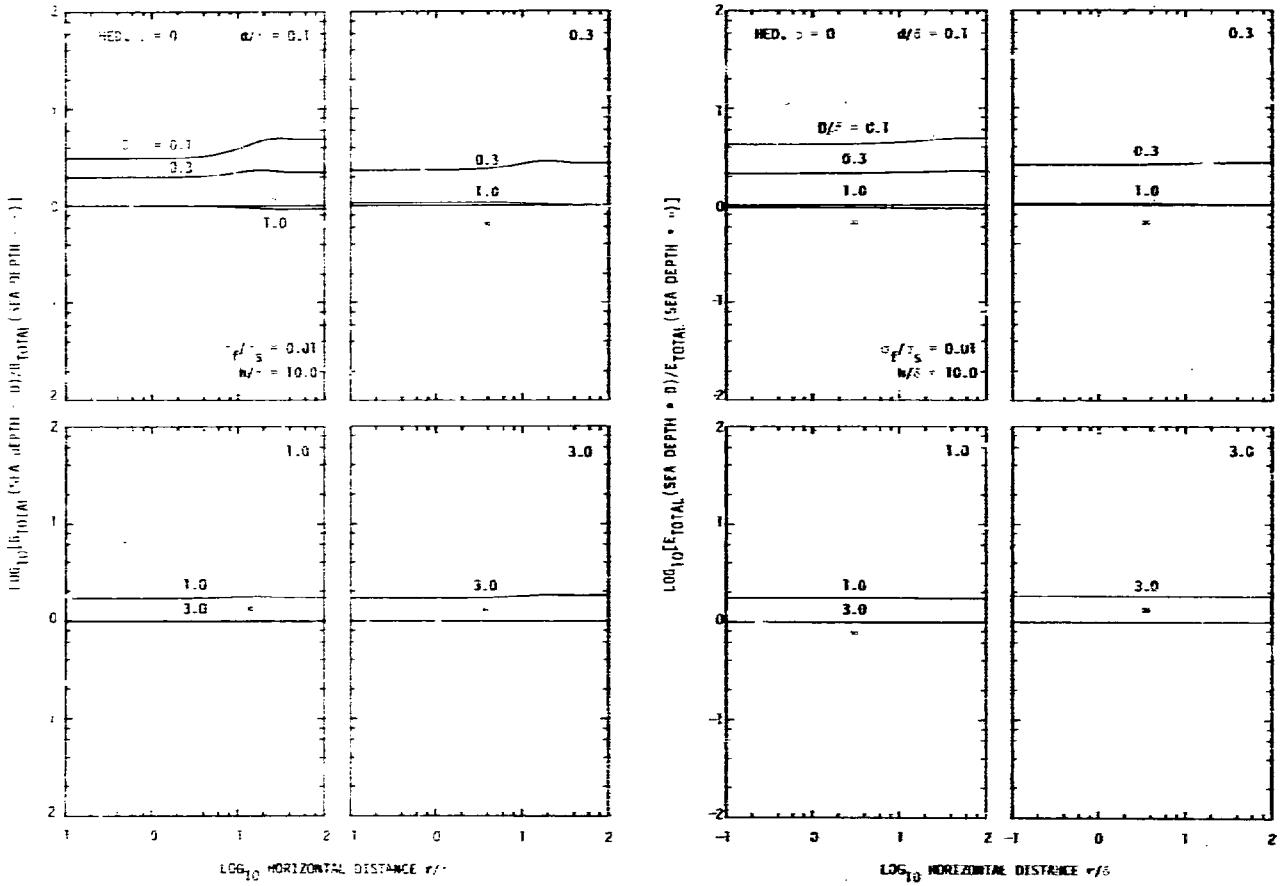

Figure 28. Curves illustrating the changes produced in the magnetic and electric field data presented in Figure 16 for a receiver altitude of ten sea water skin depths ($h/\delta = 10.0$) when an electrically conducting sea floor (conductivity $\sigma_f = 0.01\ \sigma_s$, depth D) is introduced. The conductivity of this sea floor is one tenth the conductivity of the sea floor used in Figure 26.

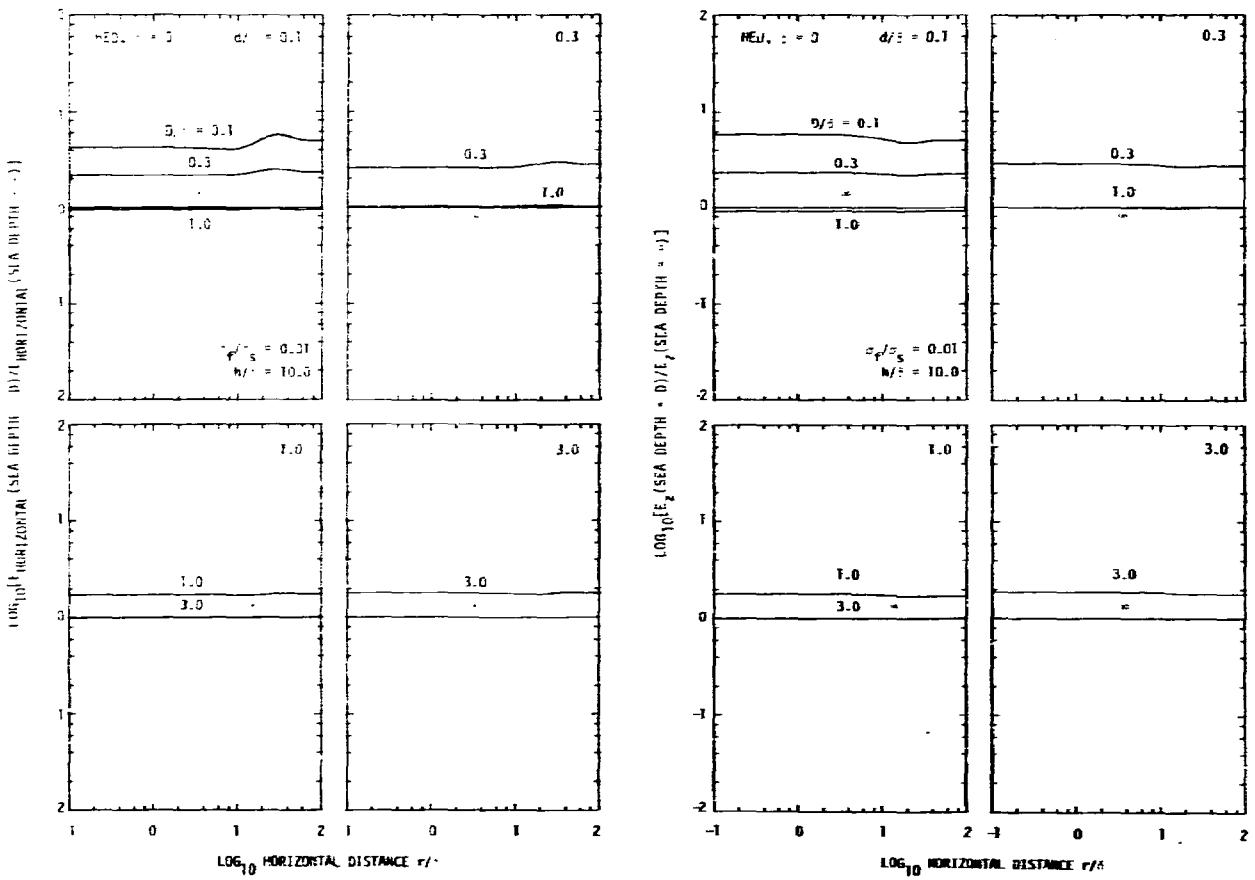

Figure 29. Curves illustrating the changes produced in the electric field component data presented in Figure 17 for a receiver altitude of ten sea water skin depths ($h/\delta = 10.0$) when an electrically conducting sea floor (conductivity $\sigma_f = 0.01\ \sigma_s$, depth D) is introduced. The conductivity of this sea floor is one tenth the conductivity of the sea floor used in Figure 27.

Figures for the

HORIZONTAL ELECTRIC DIPOLE, $\phi = 90°$

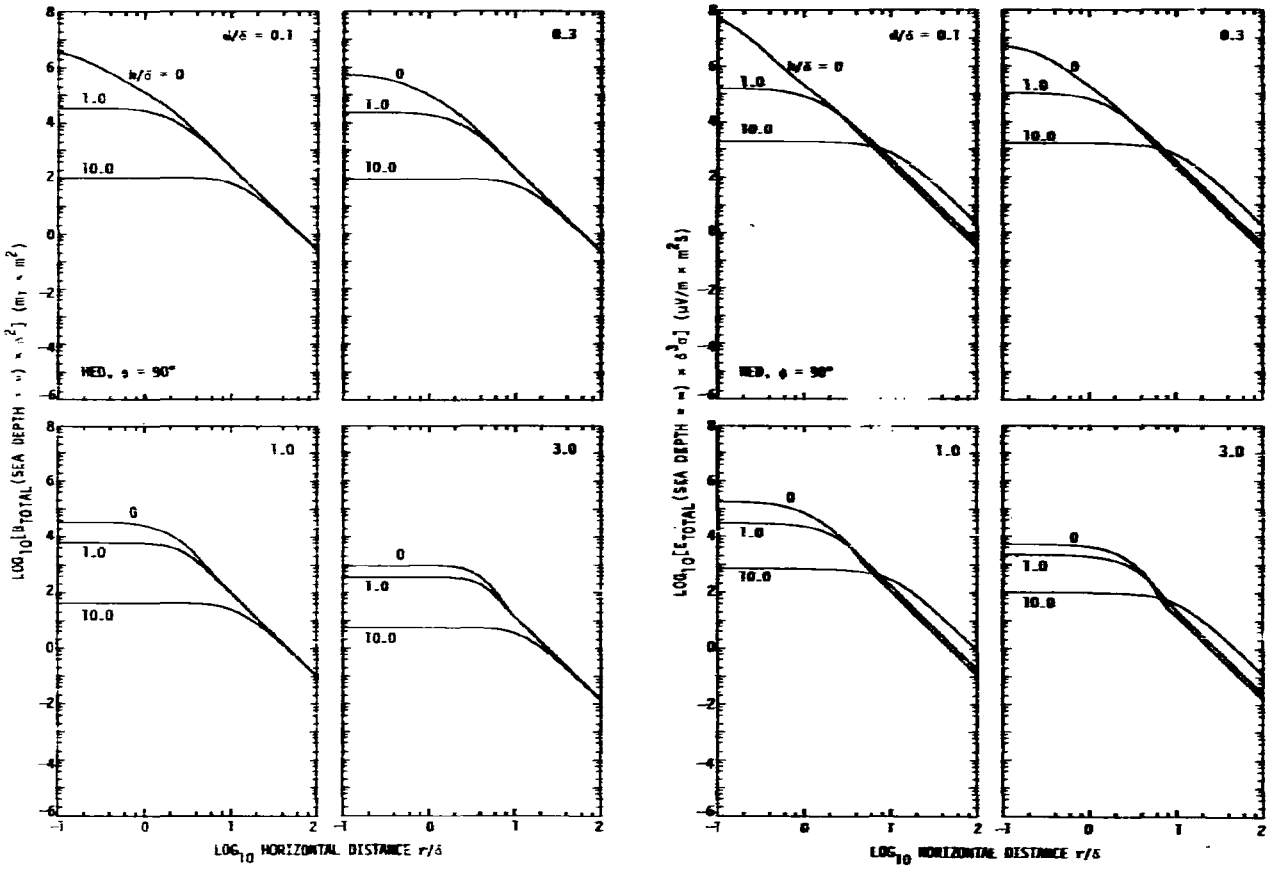

Figure 30. Variation with horizontal distance of the amplitudes of the total magnetic (B_{TOTAL}) and electric (E_{TOTAL}) fields produced on and above the surface of an infinitely deep sea by a submerged horizontally directed electric dipole (HED). The fields are given for an azimuthal angle (ϕ) of 90°.

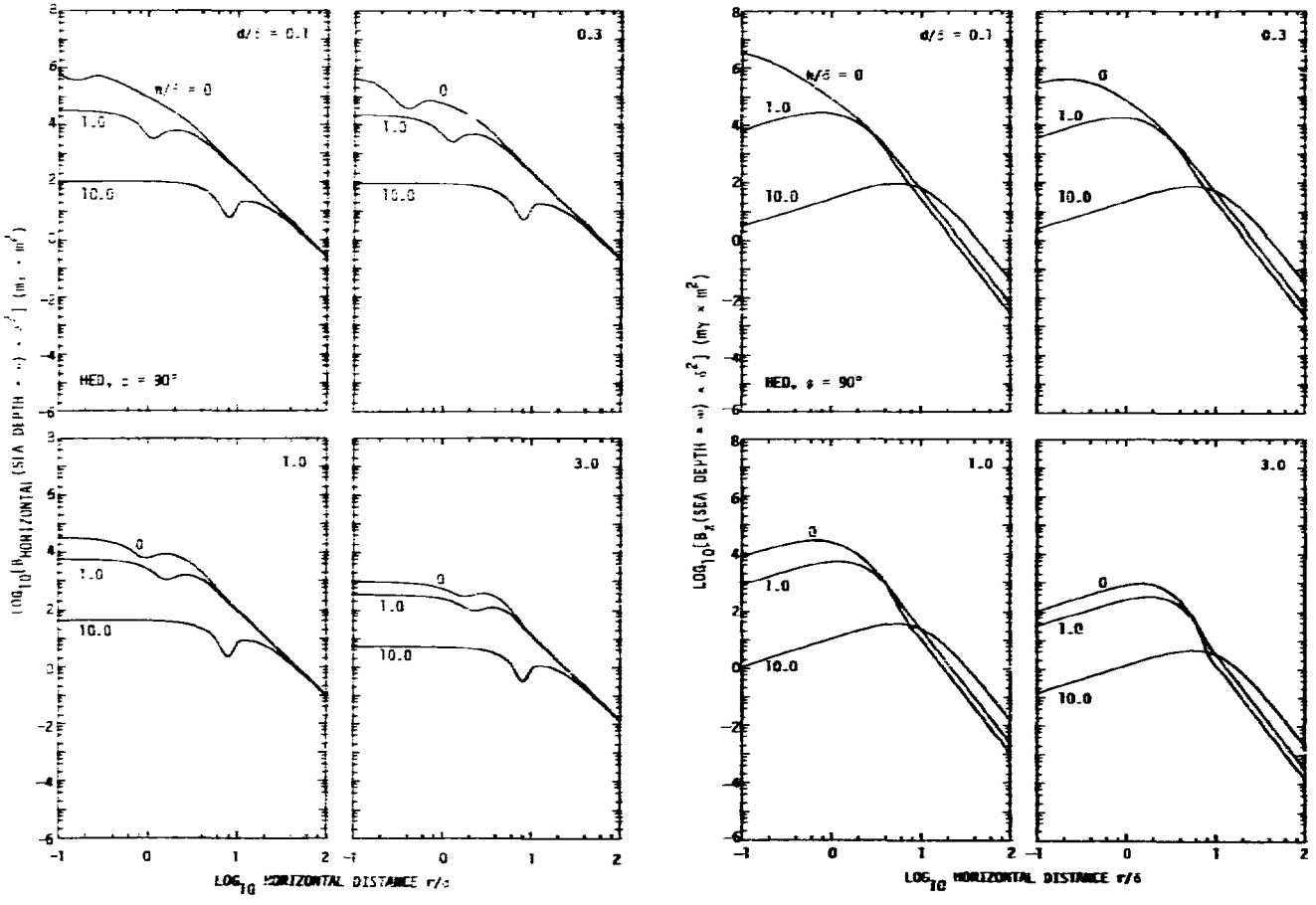

Figure 31. Variation with horizontal distance of the amplitudes of the two magnetic field components $B_{HORIZONTAL}$ and B_z produced on and above the surface of an infinitely deep sea by a submerged horizontally directed harmonic electric dipole (HED). The fields are given for an azimuthal angle (ϕ) of 90°.

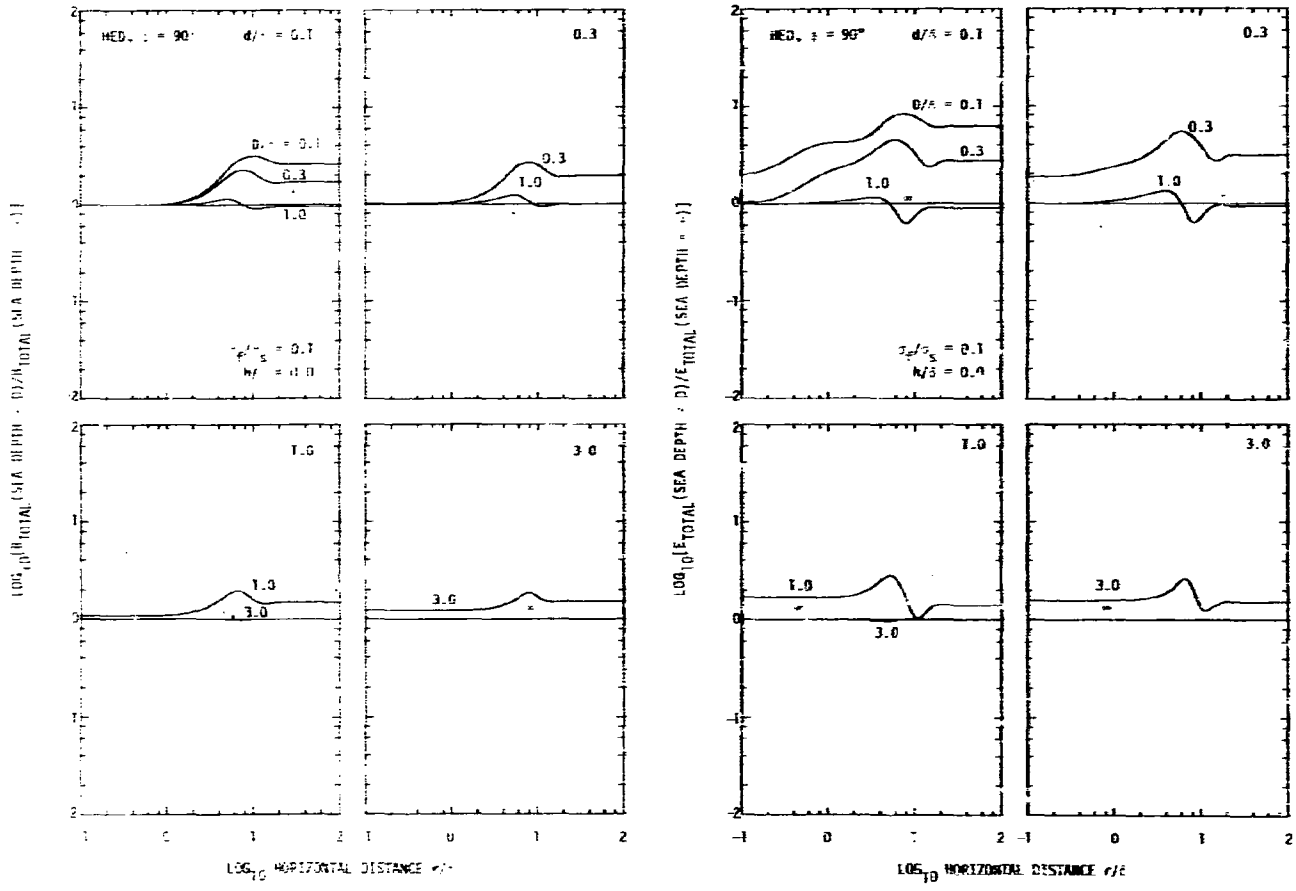

Figure 32. Curves illustrating the changes produced in the surface magnetic and electric field data presented in Figure 30 when an electrically conducting sea floor (conductivity $\sigma_f = 0.1\ \sigma_s$, depth D) is introduced.

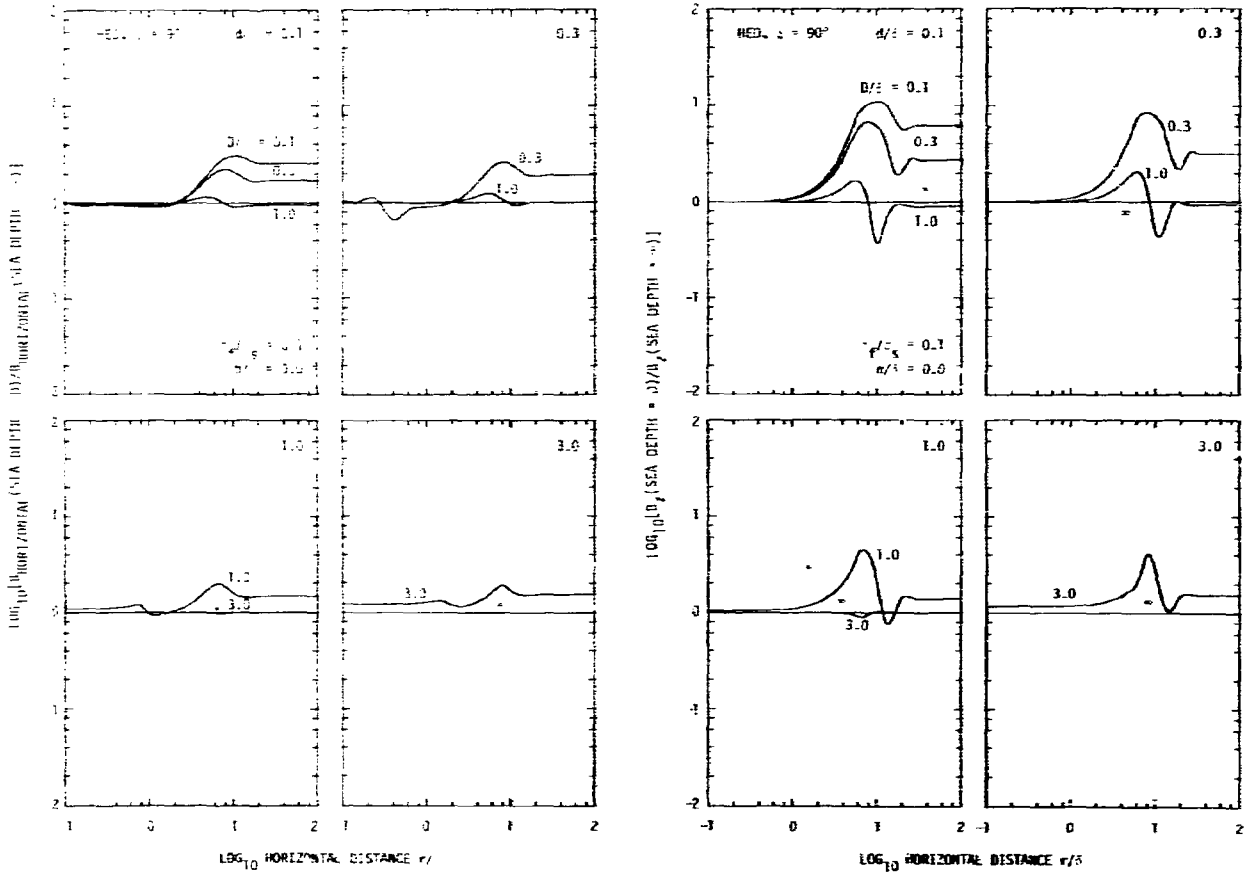

Figure 33. Curves illustrating the changes produced in the surface magnetic field component data plotted in Figure 31 when an electrically conducting sea floor (conductivity $\sigma_f = 0.1\ \sigma_s$, depth D) is introduced.

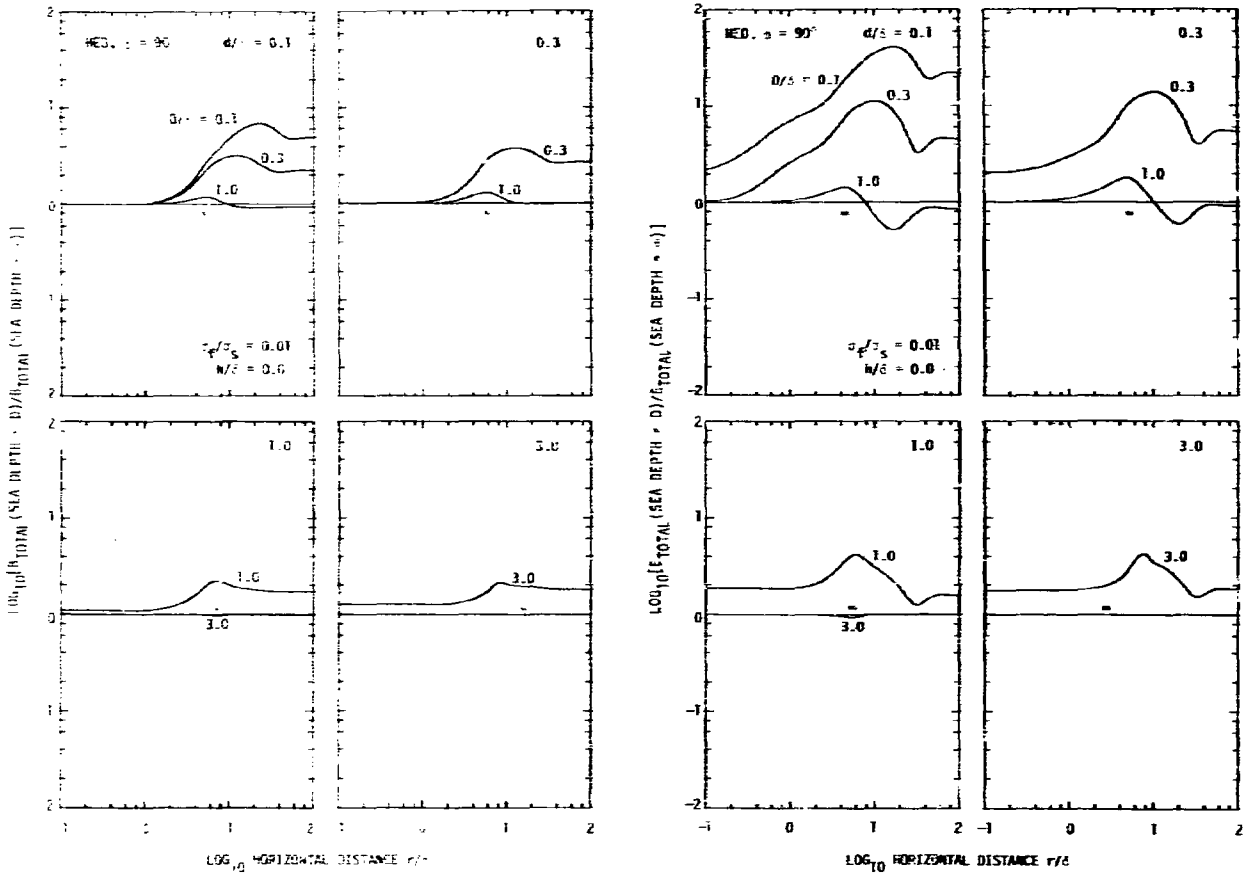

Figure 34. Curves illustrating the changes produced in the surface magnetic and electric field data presented in Figure 30 when an electrically conducting sea floor (conductivity $\sigma_f = 0.01\ \sigma_s$, depth D) is introduced. The conductivity of this sea floor is one tenth the conductivity of the sea floor used in Figure 32.

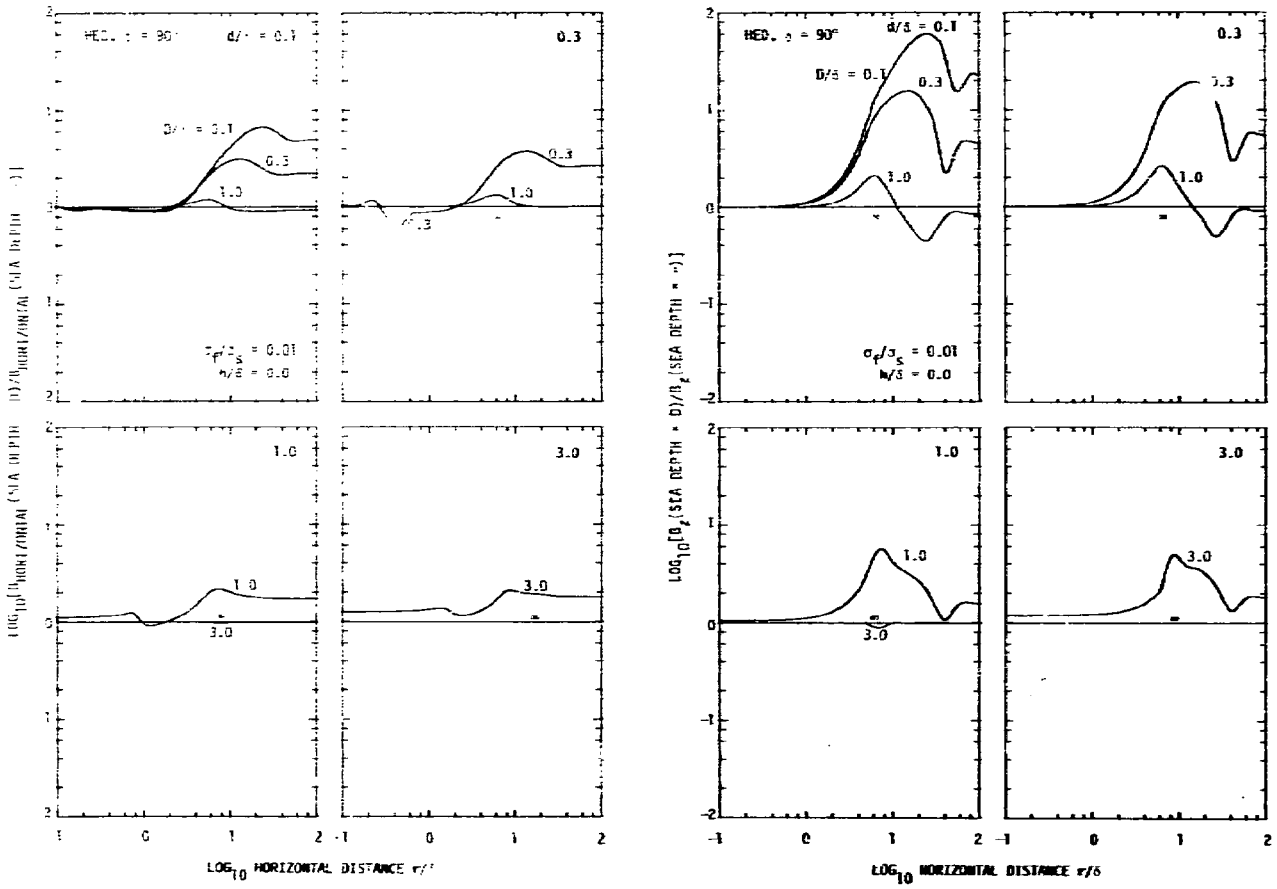

Figure 35. Curves illustrating the changes produced in the surface magnetic field component data presented in Figure 31 when an electrically conducting sea floor (conductivity $\sigma_f = 0.01\ \sigma_s$, depth D) is introduced. The conductivity of this sea floor is one tenth the conductivity of the sea floor used in Figure 33.

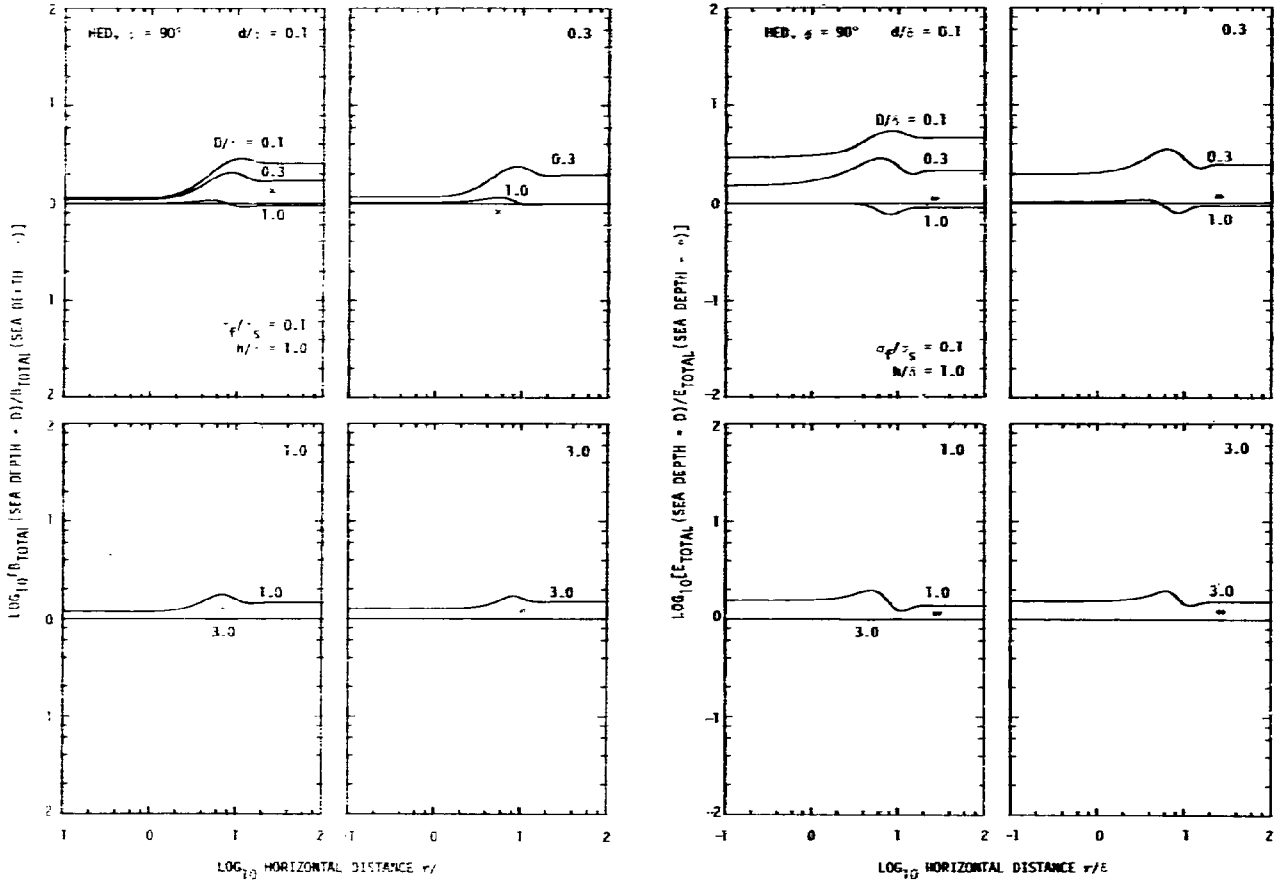

Figure 35. Curves illustrating the changes produced in the magnetic and electric field data presented in Figure 30 for a receiver altitude of one sea water skin depth ($h/\delta = 1.0$) when an electrically conducting sea floor (conductivity $\sigma_f = 0.1\ \sigma_s$, depth D) is introduced.

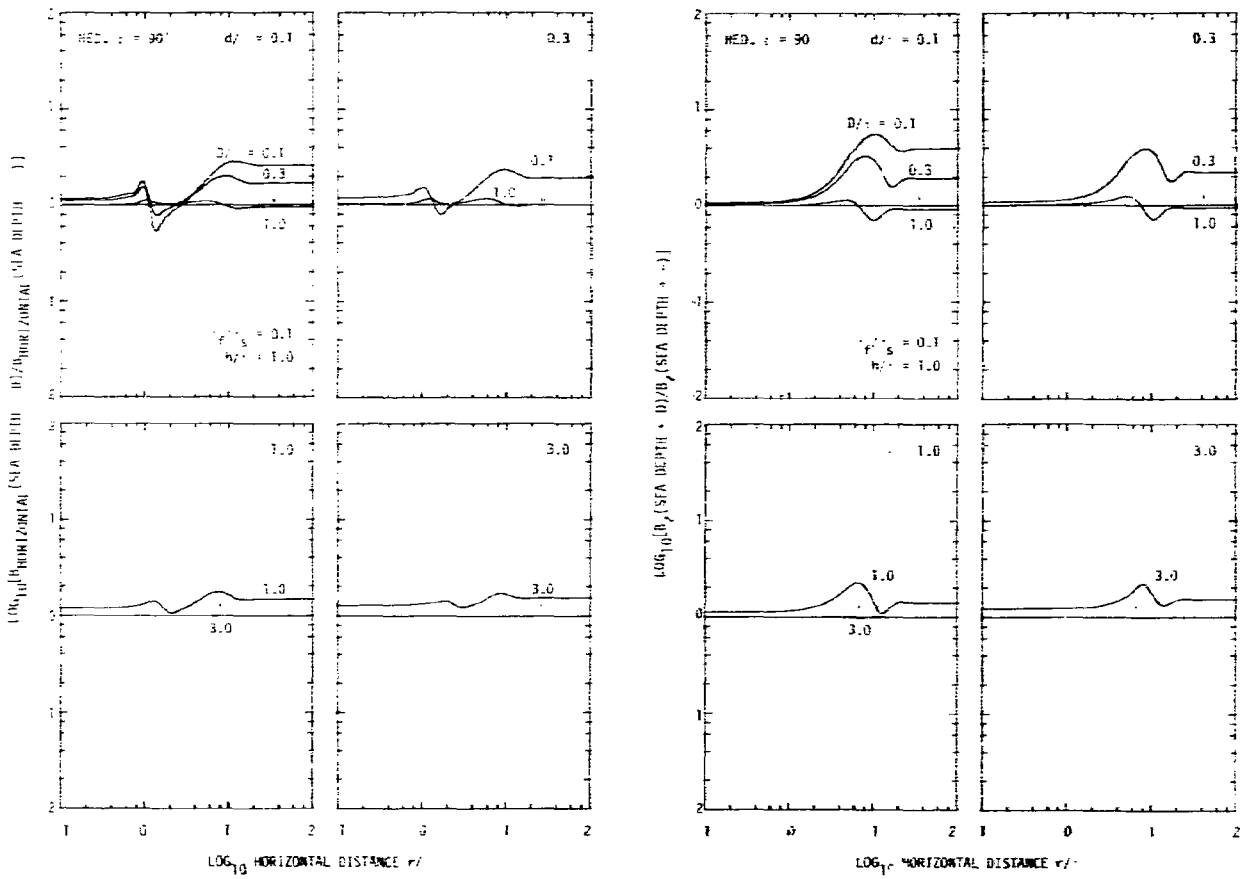

Figure 37. Curves illustrating the changes produced in the magnetic field component data presented in Figure 31 for a receiver altitude of one sea water skin depth ($h/\delta = 1.0$) when an electrically conducting sea floor (conductivity $\sigma_f = 0.1\ \sigma_S$, depth D) is introduced.

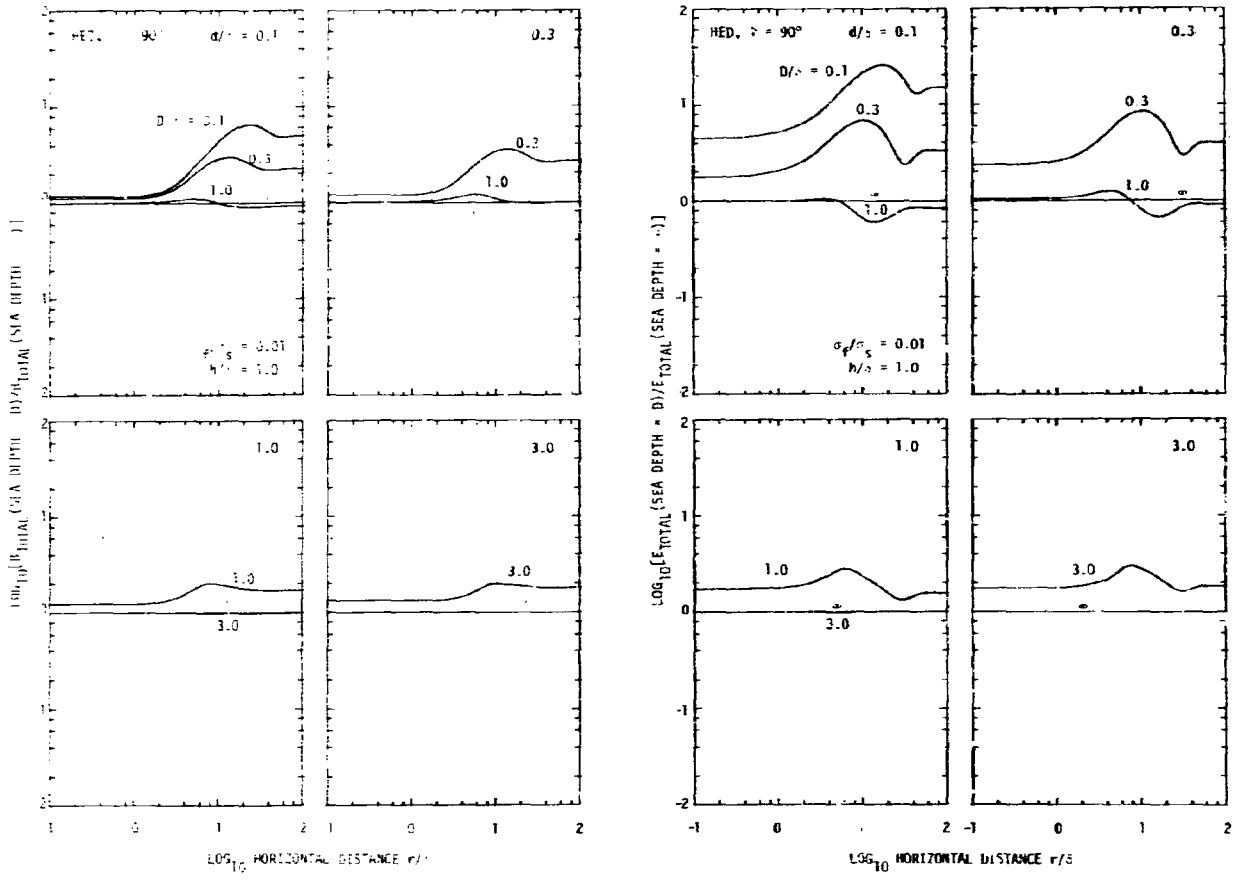

Figure 38. Curves illustrating the changes produced in the magnetic and electric field data presented in Figure 30 for a receiver altitude of one sea water skin depth ($h/\delta = 1.0$) when an electrically conducting sea floor (conductivity $\sigma_f = 0.01\ \sigma_s$, depth D) is introduced. The conductivity of this sea floor is one tenth the conductivity of the sea floor used in Figure 36.

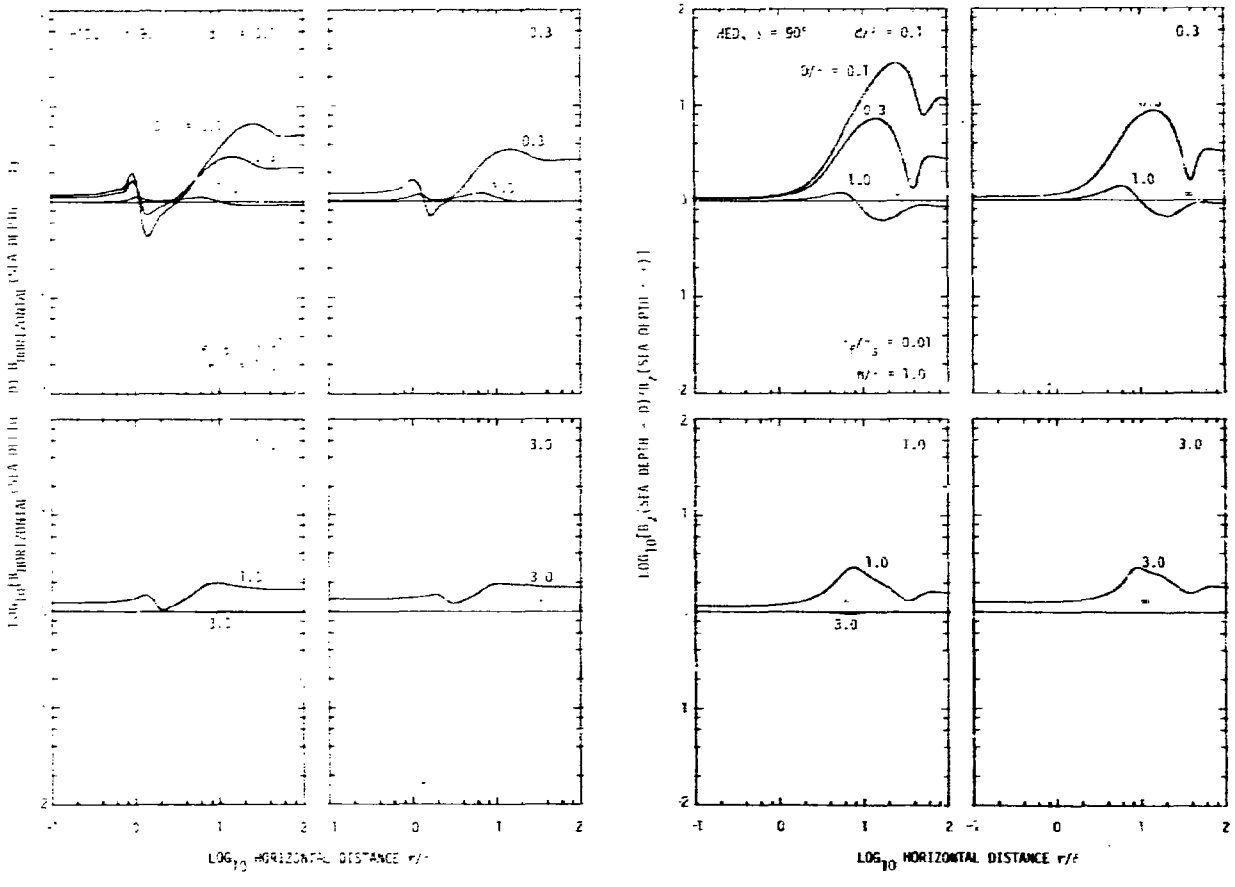

Figure 39. Curves illustrating the changes produced in the magnetic field component data presented in Figure 31 for a receiver altitude of one sea water skin depth ($h/\delta = 1.0$) when an electrically conducting sea floor (conductivity $\sigma_f = 0.01\ \sigma_s$, depth D) is introduced. The conductivity of this sea floor is one tenth the conductivity of the sea floor used in Figure 37.

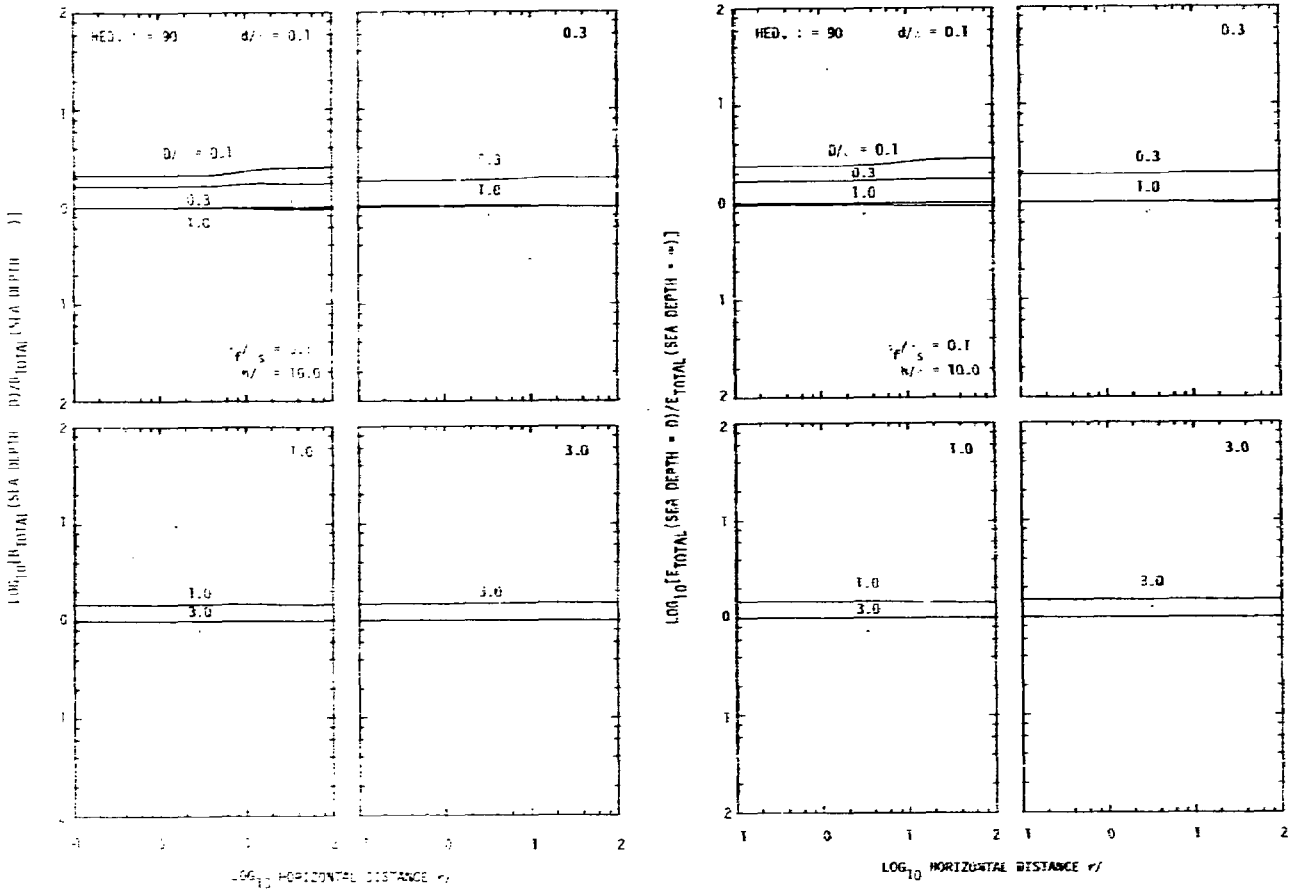

Figure 40. Curves illustrating the changes produced in the magnetic and electric field data presented in Figure 30 for a receiver altitude of ten sea water skin depths ($h/\delta = 10.0$) when an electrically conducting sea floor (conductivity $\sigma_f = 0.1\ \sigma_s$, depth D) is introduced.

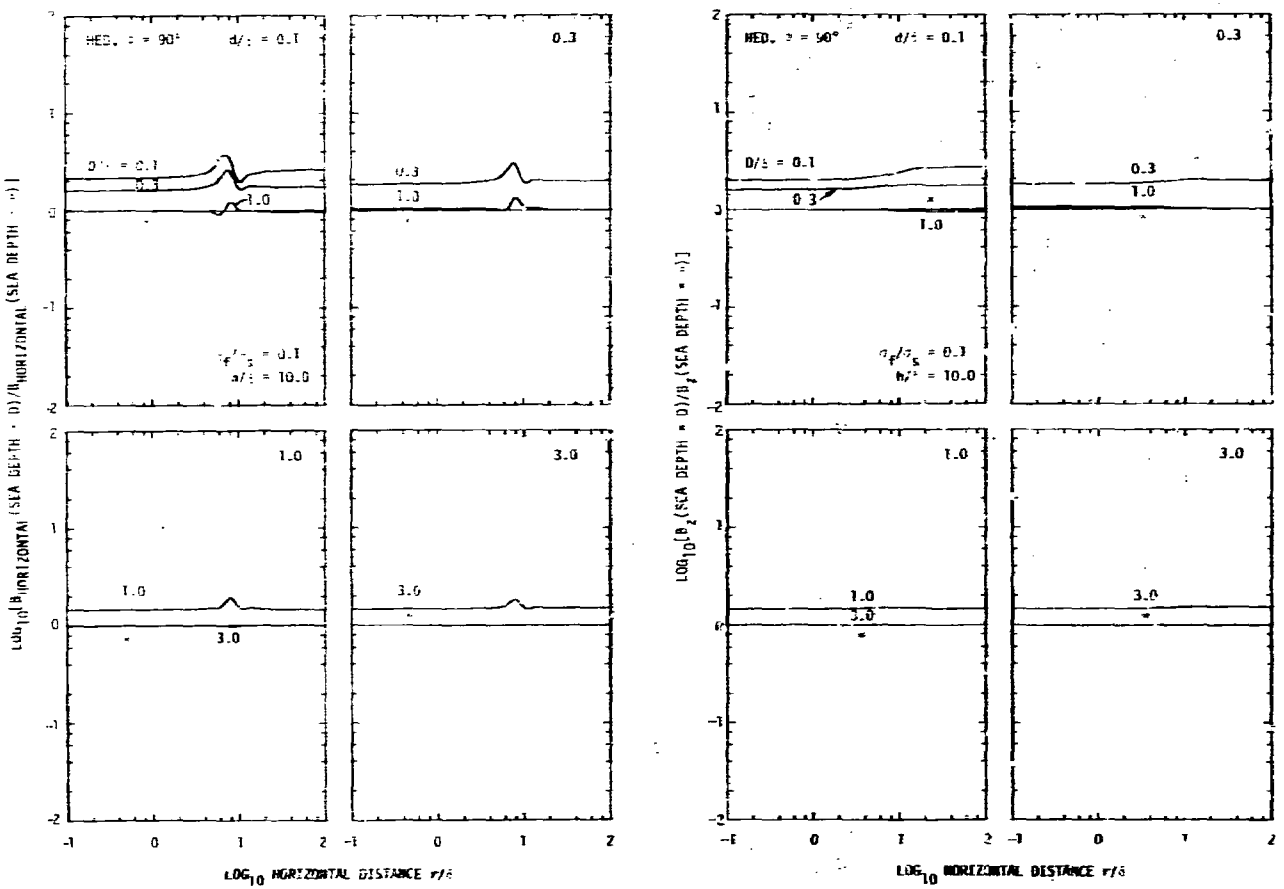

Figure 41. Curves illustrating the changes produced in the magnetic field component data presented in Figure 31 for a receiver altitude of ten sea water skin depths ($h/\delta = 10.0$) when an electrically conducting sea floor (conductivity $\sigma_f = 0.1\ \sigma_s$, depth D) is introduced.

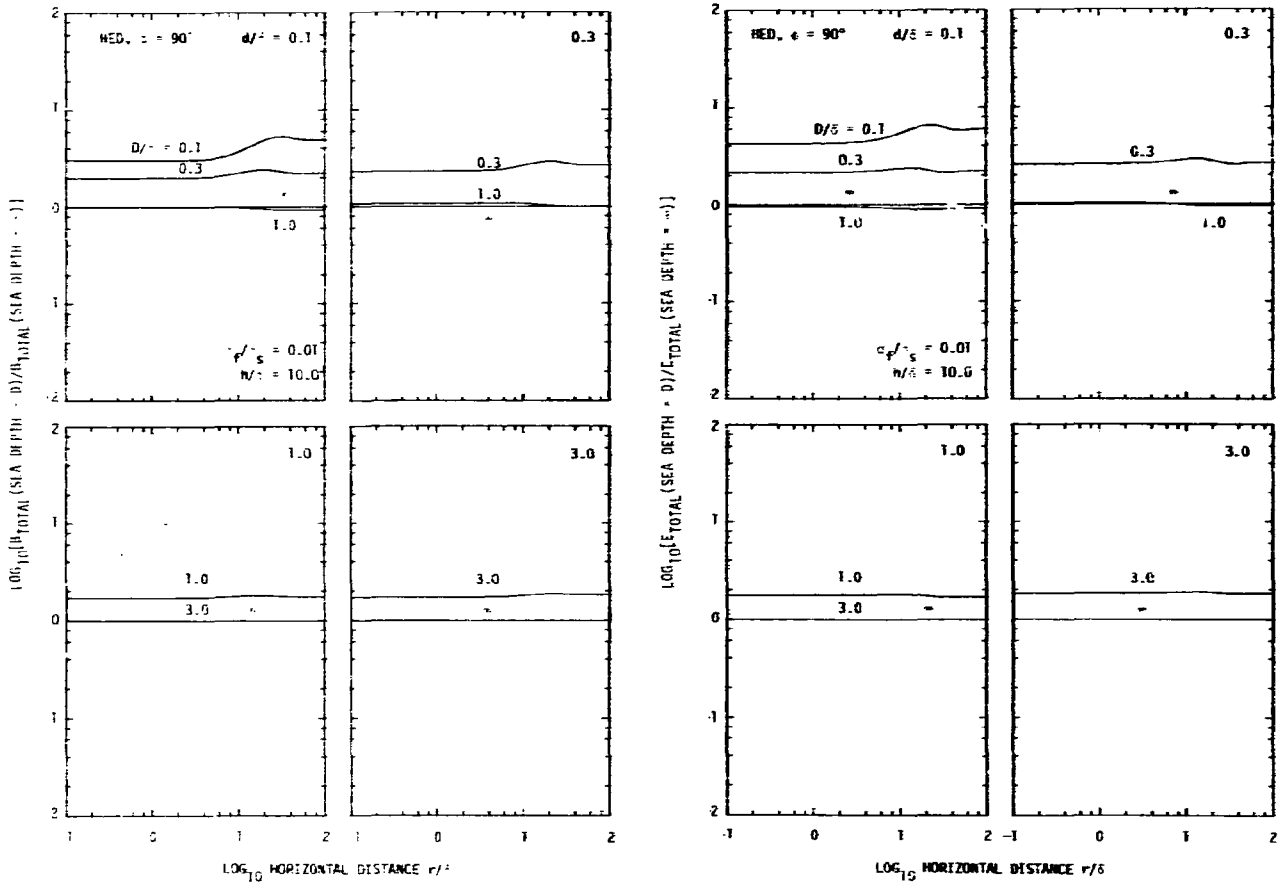

Figure 42. Curves illustrating the changes produced in the magnetic and electric field data presented in Figure 30 for a receiver altitude of ten sea water skin depths ($h/\delta = 10.0$) when an electrically conducting sea floor (conductivity $\sigma_f = 0.01\ \sigma_s$, depth D) is introduced. The conductivity of this sea floor is one tenth the conductivity of the sea floor used in Figure 40.

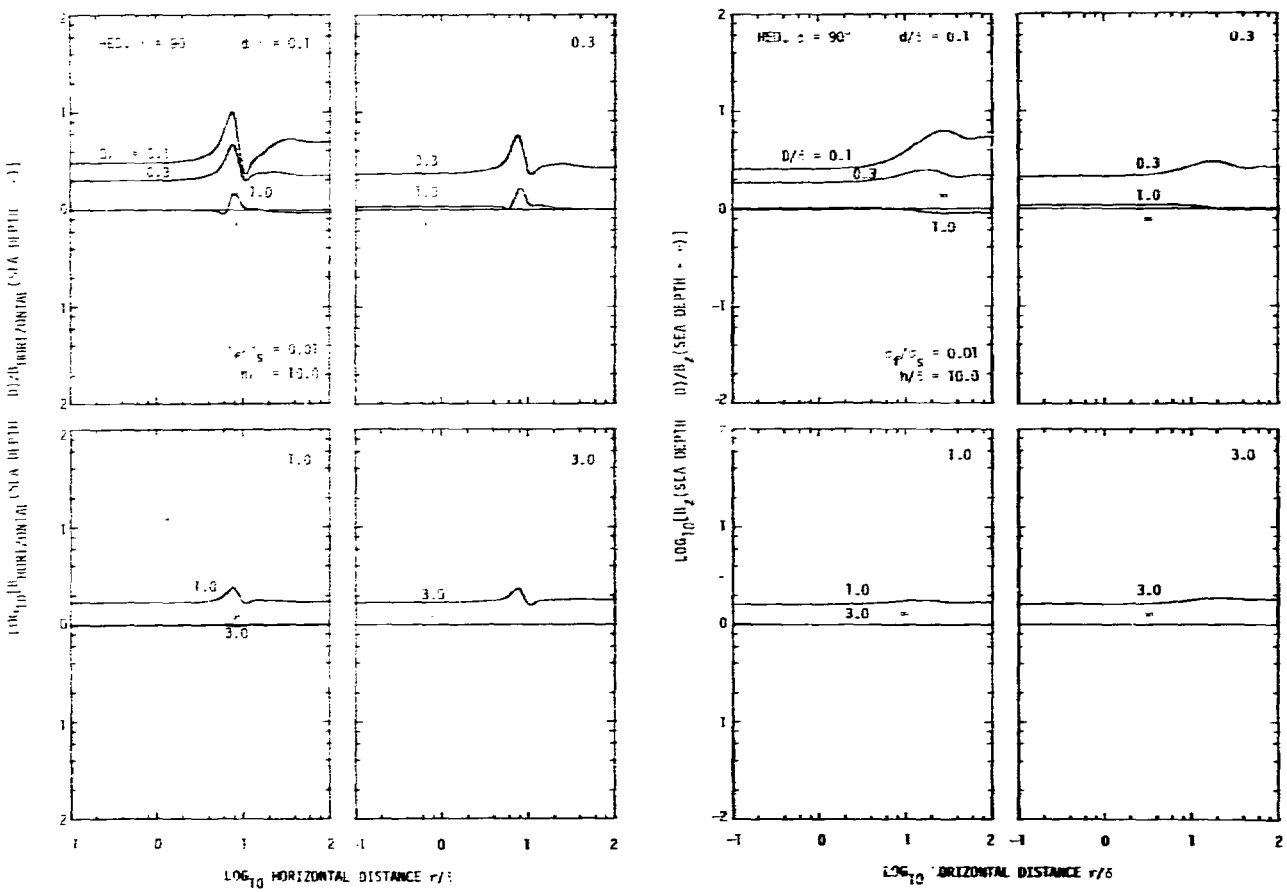

Figure 43. Curves illustrating the changes produced in the magnetic field component data presented in Figure 31 for a receiver altitude of ten sea water skin depths ($h/\delta = 10.0$) when an electrically conducting sea floor (conductivity $\sigma_f = 0.01\ \sigma_s$, depth D) is introduced. The conductivity of this sea floor is one tenth the conductivity of the sea floor used in Figure 41.

Figures for the

HORIZONTAL MAGNETIC DIPOLE, $\phi = 0°$

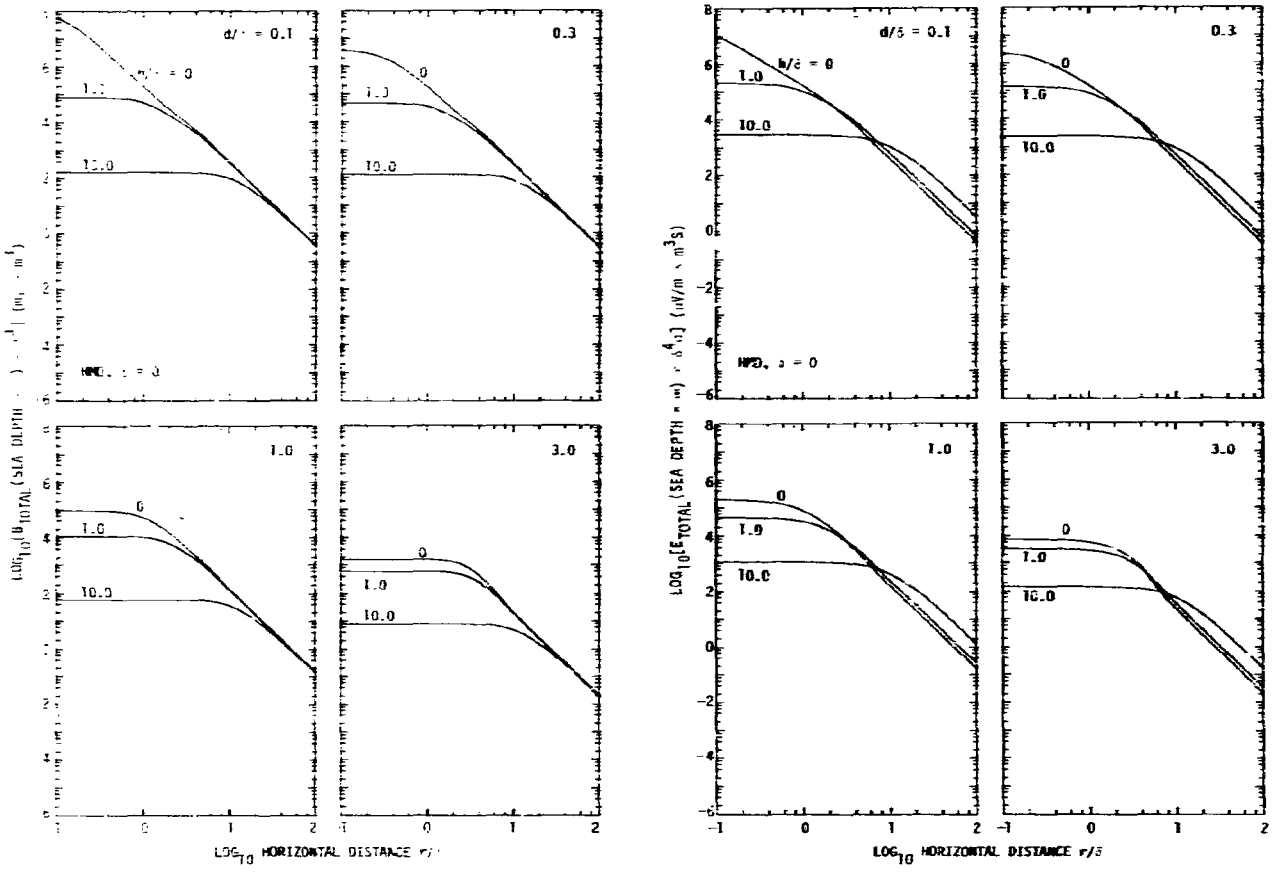

Figure 44. Variation with horizontal distance of the amplitudes of the total magnetic (B_{TOTAL}) and electric (E_{TOTAL}) fields produced on and above the surface of an infinitely deep sea by a submerged horizontally directed magnetic dipole (HMD). The fields are given for an azimuthal angle (ϕ) of 0°.

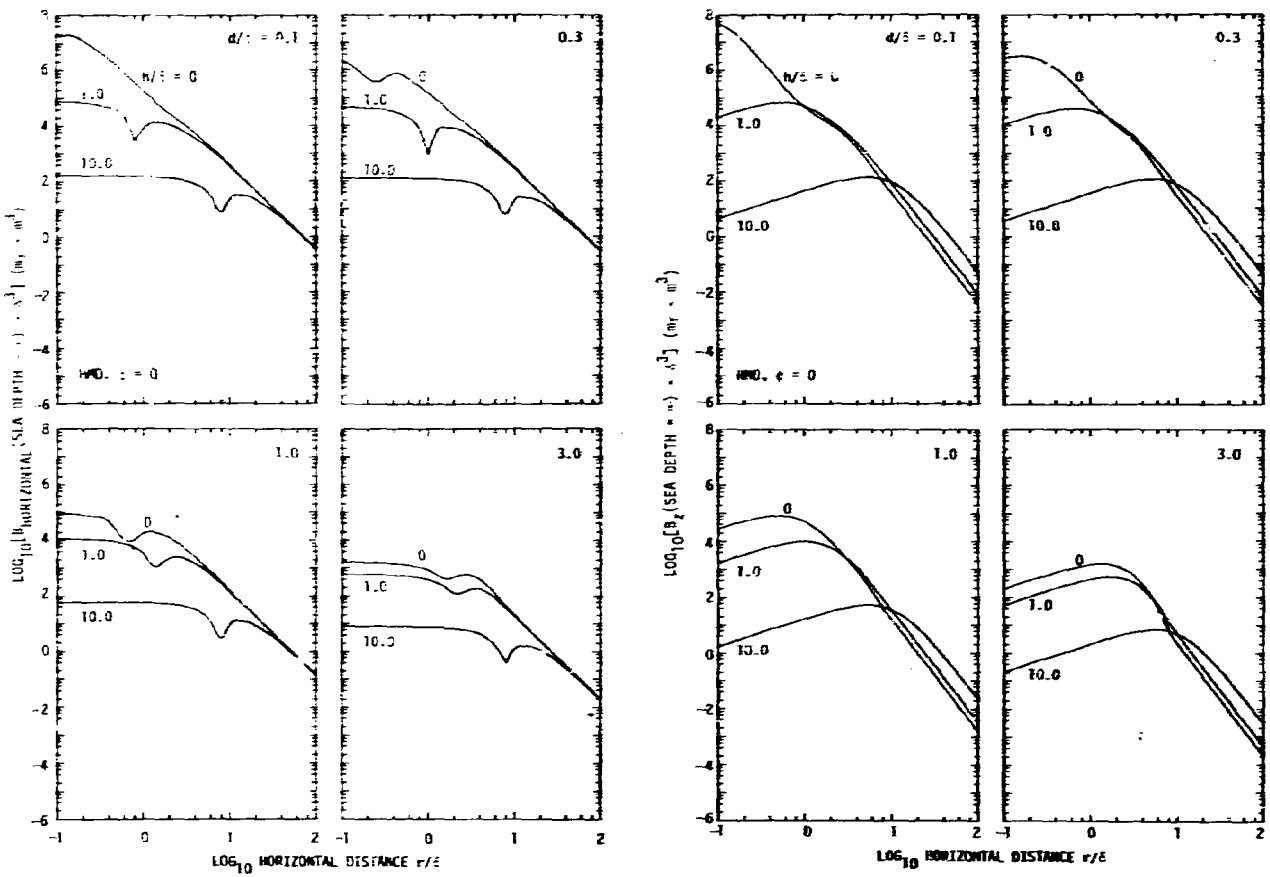

Figure 45. Variation with horizontal distance of the amplitudes of the two magnetic field components $B_{HORIZONTAL}$ and B_Z produced on and above the surface of an infinitely deep sea by a submerged horizontally directed harmonic magnetic dipole (HMD). The fields are given for an azimuthal angle (ϕ) of 0°.

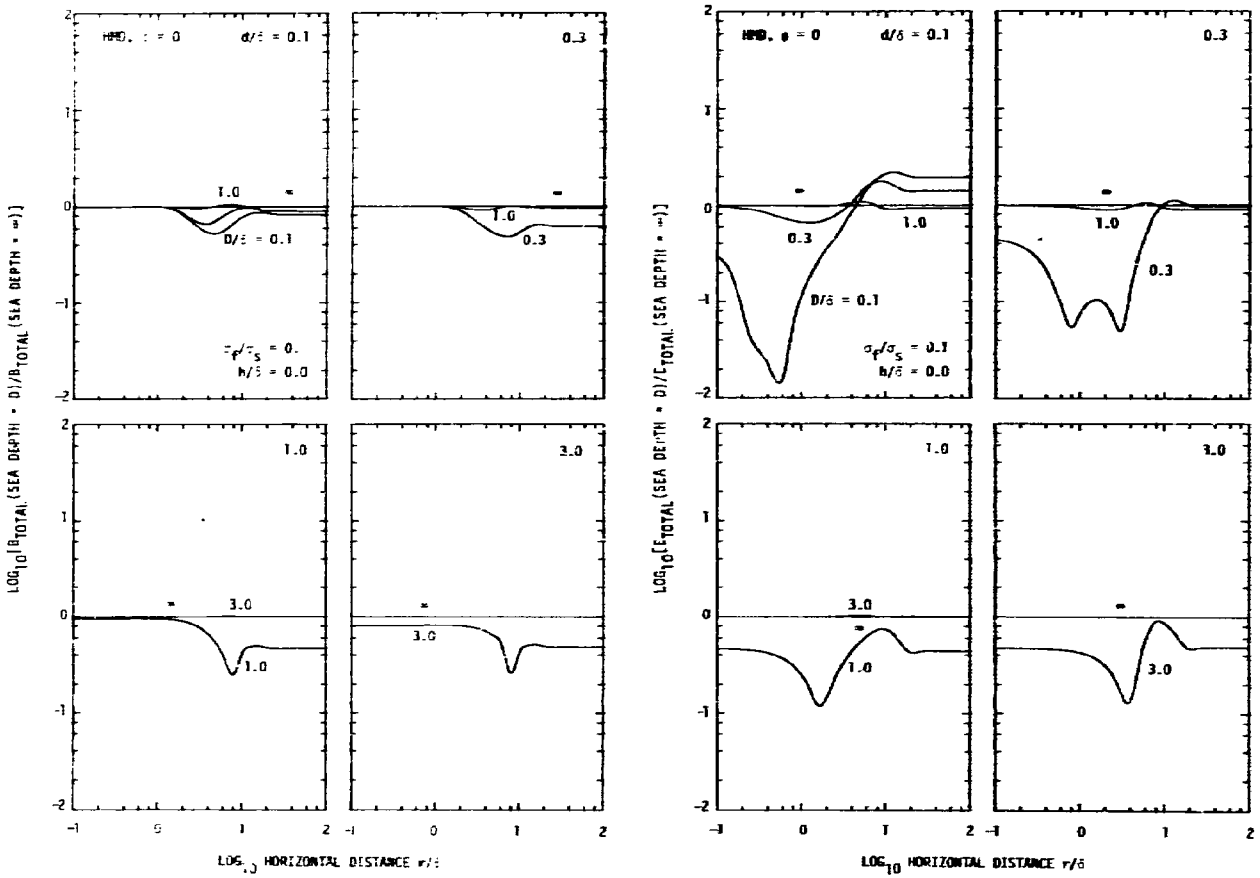

Figure 46. Curves illustrating the changes produced in the surface magnetic and electric field data presented in Figure 44 when an electrically conducting sea floor (conductivity $\sigma_f = 0.1\ \sigma_s$, depth D) is introduced.

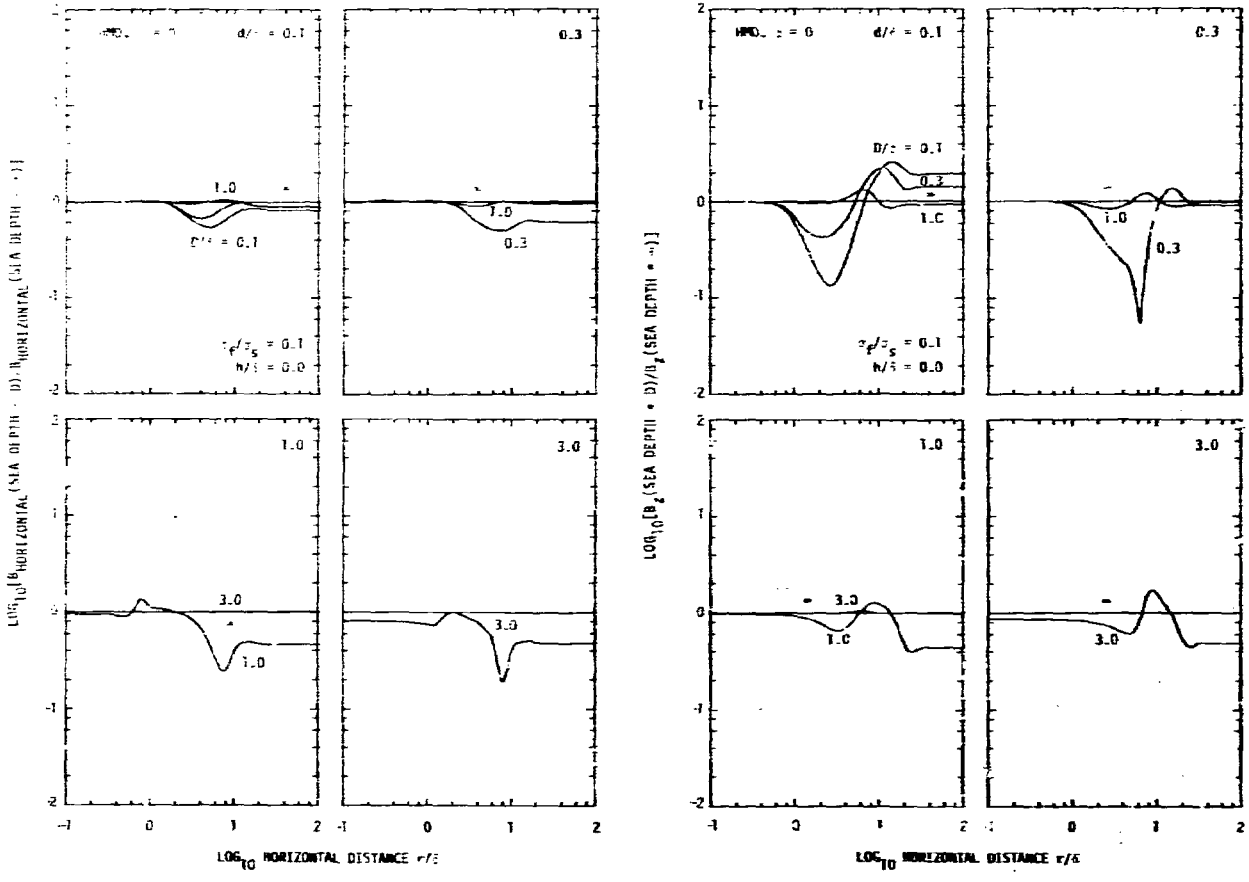

Figure 47. Curves illustrating the changes produced in the surface magnetic field component data plotted in Figure 45 when an electrically conducting sea floor (conductivity $\sigma_f = 0.1\ \sigma_s$, depth D) is introduced.

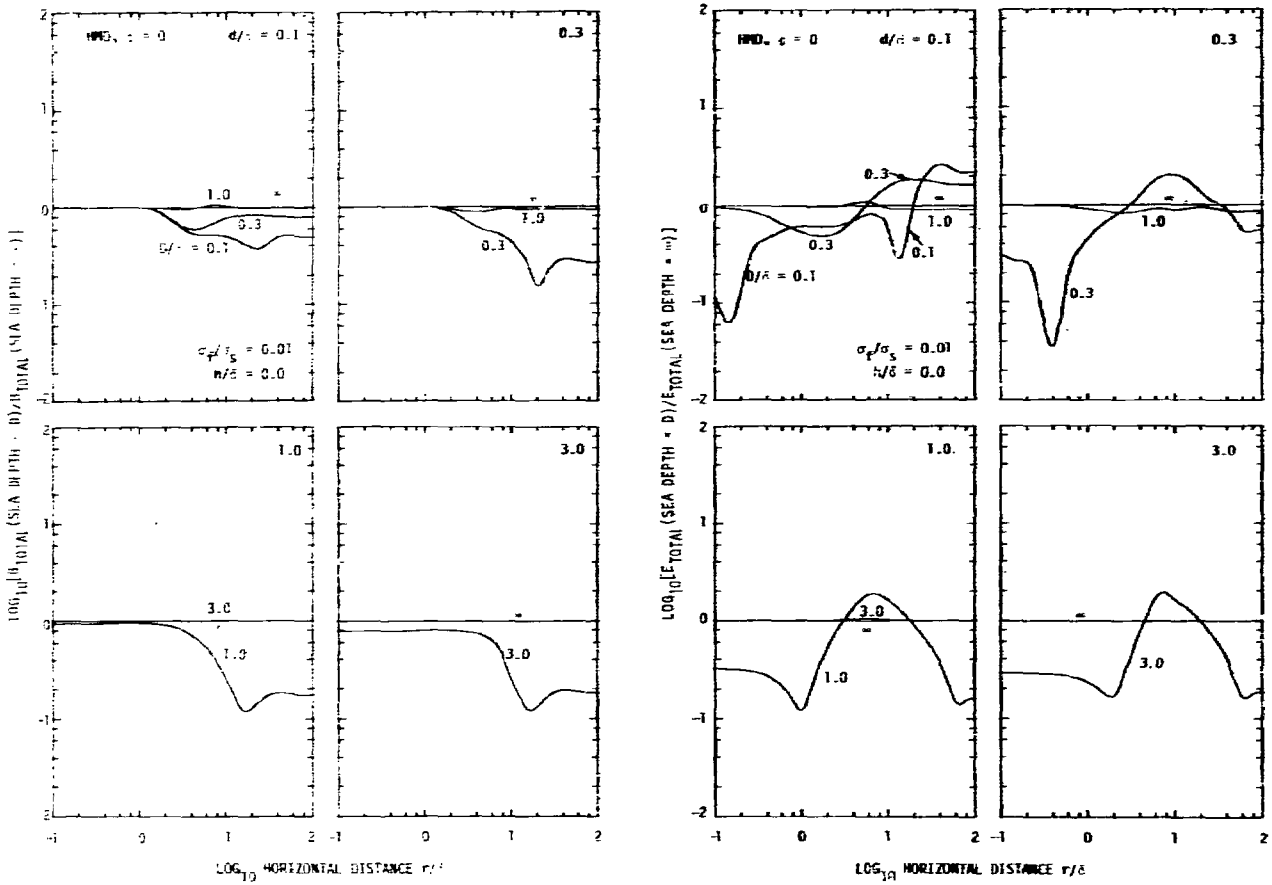

Figure 48. Curves illustrating the changes produced in the surface magnetic and electric field data presented in Figure 44 when an electrically conducting sea floor (conductivity σ_f = 0.01 σ_s, depth D) is introduced. The conductivity of this sea floor is one tenth the conductivity of the sea floor used in Figure 46.

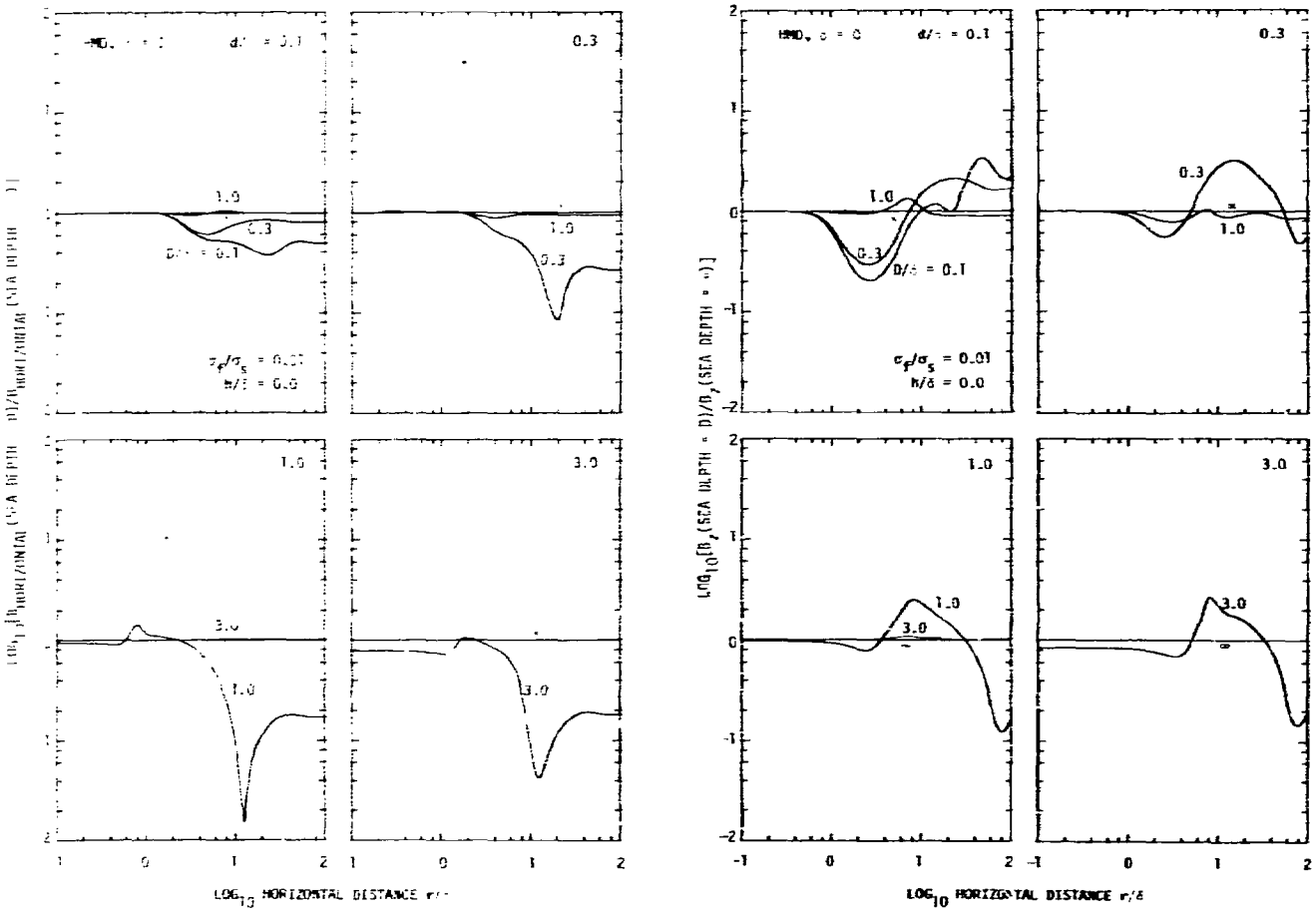

Figure 49. Curves illustrating the changes produced in the surface magnetic field component data presented in Figure 45 when an electrically conducting sea floor (conductivity $\sigma_f = 0.01\ \sigma_s$, depth D) is introduced. The conductivity of this sea floor is one tenth the conductivity of the sea floor used in Figure 47.

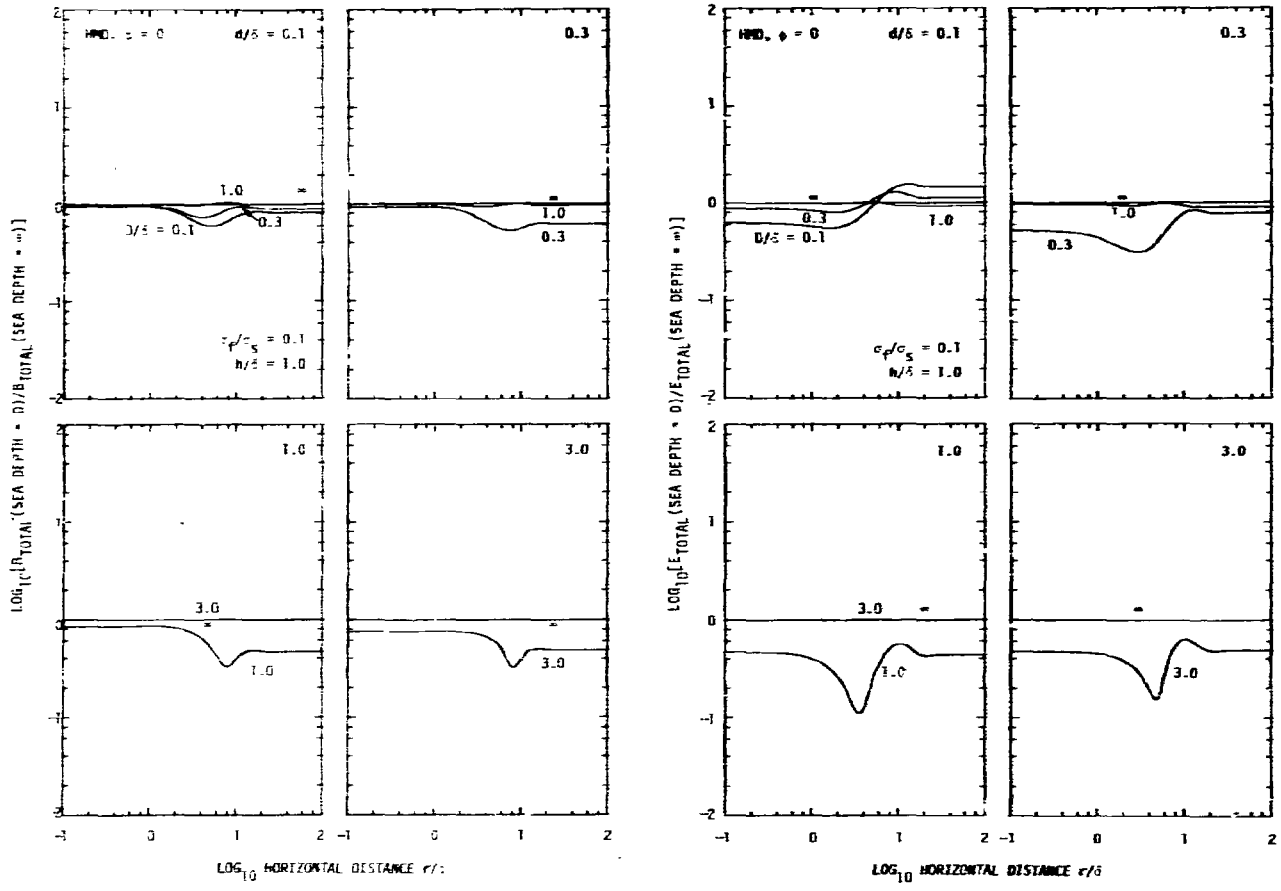

Figure 50. Curves illustrating the changes produced in the magnetic and electric field data presented in Figure 44 for a receiver altitude of one sea water skin depth ($h/\delta = 1.0$) when an electrically conducting sea floor (conductivity $\sigma_f = 0.1\ \sigma_s$, depth D) is introduced.

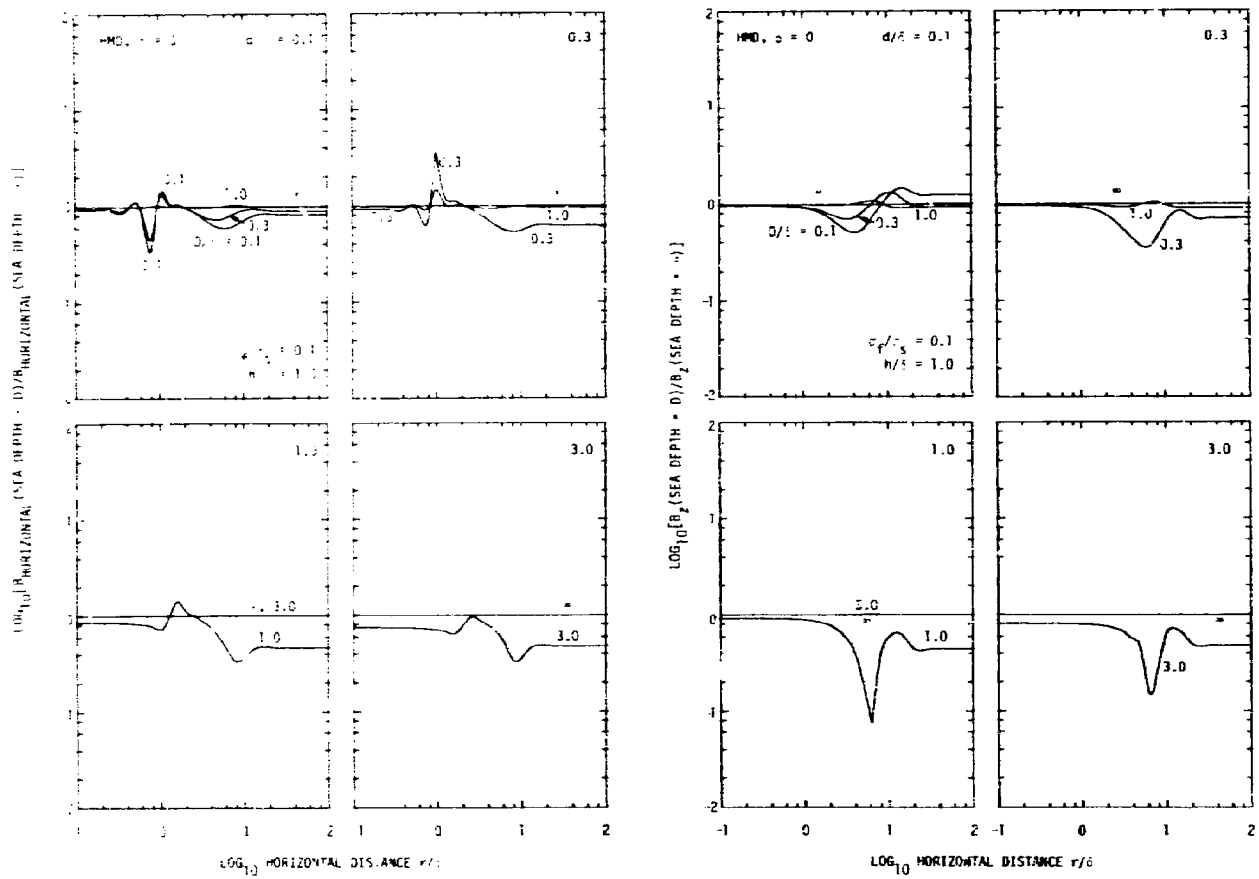

Figure 51. Curves illustrating the changes produced in the magnetic field component data presented in Figure 45 for a receiver altitude of one sea water skin depth ($h/\delta = 1.0$) when an electrically conducting sea floor (conductivity $\sigma_f = 0.1\ \sigma_s$, depth D) is introduced.

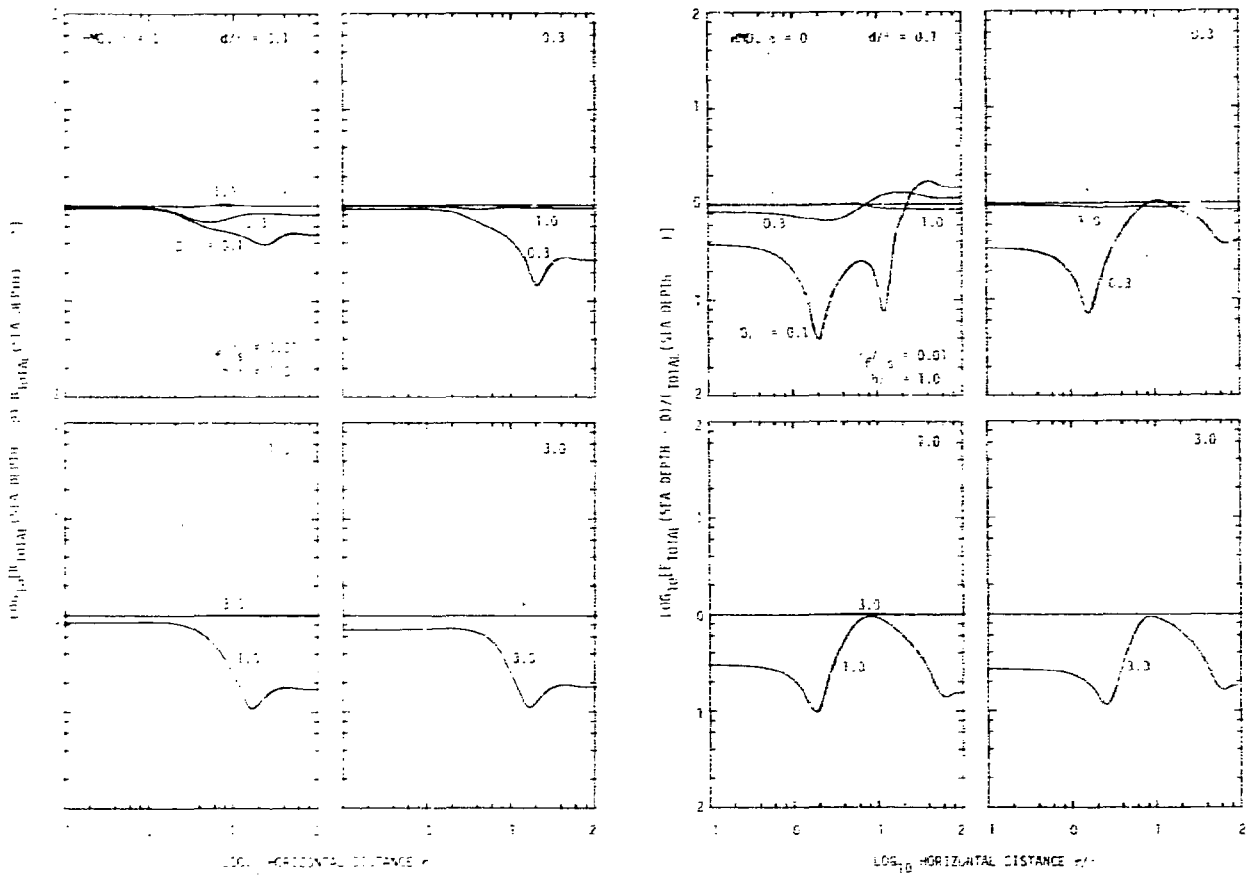

Figure 52. Curves illustrating the changes produced in the magnetic and electric field data presented in Figure 44 for a receiver altitude of one sea water skin depth ($h/\delta = 1.0$) when an electrically conducting sea floor (conductivity $\sigma_f = 0.01\ \sigma_s$, depth D) is introduced. The conductivity of this sea floor is one tenth the conductivity of the sea floor used in Figure 50.

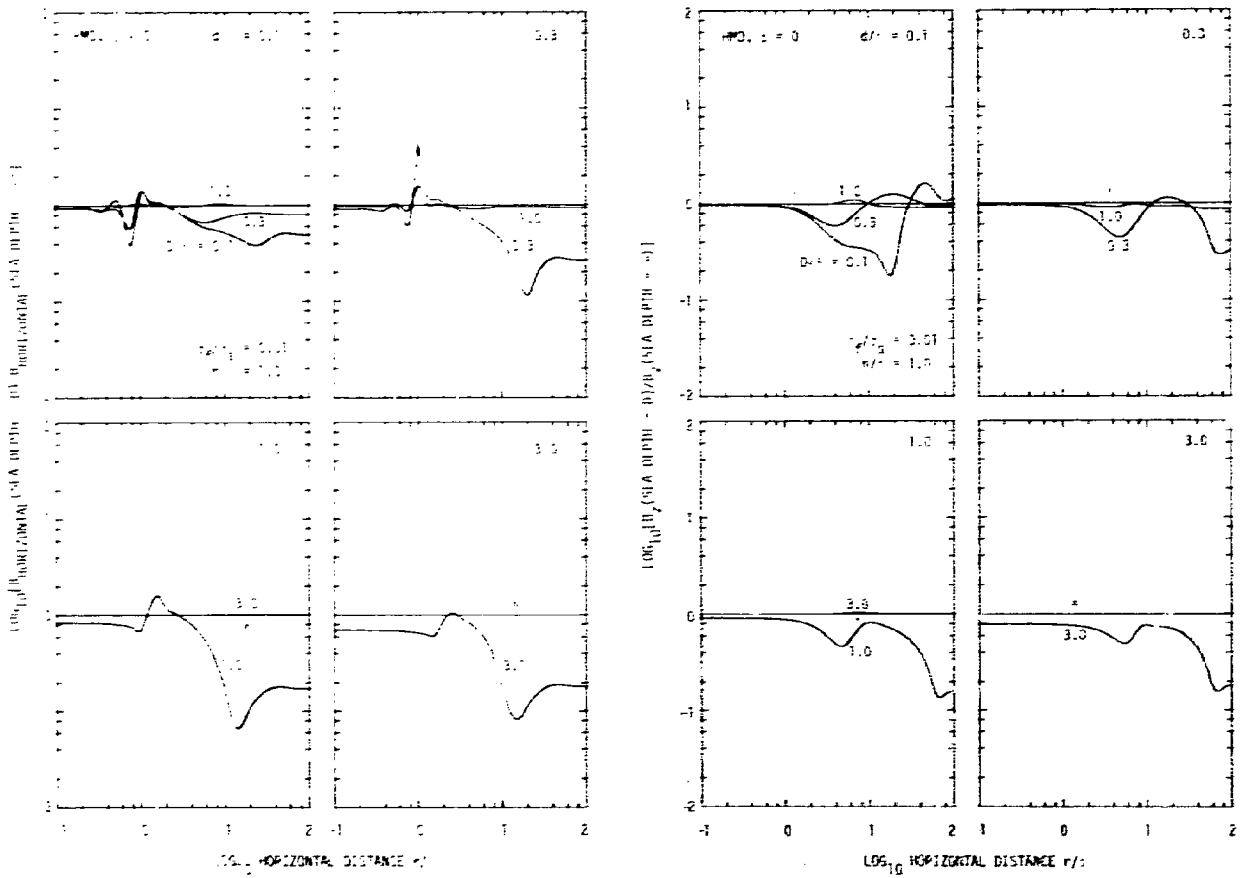

Figure 53. Curves illustrating the changes produced in the magnetic field component data presented in Figure 45 for a receiver altitude of one sea water skin depth ($h/\delta = 1.0$) when an electrically conducting sea floor (conductivity $\sigma_f = 0.01\ \sigma_s$, depth D) is introduced. The conductivity of this sea floor is one tenth the conductivity of the sea floor used in Figure 51.

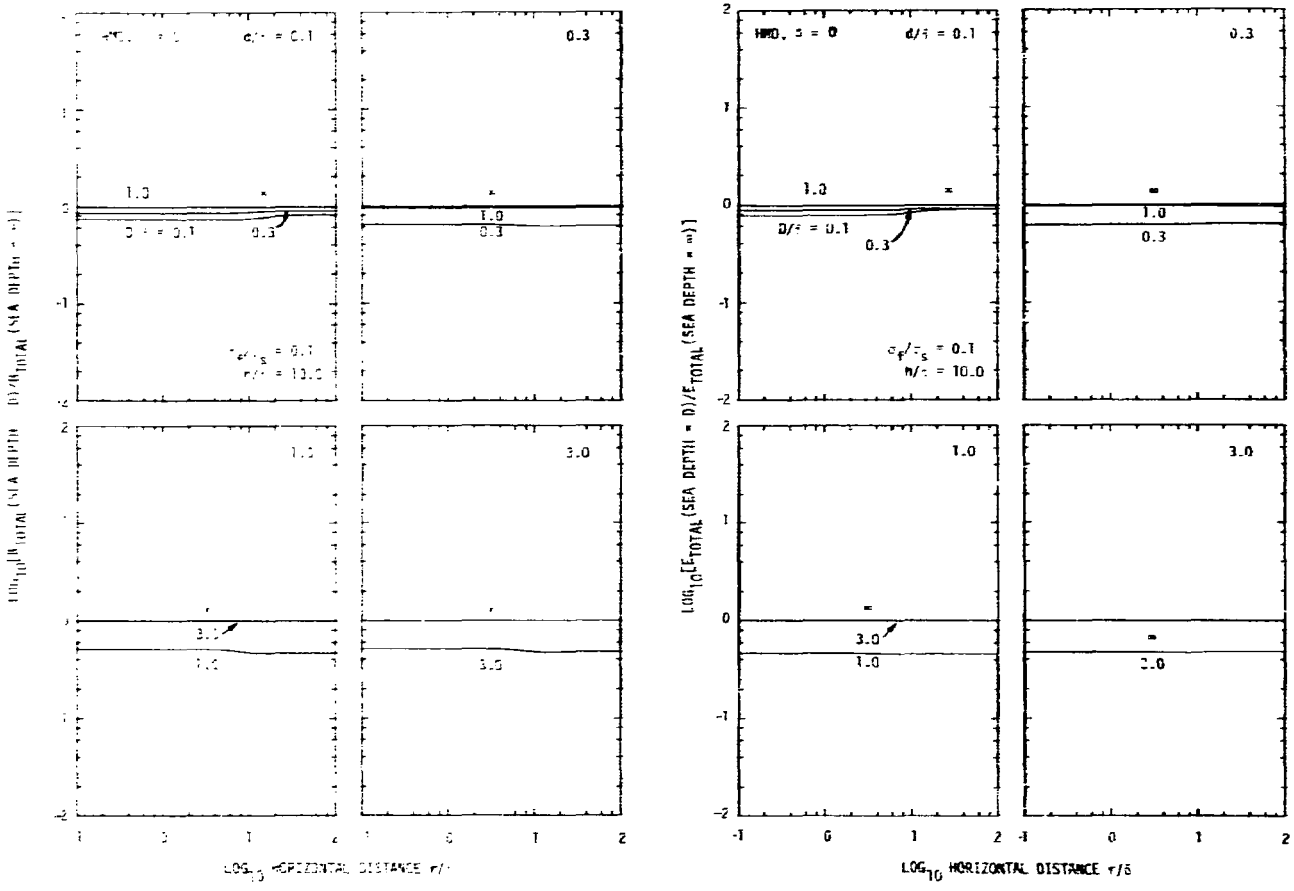

Figure 54. Curves illustrating the changes produced in the magnetic and electric field data presented in Figure 44 for a receiver altitude of ten sea water skin depths ($h/\delta = 10.0$) when an electrically conducting sea floor (conductivity $\sigma_f = 0.1\ \sigma_s$, depth D) is introduced.

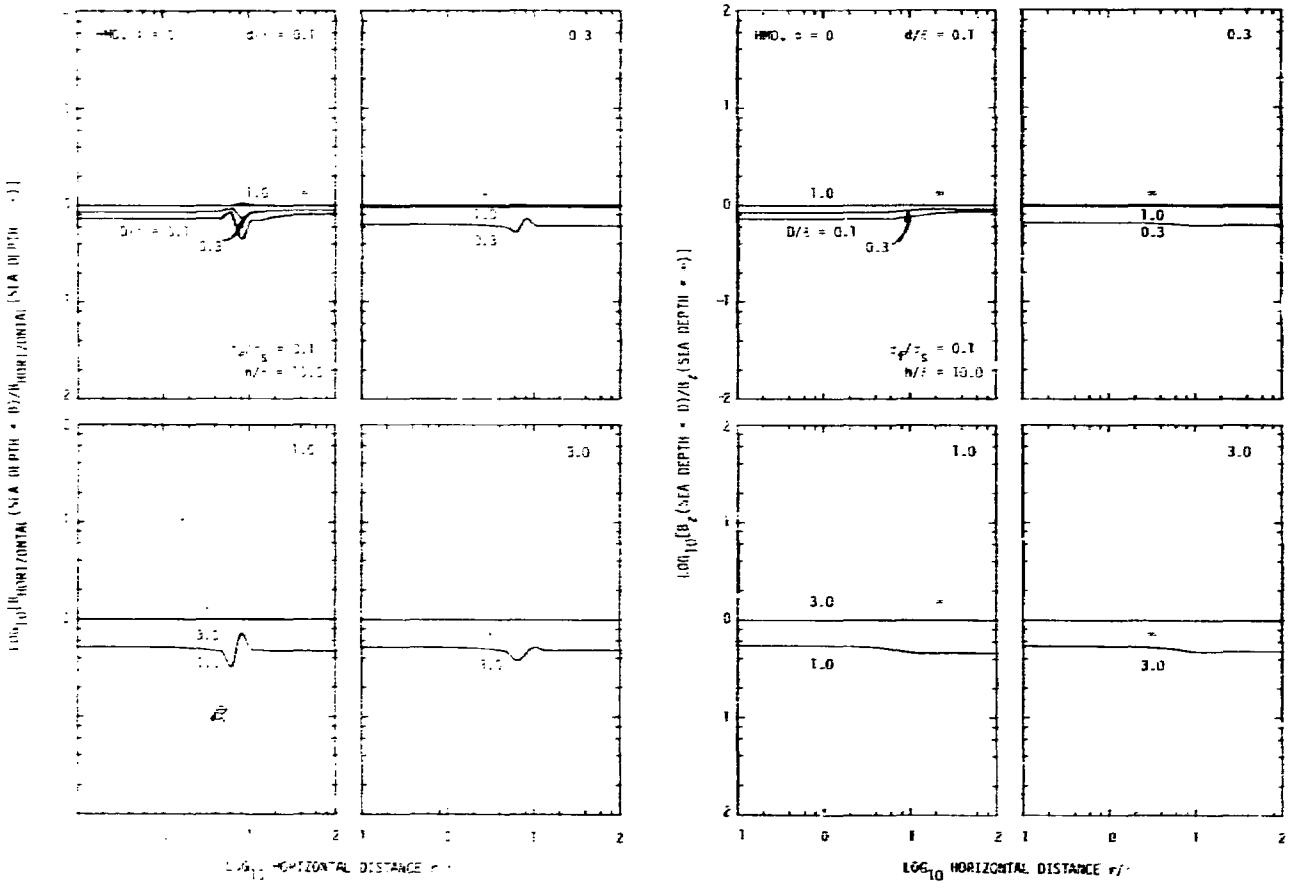

Figure 55. Curves illustrating the changes produced in the magnetic field component data presented in Figure 45 for a receiver altitude of ten sea water skin depths ($h/\delta = 10.0$) when an electrically conducting sea floor (conductivity $\sigma_f = 0.1\ \sigma_s$, depth D) is introduced.

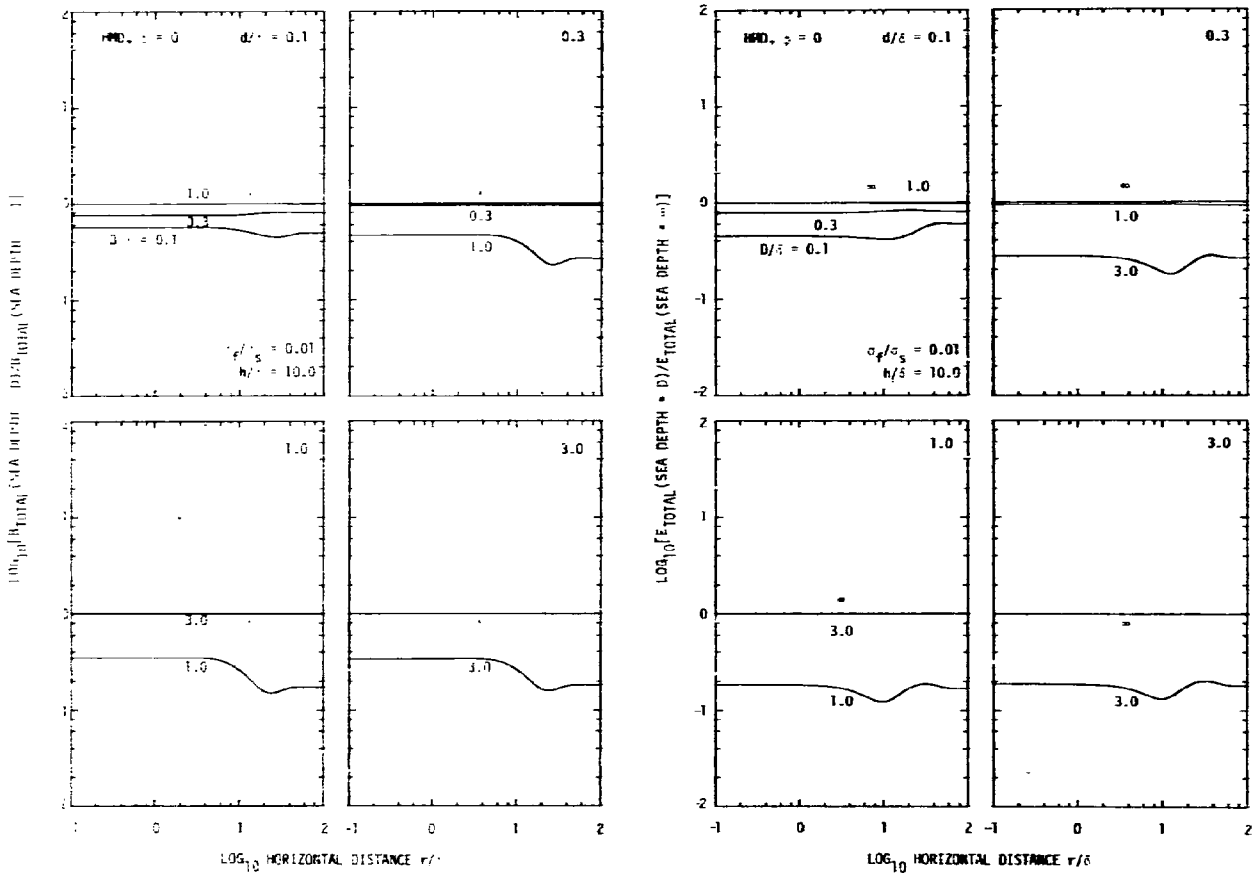

Figure 56. Curves illustrating the changes produced in the magnetic and electric field data presented in Figure 44 for a receiver altitude of ten sea water skin depths ($h/\delta = 10.0$) when an electrically conducting sea floor (conductivity $\sigma_f = 0.01\ \sigma_s$, depth D) is introduced. The conductivity of this sea floor is one tenth the conductivity of the sea floor used in Figure 54.

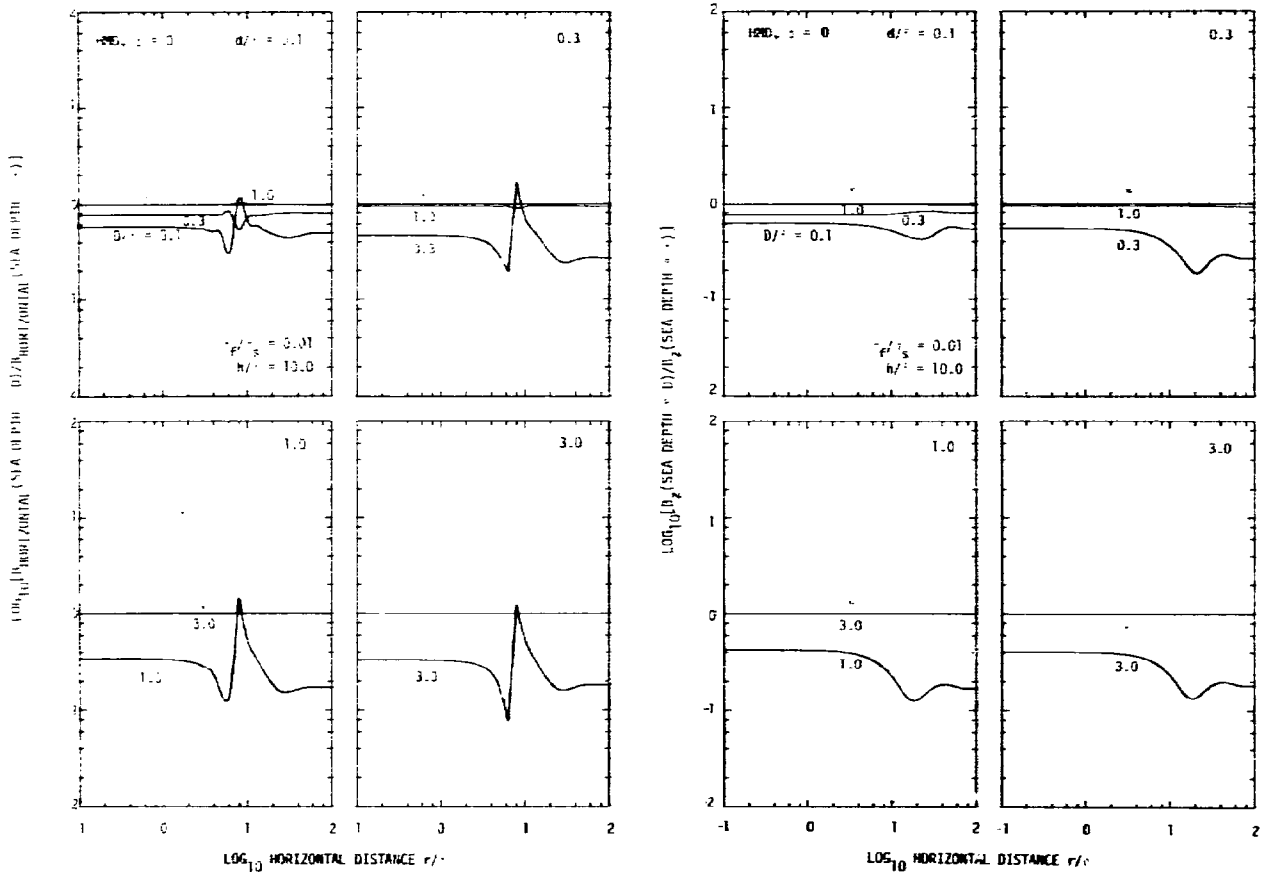

Figure 57. Curves illustrating the changes produced in the magnetic field component data presented in Figure 45 for a receiver altitude of ten sea water skin depths ($h/\delta = 10.0$) when an electrically conducting sea floor (conductivity $\sigma_f = 0.01\ \sigma_s$, depth D) is introduced. The conductivity of this sea floor is one tenth the conductivity of the sea floor used in Figure 55.

Figures for the

HORIZONTAL MAGNETIC DIPOLE, $\phi = 90°$

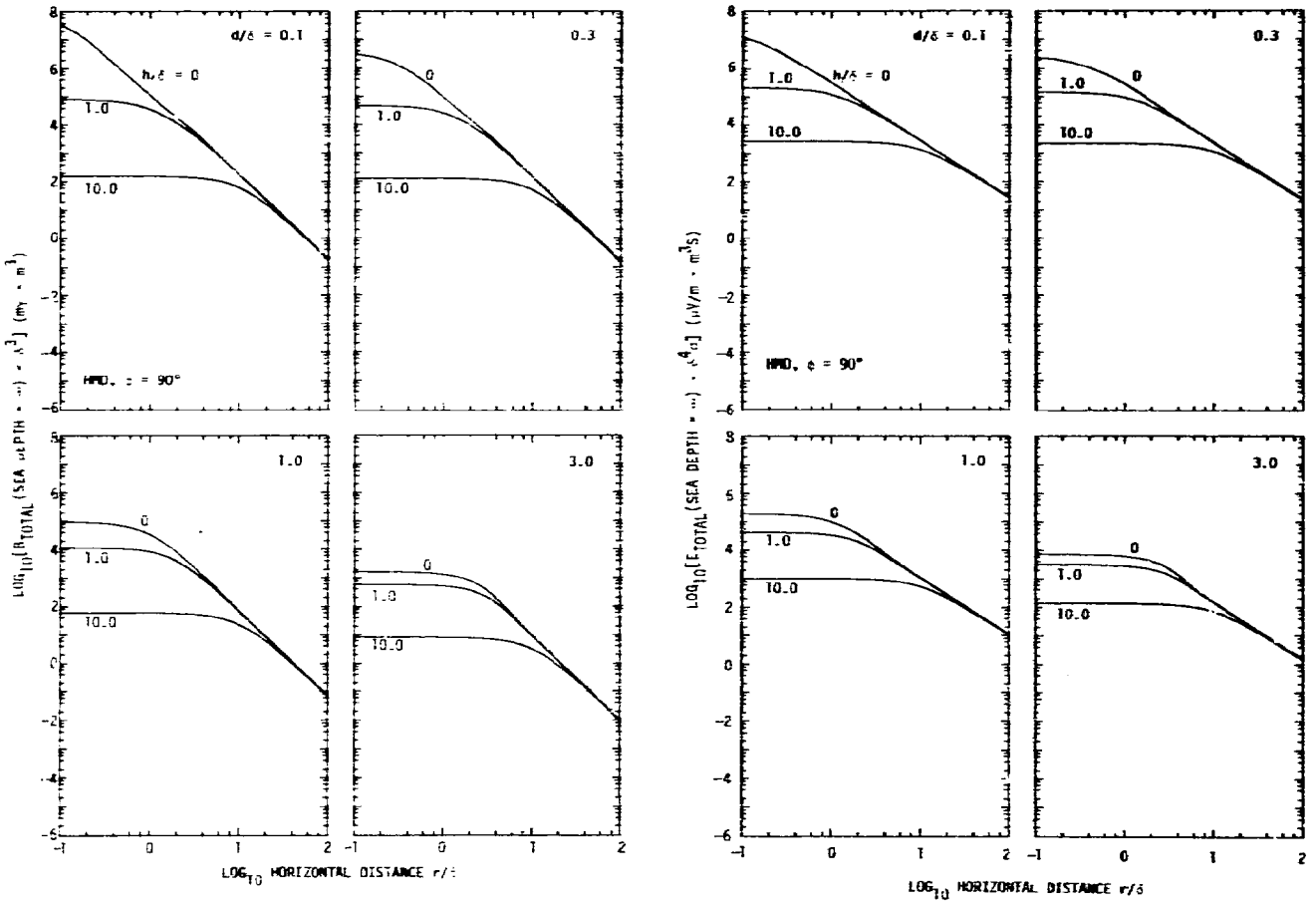

Figure 58. Variation with horizontal distance of the amplitudes of the total magnetic (B_{TOTAL}) and electric (E_{TOTAL}) fields produced on and above the surface of an infinitely deep sea by a submerged horizontally directed magnetic dipole (HMD). The fields are given for an azimuthal angle (ϕ) of 90°.

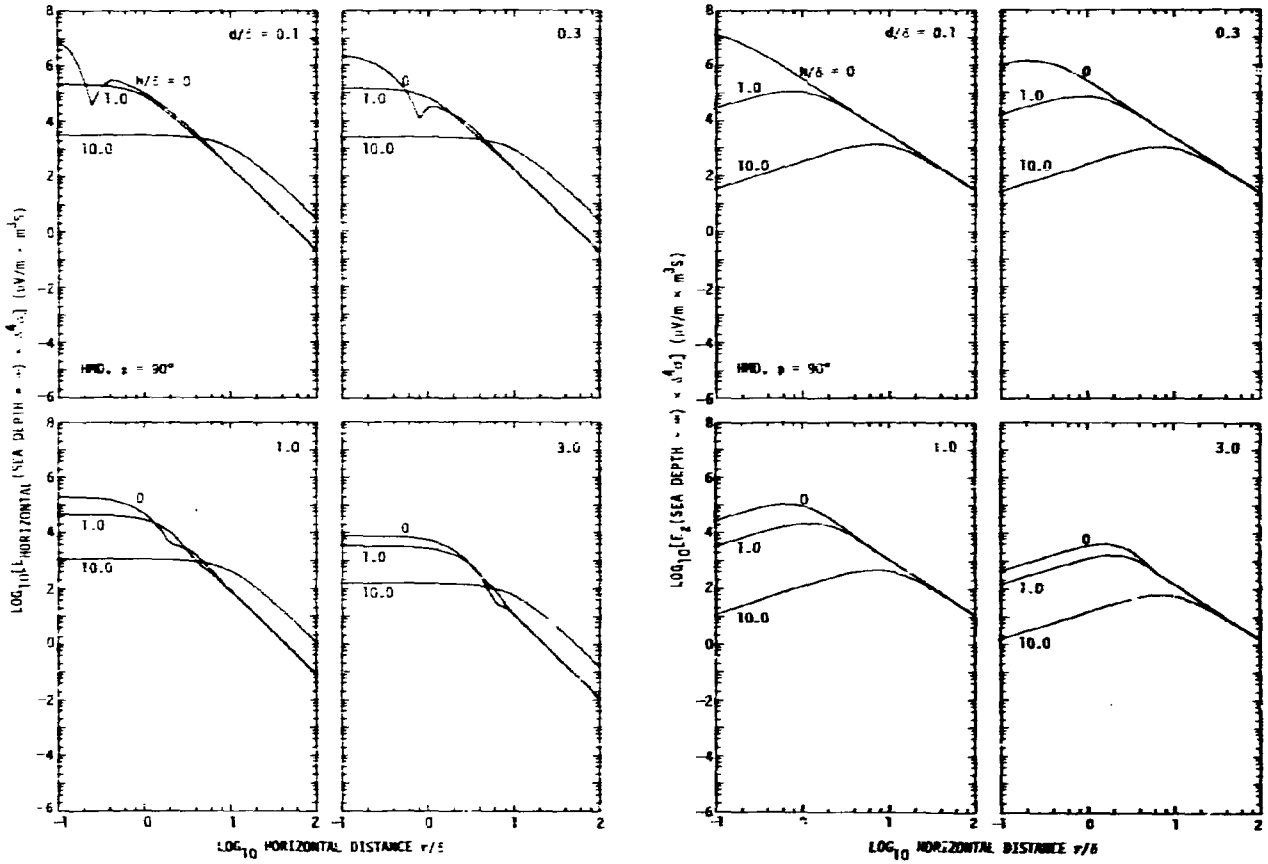

Figure 59. Variation with horizontal distance of the amplitude of the two electric field components $E_{HORIZONTAL}$ and E_z produced on and above the surface of an infinitely deep sea by a submerged horizontally directed harmonic magnetic dipole (HMD). The fields are given for an azimuthal angle (ϕ) of 90°.

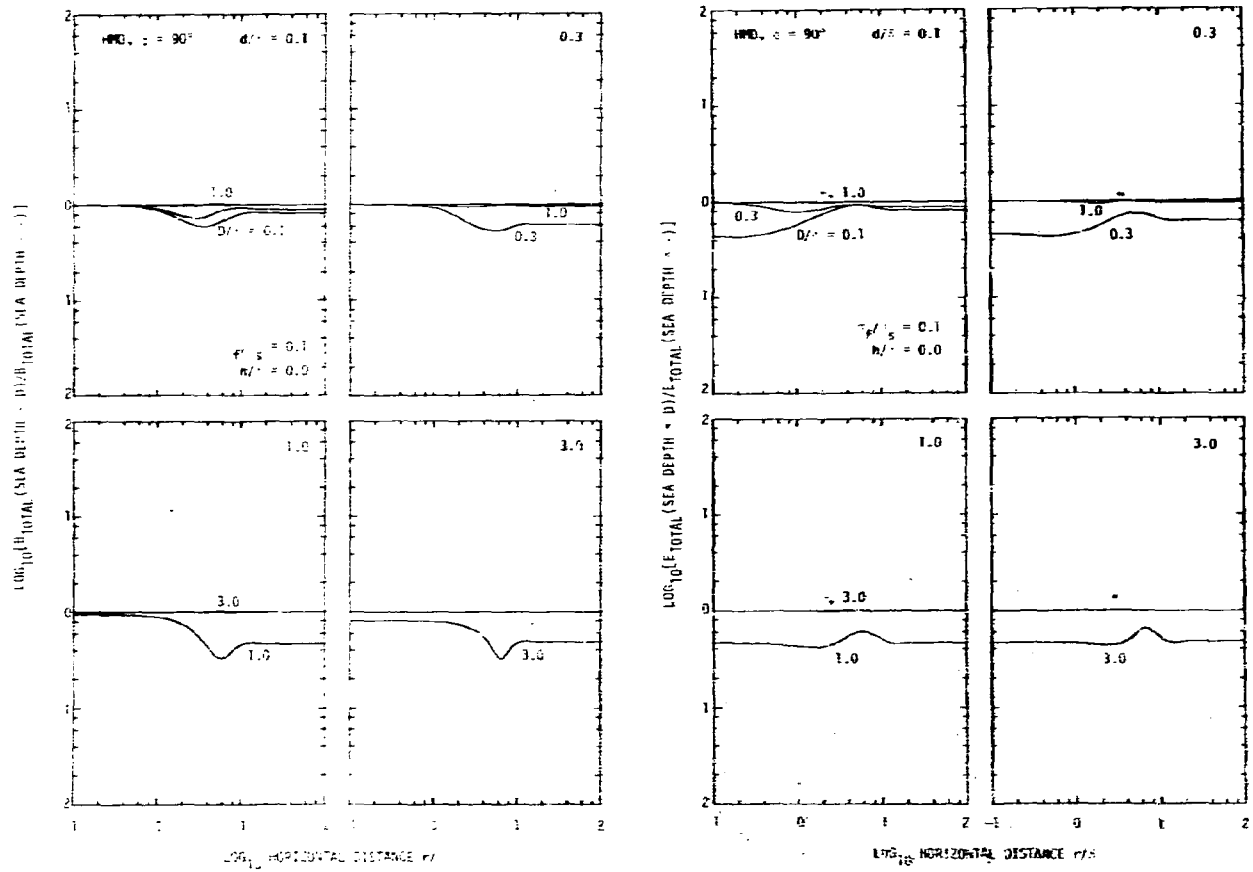

Figure 60. Curves illustrating the changes produced in the surface magnetic and electric field data presented in Figure 58 when an electrically conducting sea floor (conductivity $\sigma_f = 0.1\ \sigma_s$, depth D) is introduced.

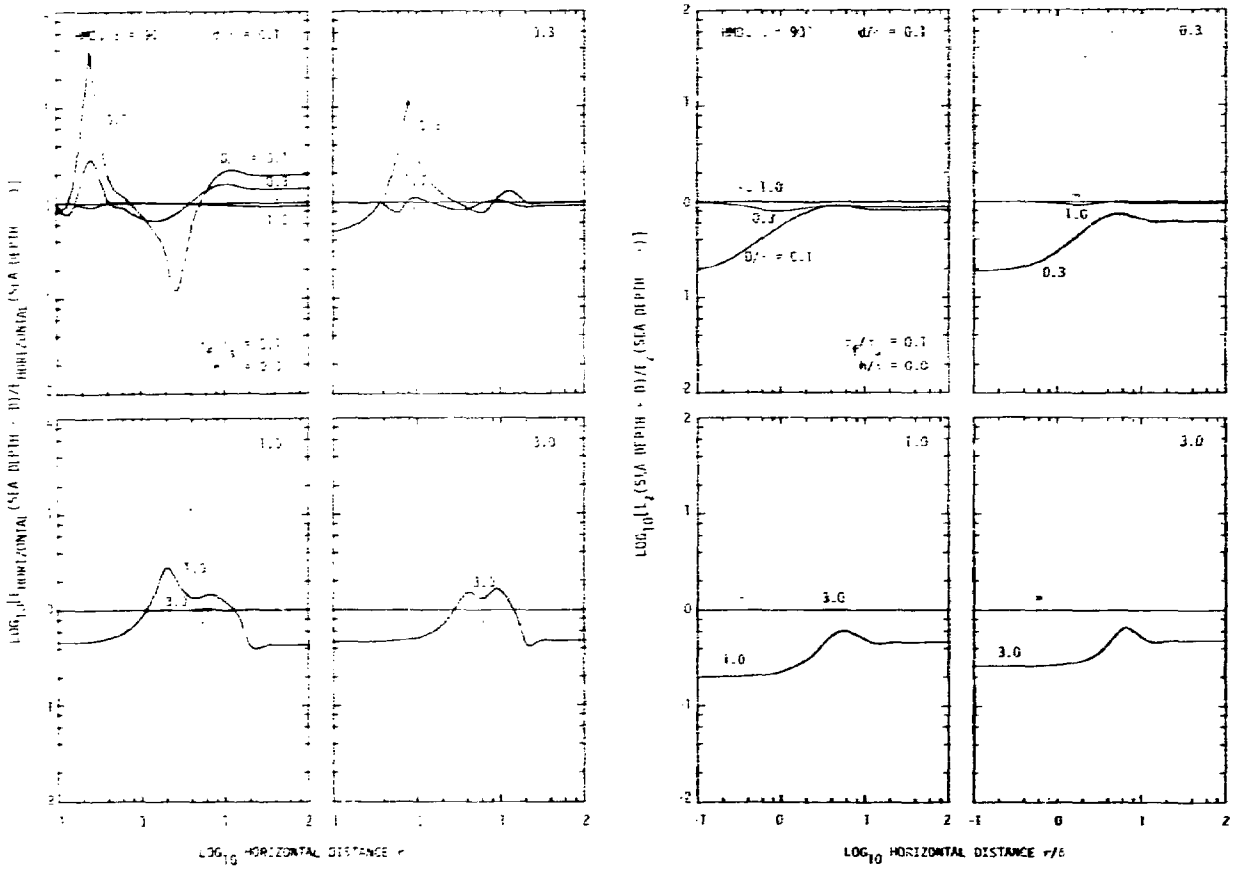

Figure 61. Curves illustrating the changes produced in the surface electric field component data plotted in Figure 59 when an electrically conducting sea floor (conductivity $\sigma_f = 0.1\ \sigma_s$, depth D) is introduced.

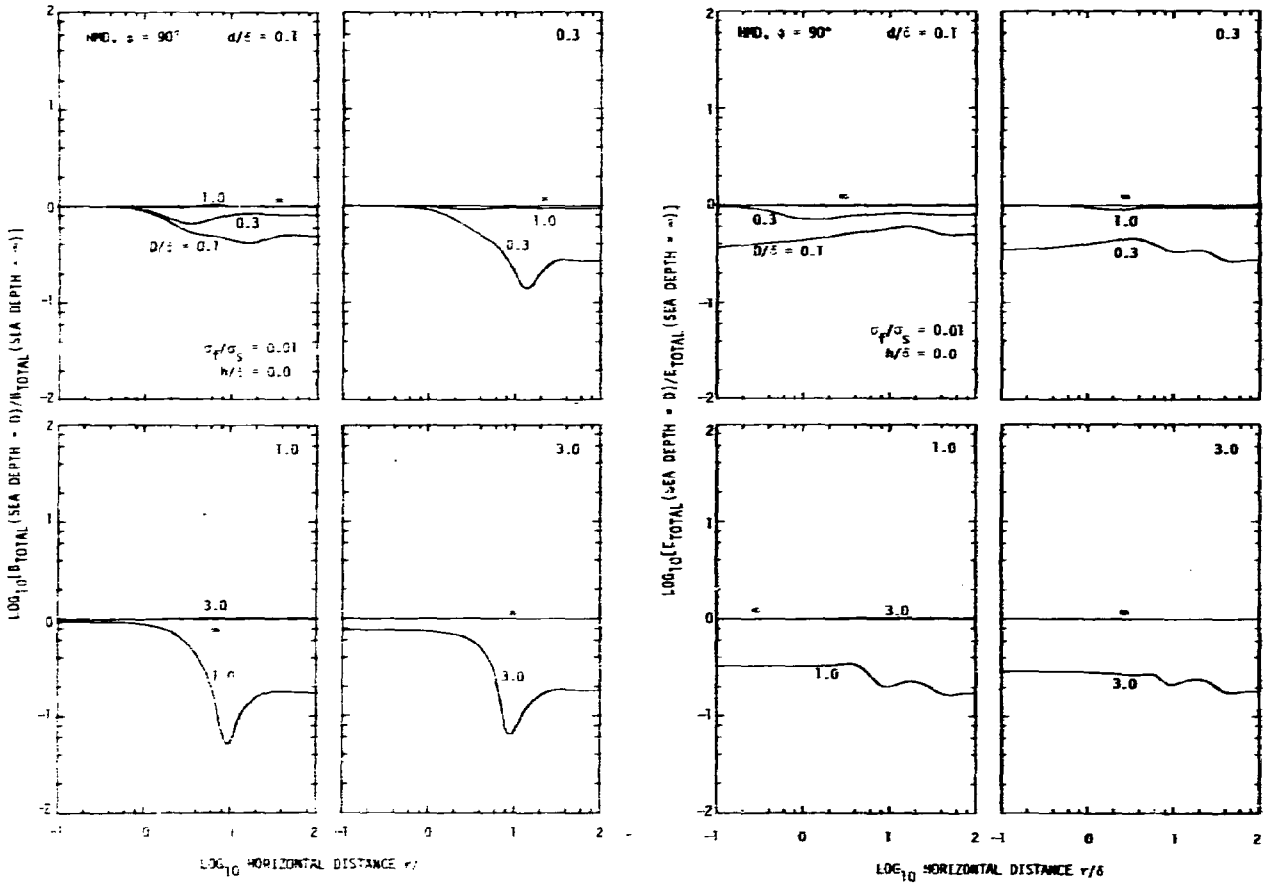

Figure 52. Curves illustrating the changes produced in the surface magnetic and electric field data presented in Figure 58 when an electrically conducting sea floor (conductivity $\sigma_f = 0.01\ \sigma_s$, depth D) is introduced. The conductivity of this sea floor is one tenth the conductivity of the sea floor used in Figure 60.

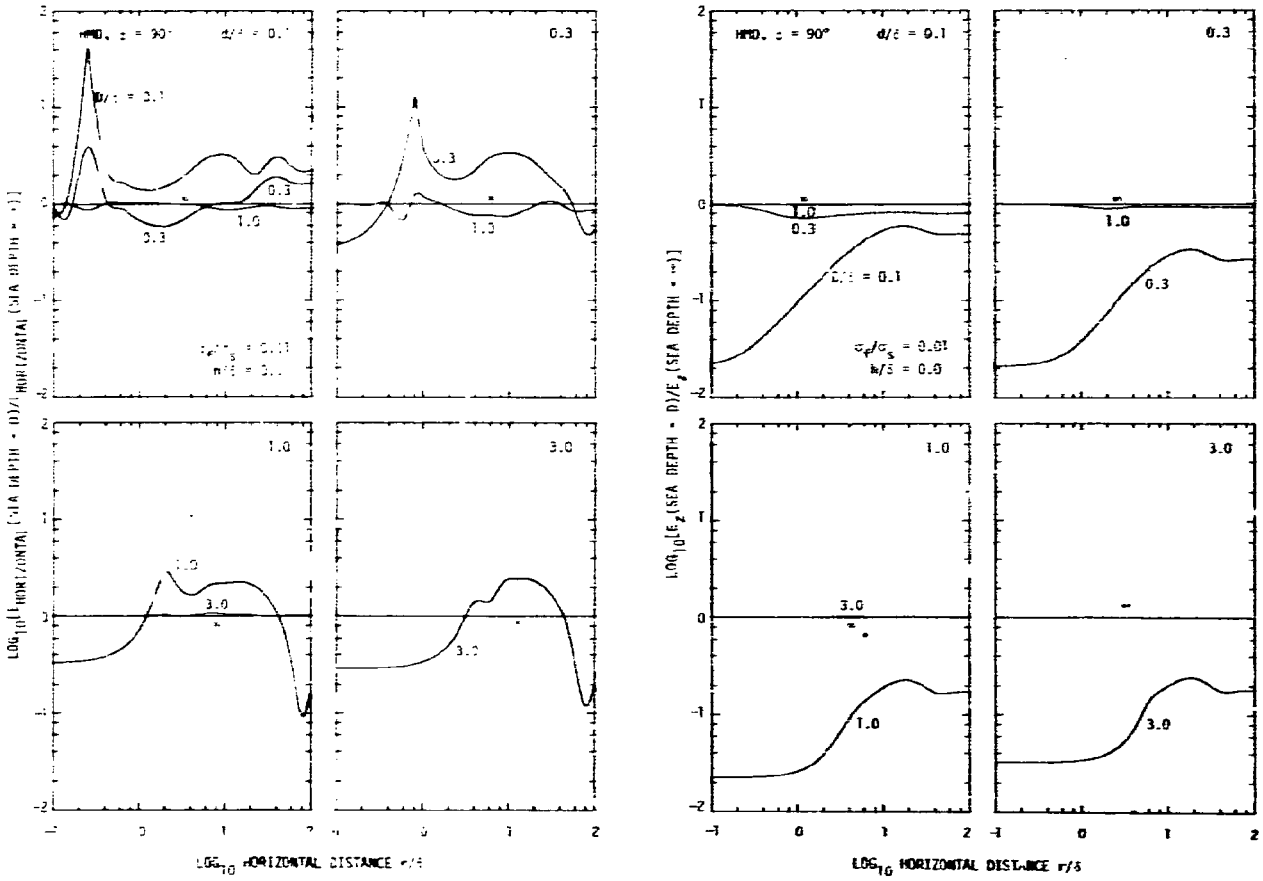

Figure 63. Curves illustrating the changes produced in the surface electric field component data presented in Figure 59 when an electrically conducting sea floor (conductivity $\sigma_f = 0.01\ \sigma_s$, depth D) is introduced. The conductivity of this sea floor is one tenth the conductivity of the sea floor used in Figure 61.

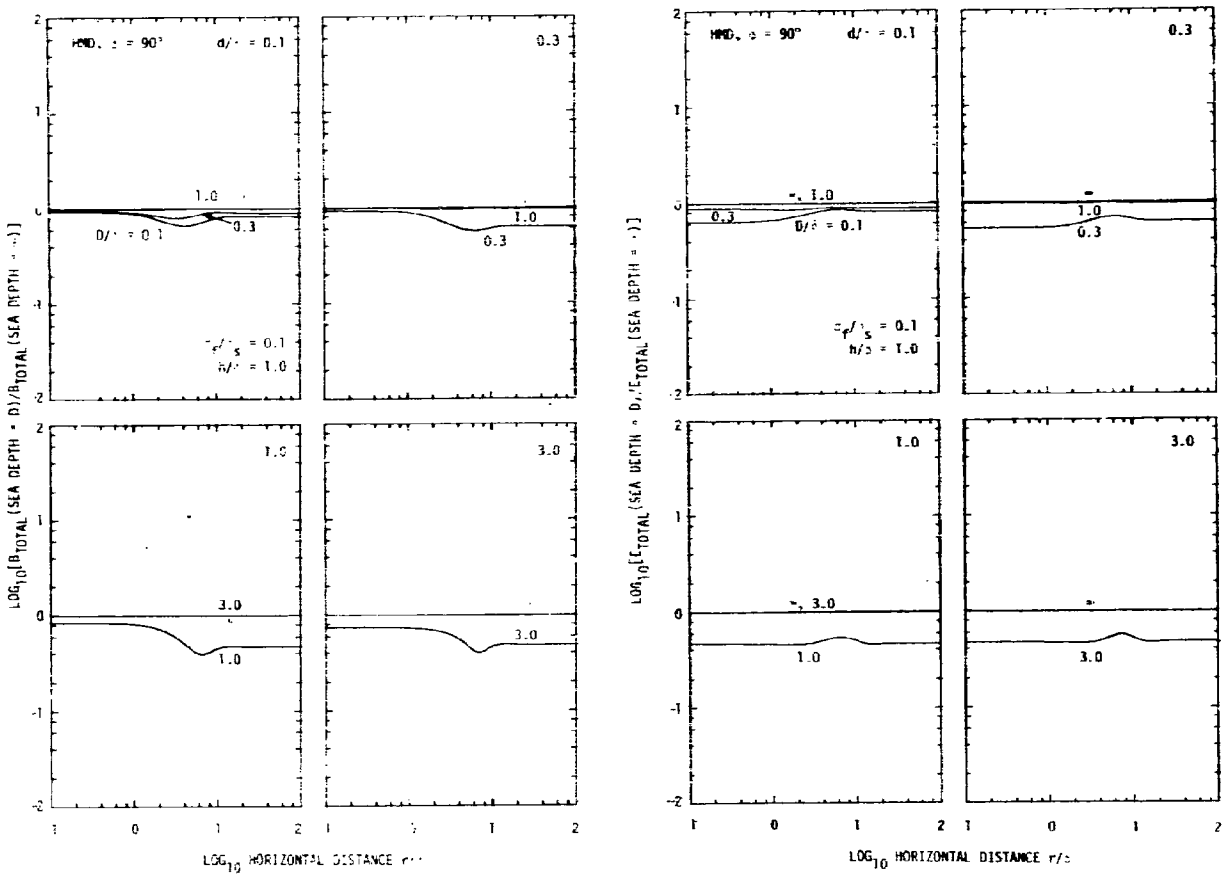

Figure 64. Curves illustrating the changes produced in the magnetic and electric field data presented in Figure 58 for a receiver altitude of one sea water skin depth ($h/\delta = 1.0$) when an electrically conducting sea floor (conductivity $\sigma_f = 0.1\ \sigma_s$, depth D) is introduced.

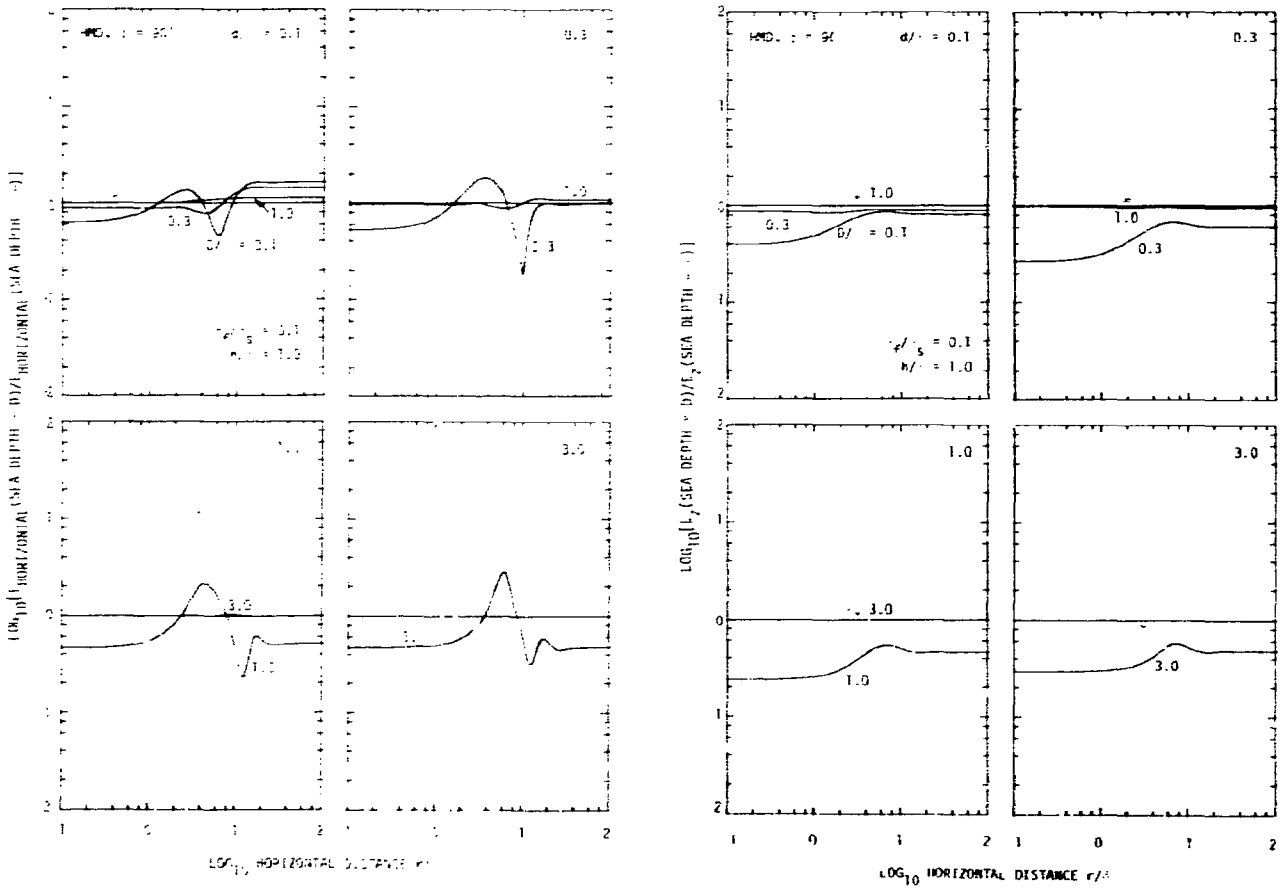

Figure 65. Curves illustrating the changes produced in the electric field component data presented in Figure 59 for a receiver altitude of one sea water skin depth ($h/\delta = 1.0$) when an electrically conducting sea floor (conductivity $\sigma_f = 0.1\ \sigma_s$, depth D) is introduced.

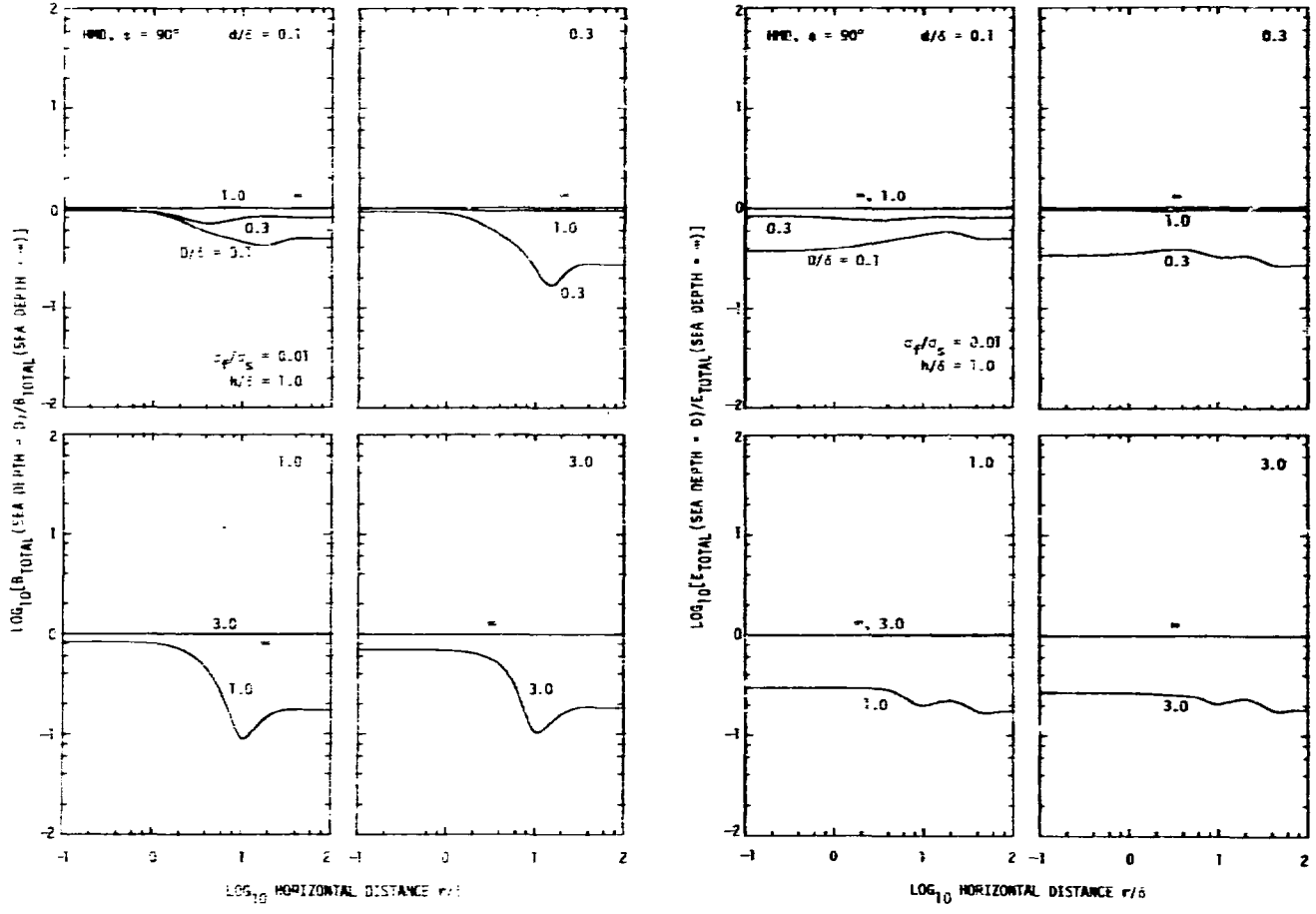

Figure 66. Curves illustrating the changes produced in the magnetic and electric field data presented in Figure 58 for a receiver altitude of one sea water skin depth ($h/\delta = 1.0$) when an electrically conducting sea floor (conductivity $\sigma_f = 0.01\ \sigma_s$, depth D) is introduced. The conductivity of this sea floor is one tenth the conductivity of the sea floor used in Figure 64.

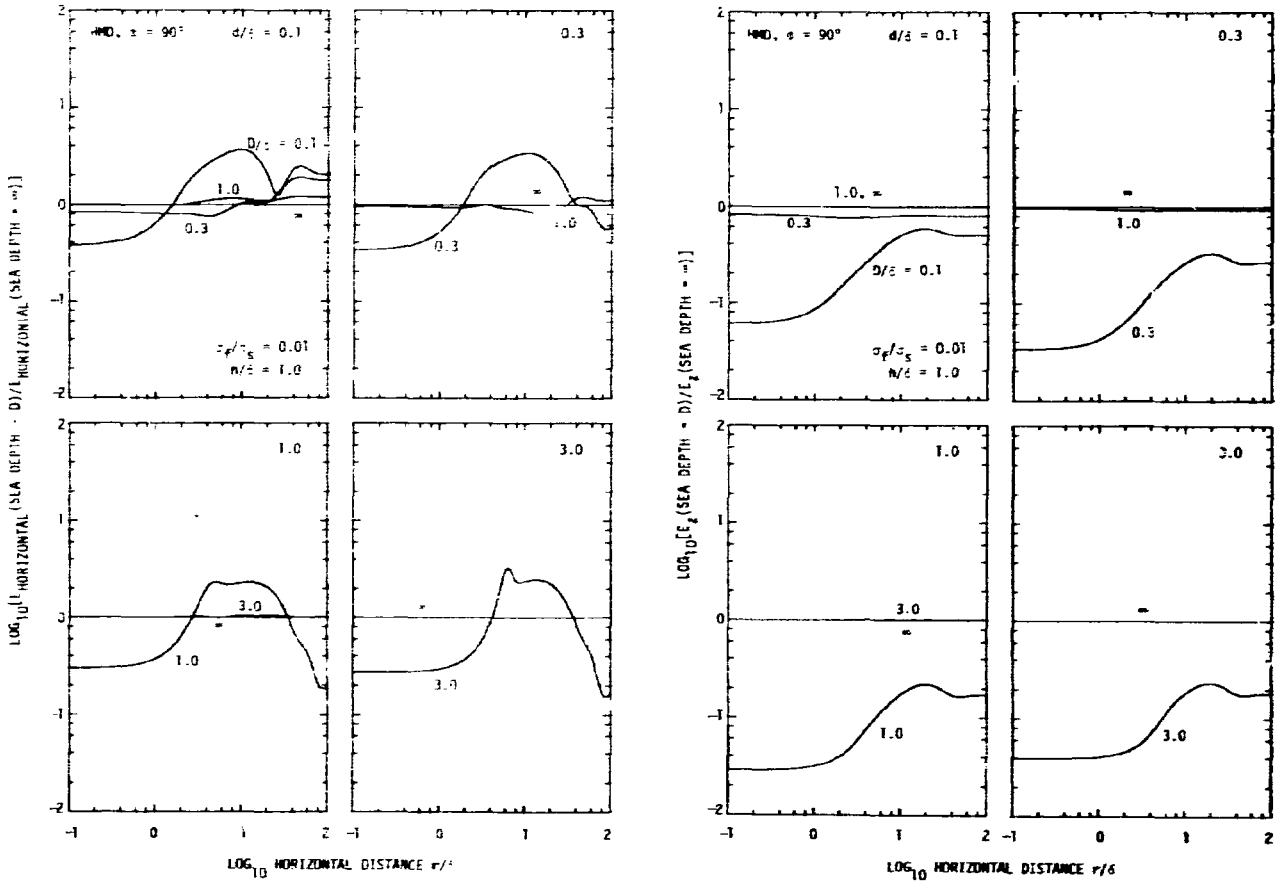

Figure 67. Curves illustrating the changes produced in the electric field component data presented in Figure 59 for a receiver altitude of one sea water skin depth ($h/\delta = 1.0$) when an electrically conducting sea floor (conductivity $\sigma_f = 0.01\ \sigma_s$, depth D) is introduced. The conductivity of this sea floor is one tenth the conductivity of the sea floor used in Figure 65.

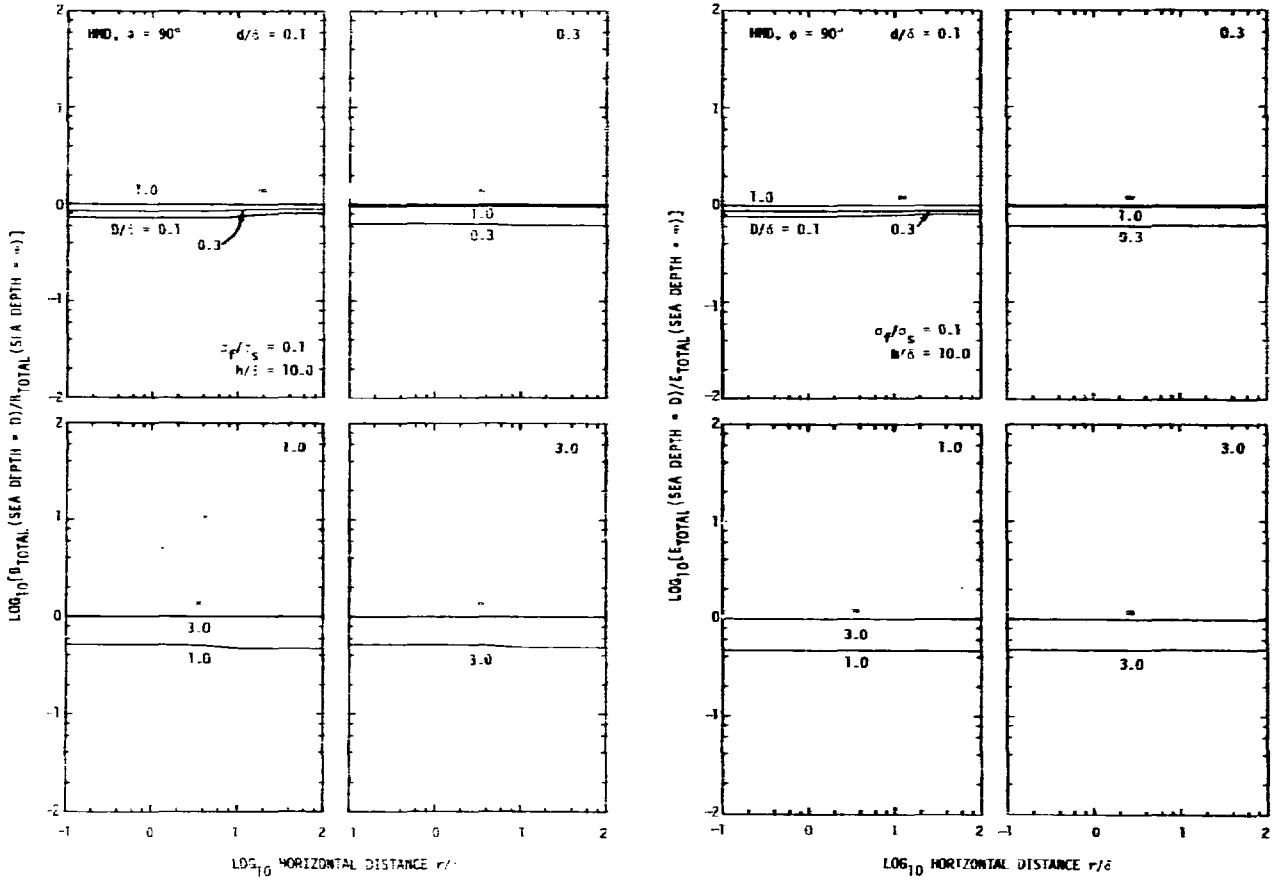

Figure 68. Curves illustrating the changes produced in the magnetic and electric field data presented in Figure 58 for a receiver altitude of ten sea water skin depths ($h/\delta = 10.0$) when an electrically conducting sea floor (conductivity $\sigma_f = 0.1\ \sigma_s$, depth D) is introduced.

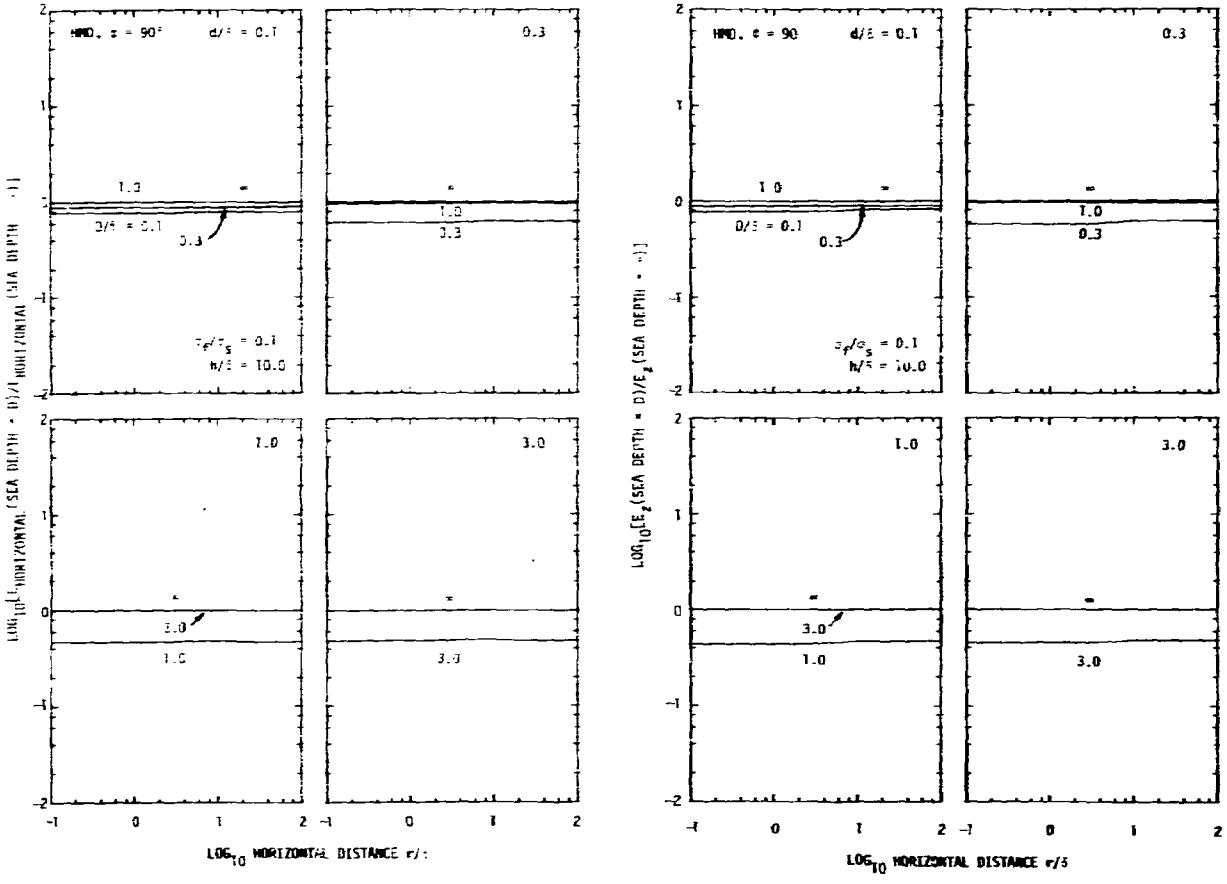

Figure 69. Curves illustrating the changes produced in the electric field component data presented in Figure 59 for a receiver altitude of ten sea water skin depths ($h/\delta = 10.0$) when an electrically conducting sea floor (conductivity $\sigma_f = 0.1\ \sigma_s$, depth D) is introduced.

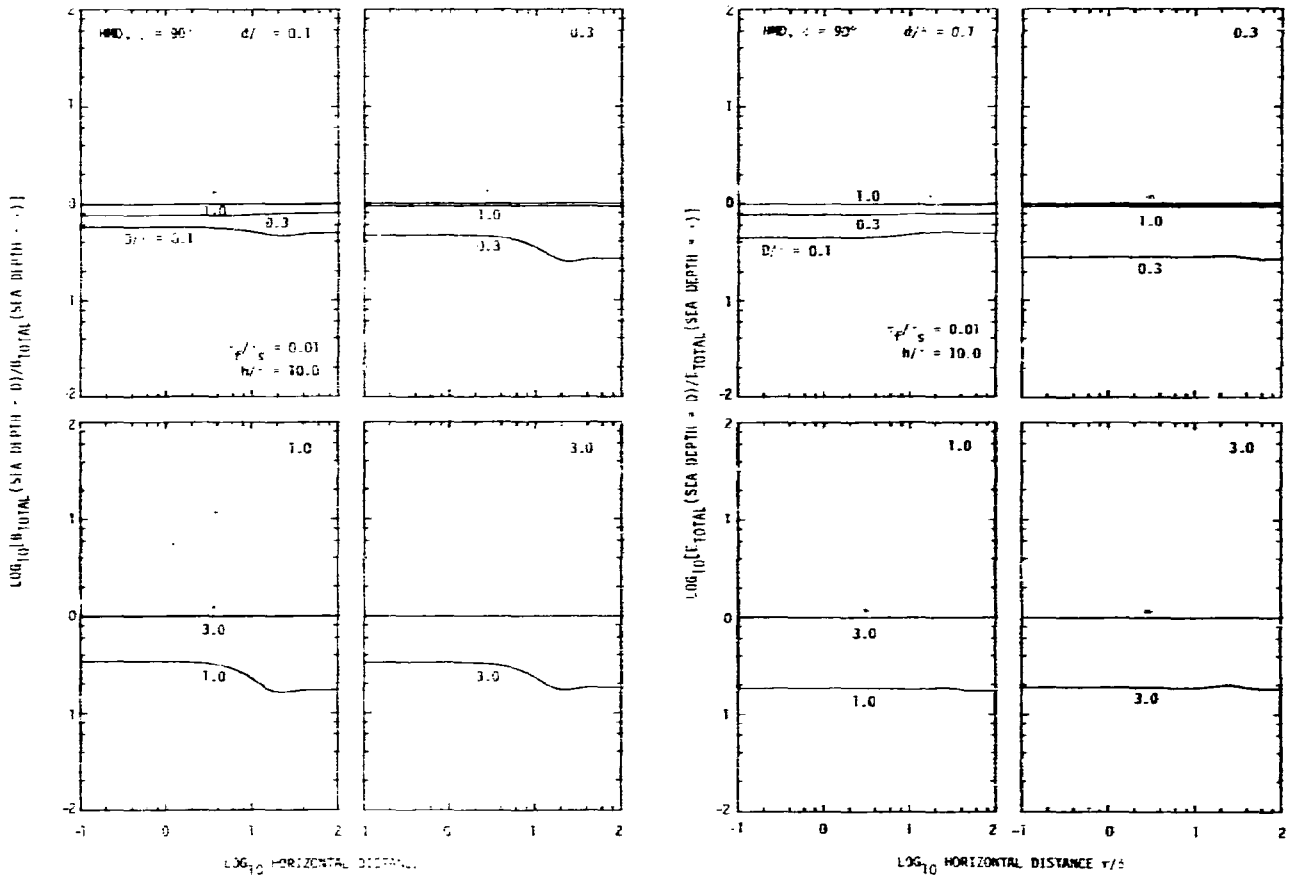

Figure 70. Curves illustrating the changes produced in the magnetic and electric field data presented in Figure 58 for a receiver altitude of ten sea water skin depths ($h/\delta = 10.0$) when an electrically conducting sea floor (conductivity $\sigma_f = 0.01\ \sigma_s$, depth D) is introduced. The conductivity of this sea floor is one tenth the conductivity of the sea floor used in Figure 68.

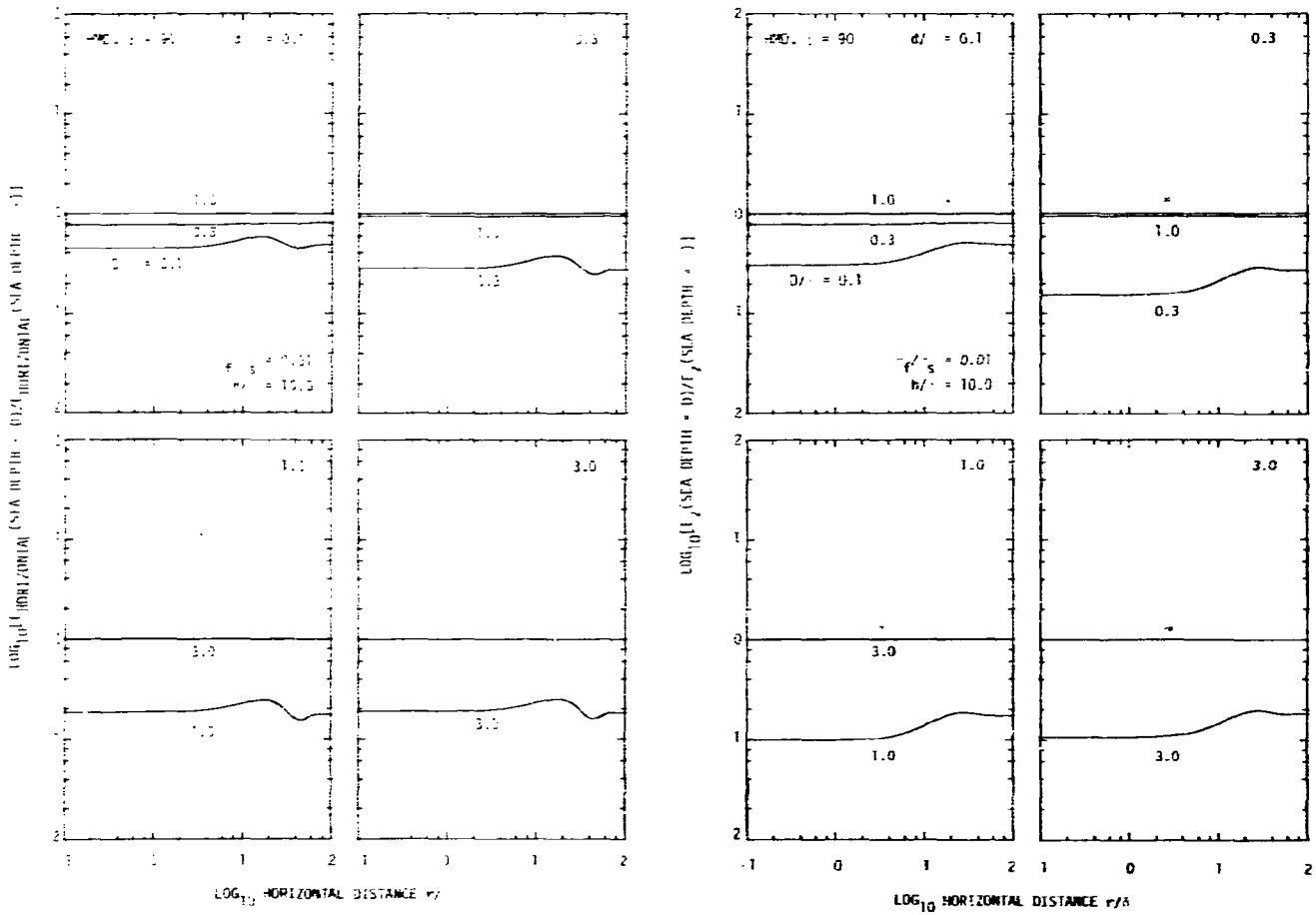

Figure 71. Curves illustrating the changes produced in the electric field component data presented in Figure 59 for a receiver altitude of ten sea water skin depths ($h/\delta = 10.0$) when an electrically conducting sea floor (conductivity $\sigma_f = 0.01\ \sigma_s$, depth D) is introduced. The conductivity of this sea floor is one tenth the conductivity of the sea floor used in Figure 69.

DISTRIBUTION LIST

Organization	No. of Copies
Director Defense Advanced Research Projects Agency	
ATTN: Program Management	2
TTO, R. A. Gustafson	1
TTO, P. A. Selwyn	1
1400 Wilson Boulevard Arlington, VA 22209	
Defense Documentation Center	12
Cameron Station Alexandria, VA 22314	
Office of Naval Research	
ATTN: Code 465	2
Code 222	1
800 North Quincy Street Arlington, VA 22217	
Office of Naval Research Resident Representative	1
University of California, San Diego La Jolla, CA 92093	
Office of Naval Research Resident Representative	1
Stanford University Room 165 - Durand Building Stanford, CA 94305	
Deputy Assistant Secretary of Defense Defense Research and Engineering for C^3	
ATTN: T. P. Quinn	1
Pentagon Washington, D.C. 20301	
Office of Assistant Secretary of the Navy (R, E&S)	
ATTN: J. Hurl	1
Pentagon, Room 5E 779 Washington, D.C. 20350	

Organization	No. of Copies
Naval Research Laboratory	
ATTN: Code 7550	
J. R. Davis	1
4555 Overlook Avenue, SW Washington, D.C. 20375	
Naval Ocean Systems Center	
ATTN: Library	1
W. Moler	1
C. F. Ramstedt	1
Y. Richter	1
C. Whitman	1
271 Catalina Boulevard San Diego, CA 95152	
Naval Electronic Systems Command	
ATTN: PME-117T	1
PME-117-21	2
Department of the Navy Washington, D.C. 20360	
Naval Underwater Systems Center New London Laboratory	
ATTN: P. Bannister	1
A. Bruno	1
J. Orr	1
E. Soderberg	1
New London, CT 06320	
Naval Surface Weapons Center White Oak Laboratory	
ATTN: J. J. Holmes	1
M. B. Kraichman	1
P. Wessel	1
Silver Spring, MD 20910	
David W. Taylor Naval Ship Research and Development Center	
ATTN: W. Andahazy	1
F. E. Baker	1
P. Field	1
Annapolis, MD 21402	

DISTRIBUTION LIST (Continued)

Organization	No. of Copies
Naval Postgraduate School Department of Physics and Chemistry	
ATTN: O. Heinz	1
P. Moose	1
Monterey, CA 93940	
Naval Coastal Systems Center	
ATTN: K. R. Allen	1
R. H. Clark	1
M. J. Wynn	1
Panama City, FL 32407	
Director Defense Nuclear Agency	
ATTN: RAAE	2
DDST	1
RAEV	2
Washington, D.C. 20305	
P&D Associates	
ATTN: C. Greifinger	1
P.O. Box 9695	
Marina del Rey, CA 90291	
Pacific-Sierra Research Corp.	
ATTN: E. C. Field	1
1456 Cloverfield Boulevard	
Santa Monica, CA 90404	
Johns Hopkins University Applied Physics Laboratory	
ATTN: L. Hart	1
H. Ko	1
Johns Hopkins Road	
Laurel, MD 20810	
University of California Scripps Institute of Oceanography	
ATTN: C. S. Cox, Code A-030	1
La Jolla, CA 92093	

Organization	No. of Copies
Lockheed Palo Alto Research Laboratory	
ATTN: W. Imhof	1
R. G. Johnson	1
J. B. Reagan	1
M. Walt	1
3251 Hanover Street	
Palo Alto, CA 94304	
La Jolla Institute	
ATTN: K. Watson	1
La Jolla, CA 92093	
University of Texas, Austin Geomagnetics and Electrical Geoscience Laboratory	
ATTN: F. X. Boxtick, Jr.	1
Austin, TX 78712	
Chief Air Force Technical Applications Center	1
HQUSAF	
Patrick AFB, FL 32925	
Commander Air Force Systems Command	2
Andrews AFB, MD 20331	
Commander Air Force Geophysics Lab	
ATTN: James Ulwick	2
Hanscom AFB, MA 01731	